Preliminary tests Part 1
Static and fatigue tests of UD and MD laminates

OB_TC_R008 rev. 000

Version 1
Confidential

OPTIMAT BLADES

TC

P.A. Joosse
D.R.V. van Delft
R.P.L. Nijssen
A.M. van Wingerde

TU Delft
Delft University of Technology

ECN

DLR

UNIVERSITY OF PATRAS

RISØ

CLRC

Table of Contents

Note: Appendix A is made available as a separate pdf document

1 INTRODUCTION

Contents of this report

In this document tests reported which form part of the so-called 'Preliminary Tests' of the "Optimat Blades" project. These tests were carried out prior to the manufacturing of the main body of standard OPTIMAT test specimens.
The objectives of this test campaign were:

1. to anticipate problems with the standard geometry and lay-up (e.g. regarding influence of geometry on strength, Euler buckling, capability of test rigs, etc.
2. to choose the best geometry for the standard OPTIMAT specimen.

To this end, specimens with different gauge lengths, lay-up and geometry were tested. Preliminary tests were also conducted at other institutes: UP [5], DLR [6] and RISØ [7].

This report contains the results, graphs and photos from static and fatigue tests carried out at the Knowledge Centre WMC (a co-operation between Delft University of Technology and ECN. It consists of 27 static compression tests, 13 static tensile test and 12 fatigue tests for four series with different geometries. The results will also be included in optiDAT.

Changes made in this revision

-

Acknowledgements

Special thanks to Ed van der Harst for his help in carrying out the tests.

2 TEST SET-UP AND PROCEDURE

Overview

Three kinds of tests were performed on the thin, flat laminate specimens: static tension and compressive tests and fatigue tests with R=-1. Most of the tests have been carried out in the 100 kN Schenck test machine, the other tests in the 250 kN in-house developed test machine.

Materials tested and notation

The tested coupons are made of the reference E-glass/epoxy materials for the Optimat Blades project [1]. These are:

- 'UD' or 'unidirectional material': 1150 g/m^2 in 0° direction and 50 g/m^2 in 90° direction with a 50 g/m^2 Chopped Strand Mat
- '±45°' or 'biaxial material': non-woven stitch-bonded glass roving in 2 layers, 400 g/m^2 in +45° and 400 g/m^2 in –45° with a two thin additional layers of 2 g/m^2 in 0° and 90°

For the matrix material, SP systems Prime 20 epoxy is used with slow hardener. The tabs for the tests are made out of GRP.
The thickness per layer was specified by LM to be about 0.88 mm for the unidirectional material and 0.61 mm for the biaxial material.
Test specimens were provided by LM Glasfiber A/S Denmark, cut from different plates.

	# of layers		lay-up	OptiDAT name	nominal thickness [mm]
	UD	biaxial			
plate 1	5	--	UD_5	UD1	4.5
plate 2	5	2	bi/UD_5/bi	MUD1	5.6
plate 3	5	6	$(bi,UD)_5$;bi	MD1	7.8
plate 5	4	5	$(bi,UD)_4$;bi	MD2	6.5

Table 1: Laminate lay-up and nominal thickness of the test plates

The tests are denoted by P***V(W)xxYz(z)z*** in which:

V	D or R	test specimen shape (Dog bone or Rectangular).
W	A, B, or C	(for plate 5) free length between the tabs of 35, 40 and 45 mm respectively.
xx		number LM used for the plate, in this series 04 (= GEV)
Y	T,C or F	type of test (static Tension, static Compression , or Fatigue)
zz(z)		number of the individual test specimens; for plate 5 three digits are used.

These plate numbers are included in optiDAT in the column 'delivered under name'.

Strain gauges

Where strain gauges have been used, strain gauge 001S000 denotes the front side of the test specimen and strain gauge 002S000 denotes the back side. The strain gauges used were 10 mm gauge length TML FLA-10-11 strain gauges, from Tokyo Sokki Kenkyujo Co.

3 STATIC TESTS

Test specimen geometry

The test specimens have been cut from the plates, described in Table 1. The plan form of the specimens is either rectangular or dog bone-shaped, see Figure 1. The actual thickness t, width and free length L (between the grips) of the tested specimens is given in Table 2.

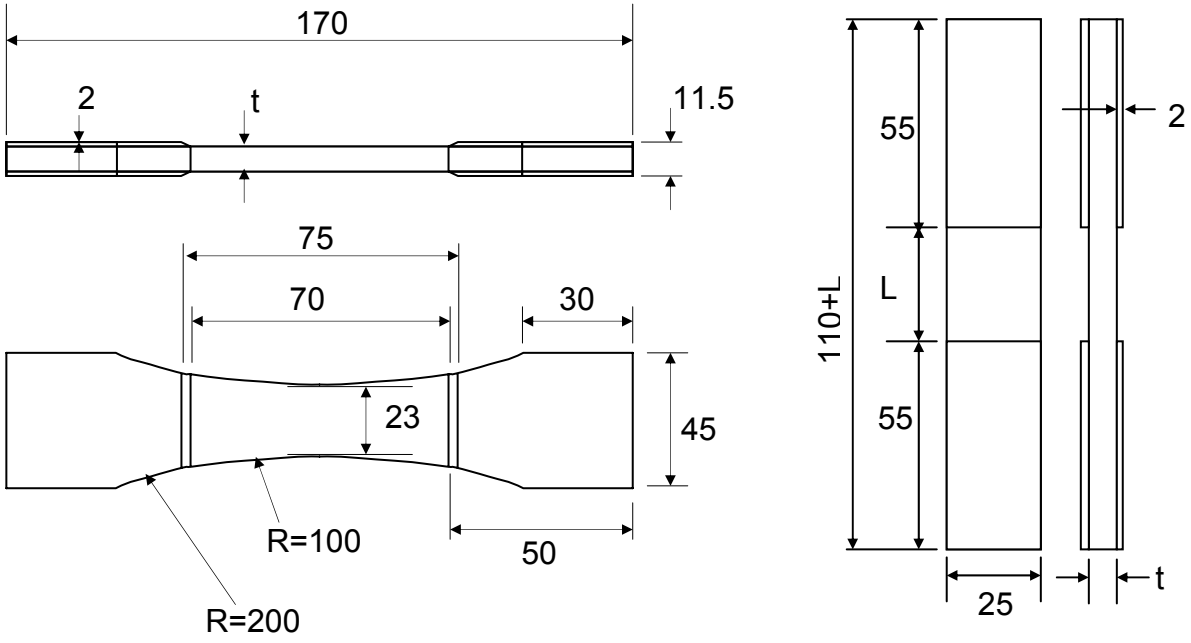

Figure 1: Dimensions of specimens D01 (dog bone shaped, left) and R01

Overview of measurement results

The mounting procedure of the specimens is as follows:

a. the specimen is mounted in the lower grips of the test machine
b. the strain gauge channel values are set to zero
c. the upper grips are closed.

The tests have been executed in displacement control with a speed of approx. 2 mm/min.

In Table 2 the actual geometry and measured data are presented for the static tests. The stress and strain given in the table are the values at failure. For the stress the applied force is divided by the initial cross sectional area in the middle of the specimen. In case of the strain, the mean value is taken of the two strain gauge readings, unless one of the gauges clearly produced erroneous data. The strain gauge measurement system normally reaches up to 18500 μ, although the strain gauge accuracy is not guaranteed for those strain levels.
The Young's modulus (E) has been determined based on linear regression of the stress-strain curve for strains between 500 and 2500 μstrain.

In the appendix, per static test one graph is presented containing the force versus the displacement of the actuator and the force against the strain gauge readings (if strain gauges

were present). Furthermore, 2 photos of each failed test specimen are presented, taken from each side.

name	width [mm]	free length [mm]	t_1 [mm]	t_2 [mm]	F_{max} [kN]	σ_{max} [Mpa]	E [Mpa]	ε_{max} [%]
compression								
PD01C01	23.28	70	4.49	4.41	-42.72	-412.4	44847	0.901
PD01C06	23.35	70	4.56	4.44	-42.58	-405.2	45844	0.885
PD01C11	23.03	70	4.54	4.51	-40.82	-391.7	44863	0.867
PR01C06	25.21	50	4.53	4.56	-53.91	-470.5	39781	1.191
PR01C16	25.03	50	4.56	4.61	-58.06	-505.9	39243	1.266
PR01C21	25.13	50	4.59	4.61	-68.6	-593.4	40075	1.496
PD02C21	23.42	70	5.64	5.68	-55.79	-420.9	37454	1.137
PD02C26	23.35	70	5.61	5.68	-56.61	-429.5	38102	1.157
PD02C31	23.52	70	5.69	5.66	-52.69	-394.8	37959	1.080
PR02C26	25.26	50	5.65	5.63	-69.21	-485.8	34364	1.399
PR02C31	25.3	50	5.69	5.70	-73.49	-510.1	34254	1.543
PR02C36	24.85	50	5.62	5.63	-71.21	-509.4	35017	1.537
PD03C21	23.34	70	7.89	7.84	-91.72	-499.6		
PD03C26	23.28	70	7.61	7.62	-87.97	-496.2		
PD03C31	23.40	70	7.87	7.84	-81.58	-443.8		
PR03C26	25.64	50	7.70	7.71	-91.66	-464.0		
PR03C31	25.45	50	7.85	7.84	-97.64	-489.0		
PR03C36	25.55	50	7.74	7.88	-91.84	-460.2		
PRA05C06	24.78	35	6.30	6.44	-71.24	-451.3	27910	1.806
PRA05C11	24.73	35	6.35	6.38	-74.27	-471.8		
PRA05C16	24.85	35	6.42	6.39	-78.37	-492.4		
PRB05C55	24.55	40	6.63	6.51	-76.07	-471.6	28693	1.898
PRB05C60	24.72	40	6.47	6.53	-77.34	-481.3		
PRB05C65	24.72	40	6.41	6.49	-75.54	-473.8		
PRC05C111	24.86	45	6.39	6.51	-76.81	-479.0		
PRC05C116	24.91	45	6.49	6.51	-78.37	-484.0	28090	1.965
PRC05C121	24.86	45	6.38	6.52	-78.42	-489.1	28537	1.940
tension								
PD01T16	23.34	70	4.60	4.42	85.5	812.2	44578	2.104
PD01T31	23.35	70	4.50	4.51	90.37	859.1	44911	2.148
PR01T01	24.99	50	4.45	4.65	100	879.5	39430	
PR01T11	25.17	50	4.51	4.59	96.41	841.8	39523	
PR01T26	25.25	50	4.61	4.60	86.56	744.4	39190	1.960
PD02T01	23.19	70	5.59	5.65	92.83	712.3		
PD02T06	23.36	70	5.64	5.65	90.84	688.9		
PR02T06	24.92	50	5.63	5.61	96.58	689.6		
PR02T11	25.30	50	5.61	5.69	96.52	675.2		
PD03T01	23.04	70	7.88	7.92	100.00	549.4		
PRA05T01	24.72	35	6.33	6.26	89.06	572.3		
PRB05T70	24.73	40	6.41	6.51	93.65	586.2		
PRC05T131	25.01	45	6.50	6.51	93.85	576.9		

Table 2: Static test results

Discussion

For plates 1, 2 and 5 specimens equipped with strain gauges have been tested.
In Figure 2 an overview is given of the Young's moduli. As expected, the pure UD material results in the highest stiffness, the larger the fraction of 45° oriented layers, the lower the stiffness becomes. Based on the results for plate 1 specimens, the loading direction (tension or compression) does not have a significant effect. There is a significant effect, though, of the specimen shape. For both plate 1 and plate 2, the dog bone specimen has a significantly higher value for the Young's modulus than the rectangular specimens. Since the material and lay-up are the same, this can only be attributed to the shape. As a result of this shape, the strain in the middle of the dog bone specimen is approx. 10% lower at the same applied stress than for the rectangular specimen.

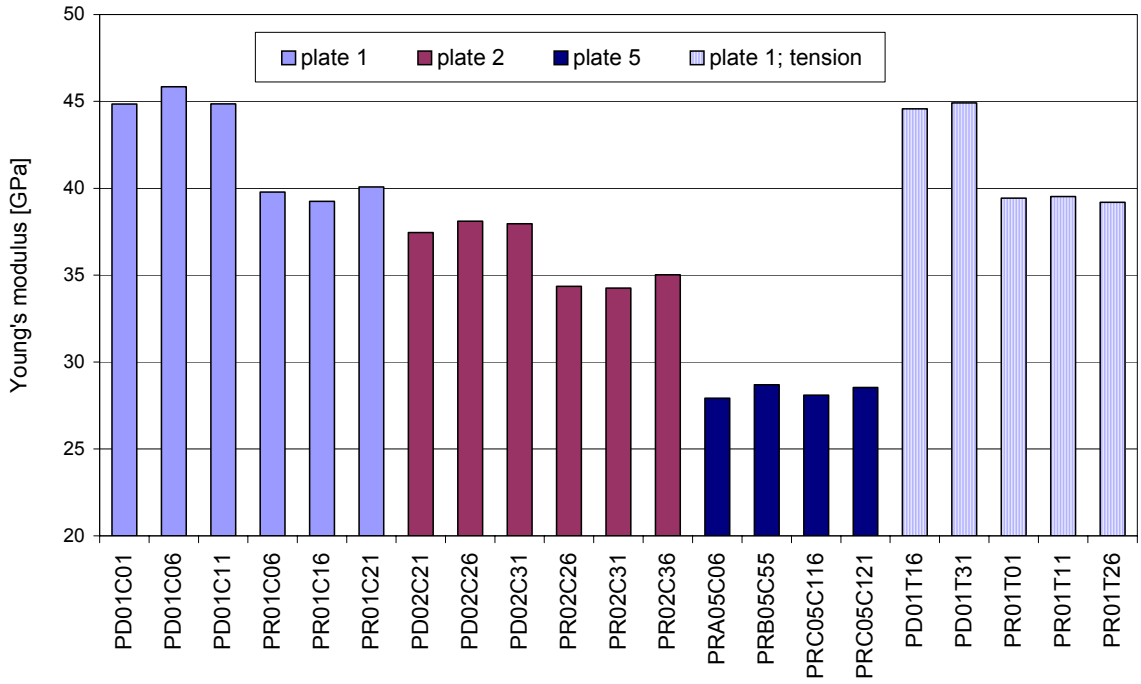

Figure 2: Young's moduli in compression for 3 plates and tensile modulus for plate 1

The strength results of the compressive tests are given in Figure 3. In this graph the failure load (in kN) is given as well as the failure strength (in MPa) for all compression tests.
From this figure it can be seen that for plates 1 and 2 the dog bone shaped specimen all fail at a lower load (either force or stress) than the rectangular specimens. For plate 3, on the other hand, the difference is small (due the relatively large scatter no 'hard' conclusions can be drawn here).

For the 'ud' specimens (plate 1), a clear difference can be observed between the dog bone and the rectangular specimens. From the test figures (e.g. figure A 1, figure A 3 and figure A 5 for the dogbone and figure A 5 etc for the rectangular specimens) it is clear that all dogbone shaped specimens encountered buckling. The strain-force curves show a strong divergent behaviour near failure. For the rectangular specimens 2 specimens fail before buckling occurs, one specimen experiences vast bending at a strain as low as 75% of the failure strain. Due to the buckling phenomena, the average dog bone specimens strength comes out 20% lower for the specimens of plates 1.

For prismatic specimens, the ASTM standard [3] states a minimum required specimen thickness, to prevent Euler buckling. This formula, which is also given in ISO 14126 [4], is as follows:

$$h > L / (0.9096 * \sqrt{ ((1 - 1.2*F^{cu}/G_{xz}) * (E_c/F^{cu})) }) \qquad \text{(eq. 1)}$$

For plate 1, the following values are applied:

- nominal thickness of h = 4.5 mm,
- E_c = 40 GPa (see above)
- out-of-plane shear modulus of G_{xz} = 5.8 GPa (assumed value)

For a free length of L=50 mm, Euler buckling is predicted at approx. 250 MPa, which is only half of the strength found for the rectangular specimens. In view of this limited accuracy, results of this equation will not be used any further in this report.

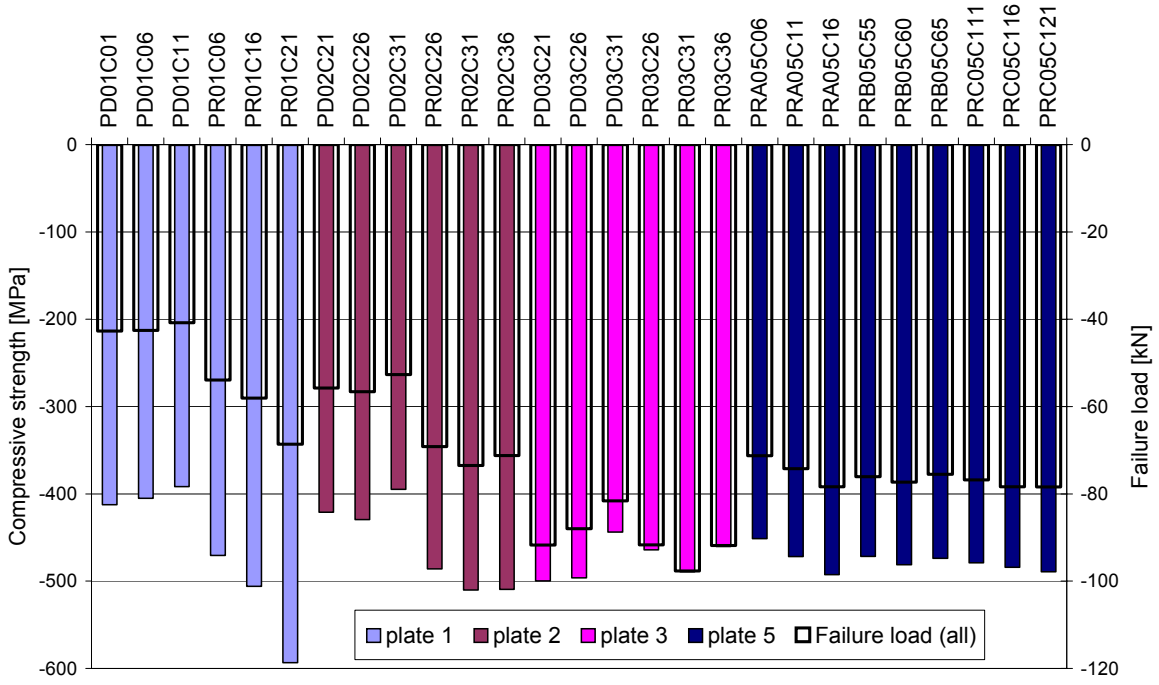

Figure 3: Compressive strength for 4 different plates

For plate 2 buckling can be observed for all specimens, either rectangular or dogbone shaped. This is a surprising outcome, since plate 2 is merely plate 1 with 2 additional layers of 45-degree oriented materials. The failure loads are higher, compared to plate 1.

For plate 3 no specimens have been equipped with strain gauges, therefore no objective data are available to decide on buckling. In view of the increased thickness, it can however be argued that Euler buckling is not expected to happen at the measured strength of 475 MPa.

For the test results of plate 5, the main difference is the free length. As can be expected, the specimens with the shortest length (35 mm) do not show any buckling, whereas the longest specimens will probably have experienced buckling. This can be judged from the two

specimens equipped with strain gauges: both show the typical divergence of the strain curves.

The tensile strength results are given in graphical form in Figure 4. The number of tests is more limited than the compressive tests. Two specimens (pr01t01 and pd03t01) shown here should be regarded as run-outs, since the specimens could not be failed in the 100 kN test machine. Specimen pr01t01 was later mounted in the 250 kN test machine and failed at 87.4 kN.

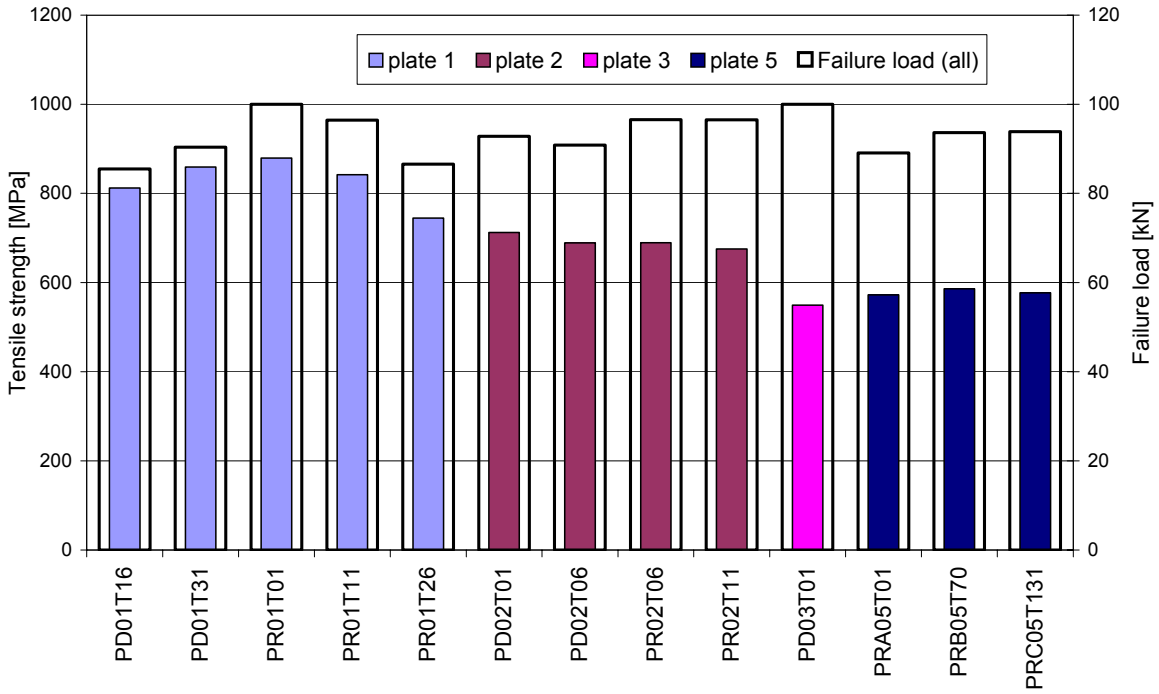

Figure 4: Tensile strength for different plates

There are no firm indications for strength differences due to the specimen shape. Although the rectangular specimens are slightly weaker, this is only a few percent and therefore not significant. The addition of ±45° layers (plate 2 and plate 3) increases the failure load, but not the in proportion to the thickness. This can be expected, since the material added is less strong than the 'ud' material.

When comparing the tensile strength to the compressive strength, for rectangular specimens, the following can be observed. For the specimens of plate 1, the 'ud' laminate, the compressive strength is approximately 65% of the tensile strength. When 45° oriented layers are added at the outside (plate 2), this ratio increases to 72%. For the test plates with an (almost) equal number of 'ud' and ±45° layers, the ratio increases to approx. 75%, due to a decreased tensile strength at almost constant compressive strength.

4 FATIGUE TESTS

Test specimen geometry

The test specimens have been cut from the plates, described in Table 1. The plan form of the specimens is either rectangular or dogbone-shaped, see [2]. The actual thickness, width and free length (between the grips) of the tested specimens is given in Table 2.

Overview of measurement results

The specimens were mounted in the test machine following the same procedure as used for the static loaded specimens. For every specimen a slow cycle is executed (and measured) first, at a frequency of 0.02 Hz. This slow cycle can be used as part of the stiffness degradation monitoring.
Following that, the fatigue tests is started in load control with a frequency of 2 Hz, except for pr01f31 which was loaded at 1 Hz.

In Table 3 the actual geometry and measured data are presented for the fatigue tests. The stress and strain given in the table are the maximum value in the fatigue cycle. For the stress the applied force is divided by the initial cross sectional area in the middle of the specimen. In case of the strain, the mean value is taken of the two strain gauge readings, unless one of the gauges clearly produced erroneous data. The Young's modulus (E) has been determined as the mean value of the linear regression slopes of the stress-strain curve for strains between 500 and 2500 μstrain and –500 and –2500 μstrain.

For the fatigue tests, two pages with graphs are given per specimen and two photographs. The first page with graphs gives the result for the slow cycle that precedes the fatigue test. The lay-out is similar as the graph for the static test. The second page gives ranges of the applied force and bench displacement and the strains (for plate 1) over the fatigue life.
Furthermore, 2 photos of each failed test specimen are presented, taken from each side.

name	width [mm]	t_1 [mm]	t_2 [mm]	F_{max} [kN]	cycles	σ_{max} [Mpa]	E [Mpa]	ε_{max} [%]
PD01F21	23.27	4.46	4.48	30	791	288.4	45024	0.642
PD01F26	23.28	4.51	4.52	30	469	285.4	44673	0.636
PR01F31	25.14	4.53	4.54	35	13655	307.0	40299	0.765
PR01F36	25.14	4.52	4.58	30	24325	262.3	39950	0.658
PD02F11	23.37	5.58	5.60	30	82468	229.6		
PD02F16	23.39	5.59	5.61	35	9305	267.2		
PR02F16	24.91	5.67	5.61	35	11674	249.1		
PR02F21	25.15	5.59	5.60	35	9153	248.7		
PD03F11	23.38	7.86	7.88	35	36165	190.2		
PD03F16	23.17	7.69	7.71	35	172	196.2		
PR03F16	25.54	7.80	7.89	35	1283	174.7		
PR03F21	25.43	7.86	7.88	35	721	174.9		

Table 3: Fatigue test results

From the specimens that have been equipped with strain gauges (plate 1), relative large bending can be observed for he dogbone specimens and some bending for the rectangular

ones. During the last phase of test pr01f31 and the first of pr01f36, wrong values of the force range were recorded, due to erroneous time averaging settings. The ranges should be 70 and 60 kN respectively, as was recorded for the rest of those specimens.
For most specimens some hysteresis has been recorded in the force – bench displacement diagram during the first (slow) cycle. In general, the hysteresis (expressed as ratio of the enclosed area to the elastic energy) increases from plate 1 to plate 3 and is higher for the dogbone shaped specimens. This hysteresis can be a result from heat build-up or damage in the specimen, it can also be caused by slip between e.g. tab and grip. Since it is not possible, at present, to pinpoint the exact cause, no conclusions can be drawn.

Discussion

The values for the Young's modulus, as given in Table 3 for the slow cycles before the fatigue tests, agree with the data found during the static tests.
The fatigue results are graphically given as S-N curve in Figure 5. Since only 2 specimens have been tested per configurations, no firm conclusions will be drawn.

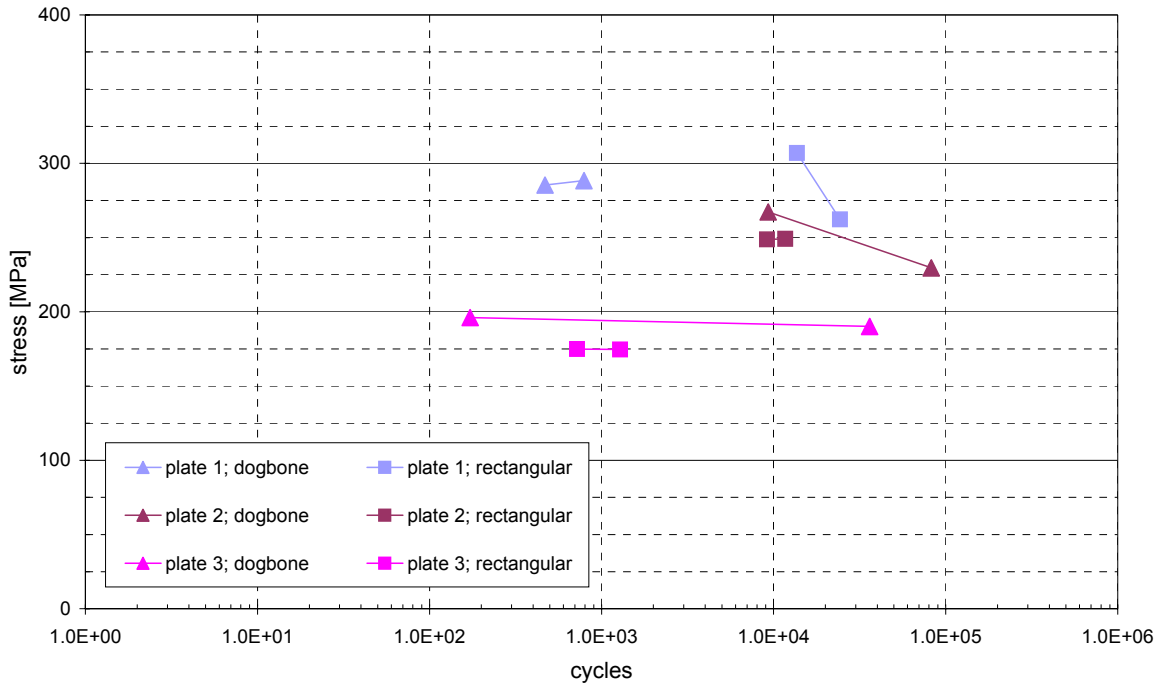

Figure 5: Fatigue results of three plates

For most configurations the two data points are relatively close together, taking into account that the dogbone specimens of plate 2 are tested at different levels. The exceptions for this are the dogbone shaped specimens from plate 3: one specimen failed in a buckling mode, at a mere 172 cycles, whereas the other one failed in an 'ordinary' manner at 36165 cycles.
When taking a closer look at the photographs, it can be seen that most of the rectangular specimens failed at the tab, although this position can be expected, it is not favoured. None of the dog bones failed near the narrowest section, most of them failed halfway the narrowest section and the tab.

5 CONCLUSIONS

- The measured Young's modulus of the dogbone specimens is typically 10% higher than for the rectangular specimens. This is a result from the non-uniform strain distribution in the measured section.
- The loading direction (tension or compression) does not have a significant effect on the measured Young's modulus.
- For the compression loaded dogbone specimens of plate 1 and 2, an Euler buckling type of failure occurred, resulting in relatively low compressive strength. For the MD1 laminate (plate 3) the dogbone and rectangular specimens resulted at similar compressive strength values.
- For the MD2 laminate (plate 5), compression tests have been accomplished with different free lengths: 35, 40 and 45 mm. Although buckling was observed for the specimens with 45 mm free length, there is no significant difference between the compression strengths.
- For the specimens that were loaded in tension, no influence of the specimen shape on the strength could be established.
- The compression strength of the MD1 and MD2 specimens (plates 3 and 5) is approx. 85% of the tensile strength. For the specimens with higher percentage of 0° fibres this ratio decreases: 72% for plate 2 and 64% for plate 1.

6 REFERENCES

[1] T. K. Jacobsen, Reference material (OPTIMAT), Glass-epoxy material, OB_SC_R001/00, 7 May 2002.

[2] A.M. van Wingerde et.al: Overview of test geometry, material lay-up and test set-up, OB_TC_R003, 30-05-2002

[3] "Standard Test Method for Determining the Compressive Properties of Polymer Matrix Composite Laminates Using a Combined Loading Compression (CLC) Test Fixture", ASTM D 6641/D 6641M – 01

[4] "Fibre-reinforced plastic composites – Determination of compressive properties in the in-plane direction", ISO 14126, September 1999

[5] T. P. Philippidis, T. T. Assimakopoulou, V. Passipoularidis, "Preliminary test results on UD reference material (2nd round)", OB_TC_R006, 29 August 2002

[6] O. Krause, "Preliminary tests – 2 (Compression of UD specimens)", OB_TC_N002, 4 September 2002

[7] M. Megnis, P. Brønsted, "Preliminary tests – 2 (Compression of UD specimens)", OB_TG3_R002, 20 August 2002

APPENDIX A TEST RESULT FIGURES AND PHOTOGRAPHS

In this annex figures are given for the static and fatigue tests and photographs of the specimens after testing.

For the static tests, the applied bench displacement and resulting force are given, e.g. in the upper figure of figure A-1. In the lower figure of figure A-1, when measured, the strains are given against the force. Following this figure with graphs, two photographs are given for each specimen, from the front side and backside of the specimen.

For the fatigue tests, two pages with graphs are given per specimen and two photographs. The first page with graphs gives the result for the slow cycle that precedes the fatigue test (see e.g. figure A 81). The lay-out is similar as the graph for the static test. The second page gives ranges of the applied force and bench displacement and the strains (when strain gauges have been mounted) over the fatigue life.

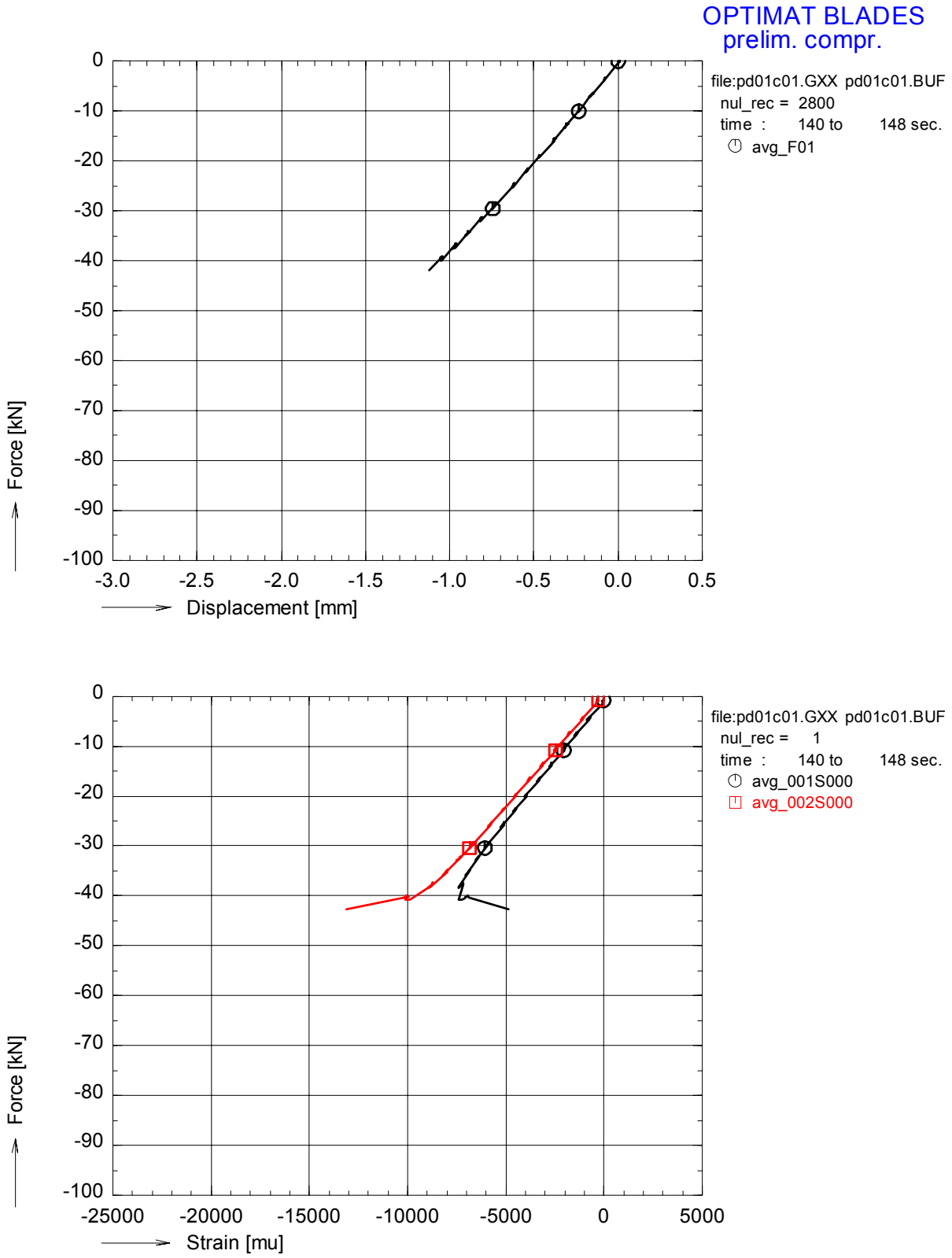

figure A 1: Axial compressive force vs. bench displacement and strains for pd01c01

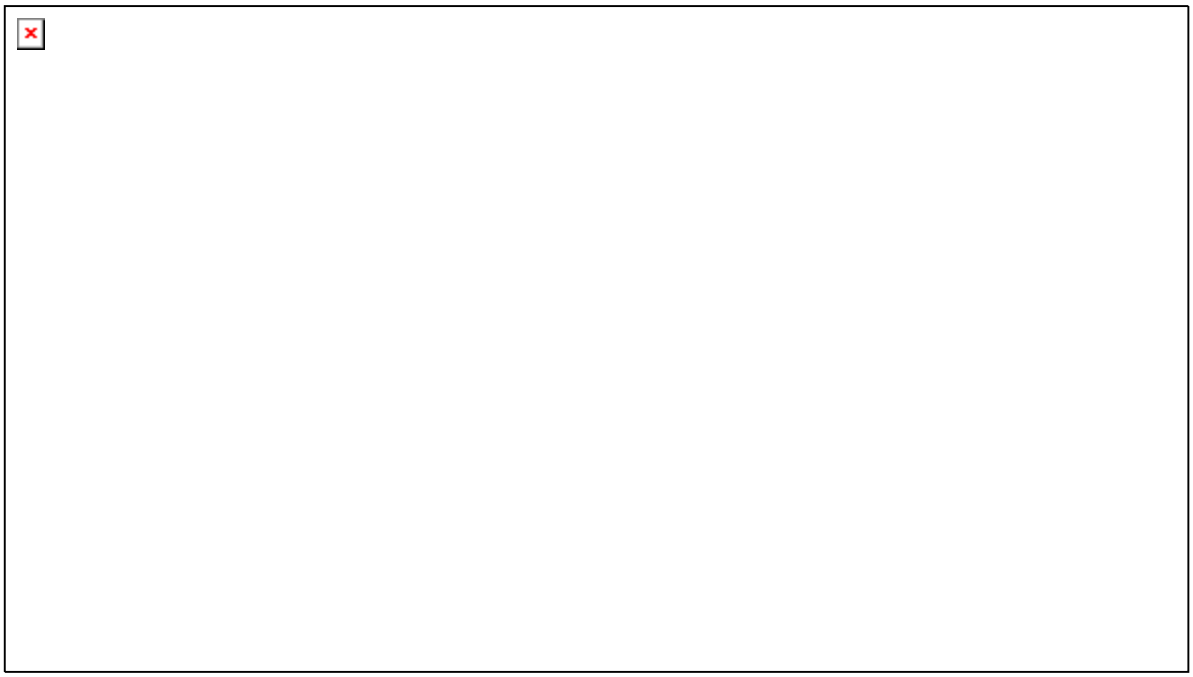

figure A 2: Photographs of failed specimen pd01c01 (top: back-side)

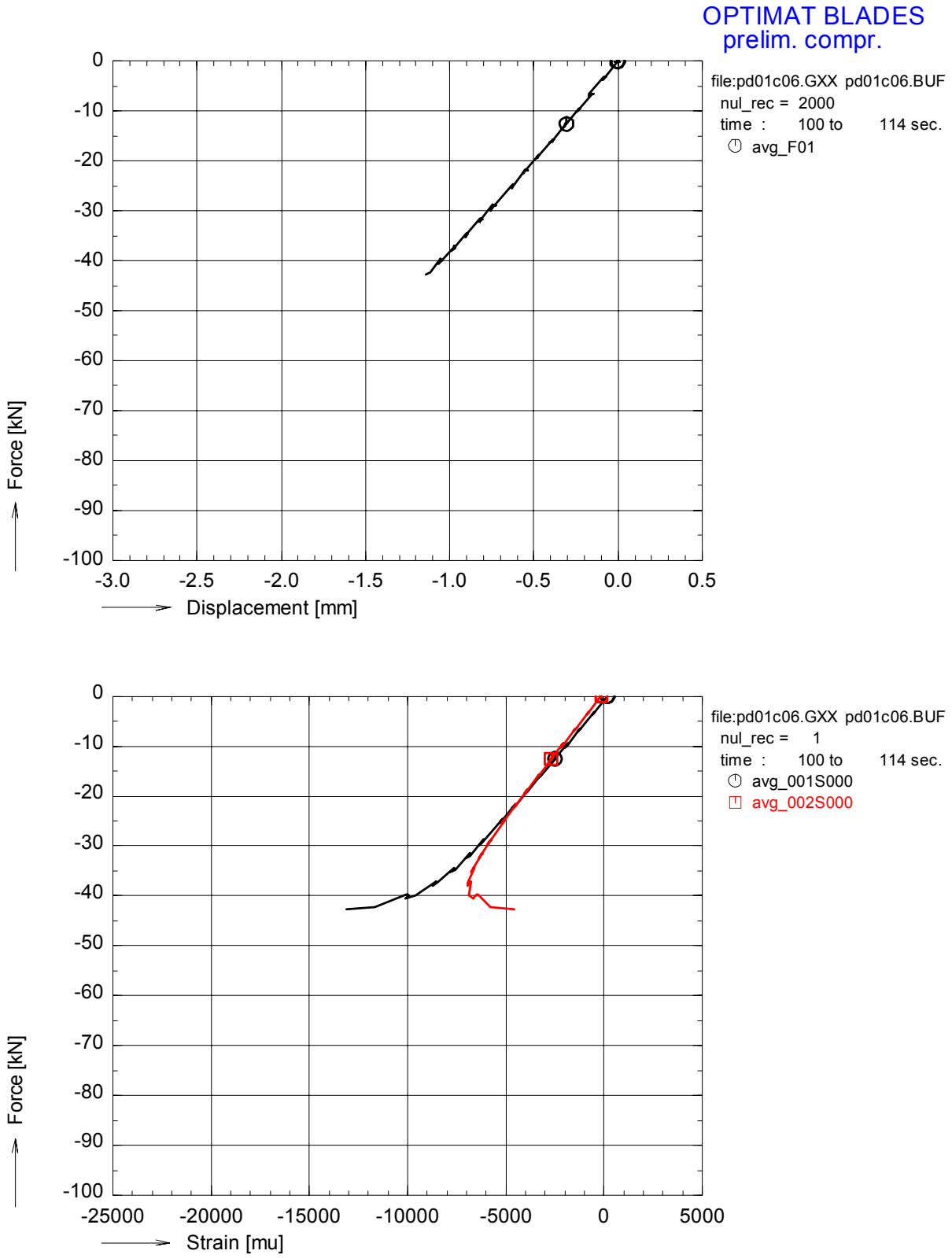

figure A 3: Axial compressive force vs. bench displacement and strains for pd01c06

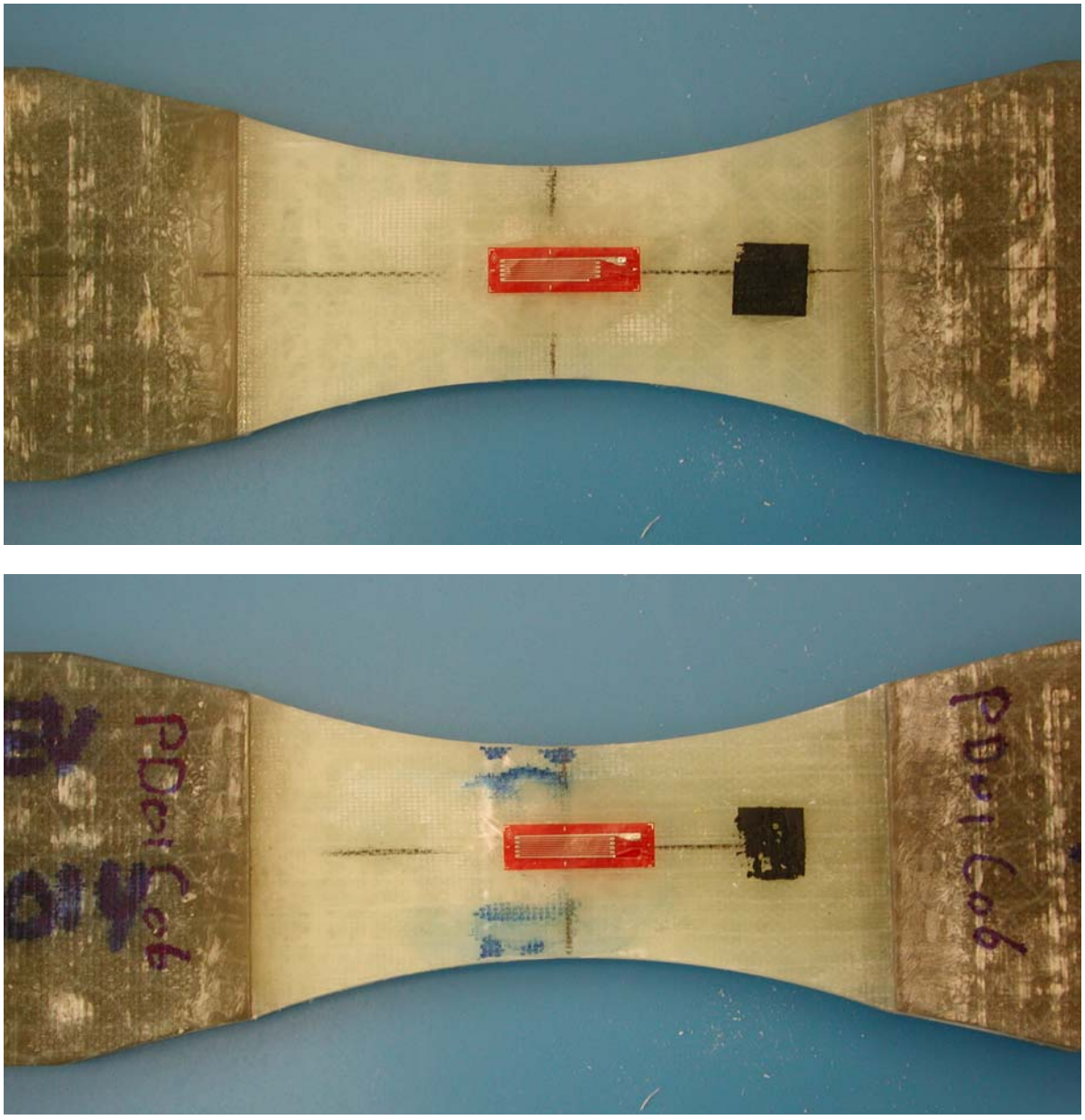

figure A 4: Photographs of failed specimen pd01c06

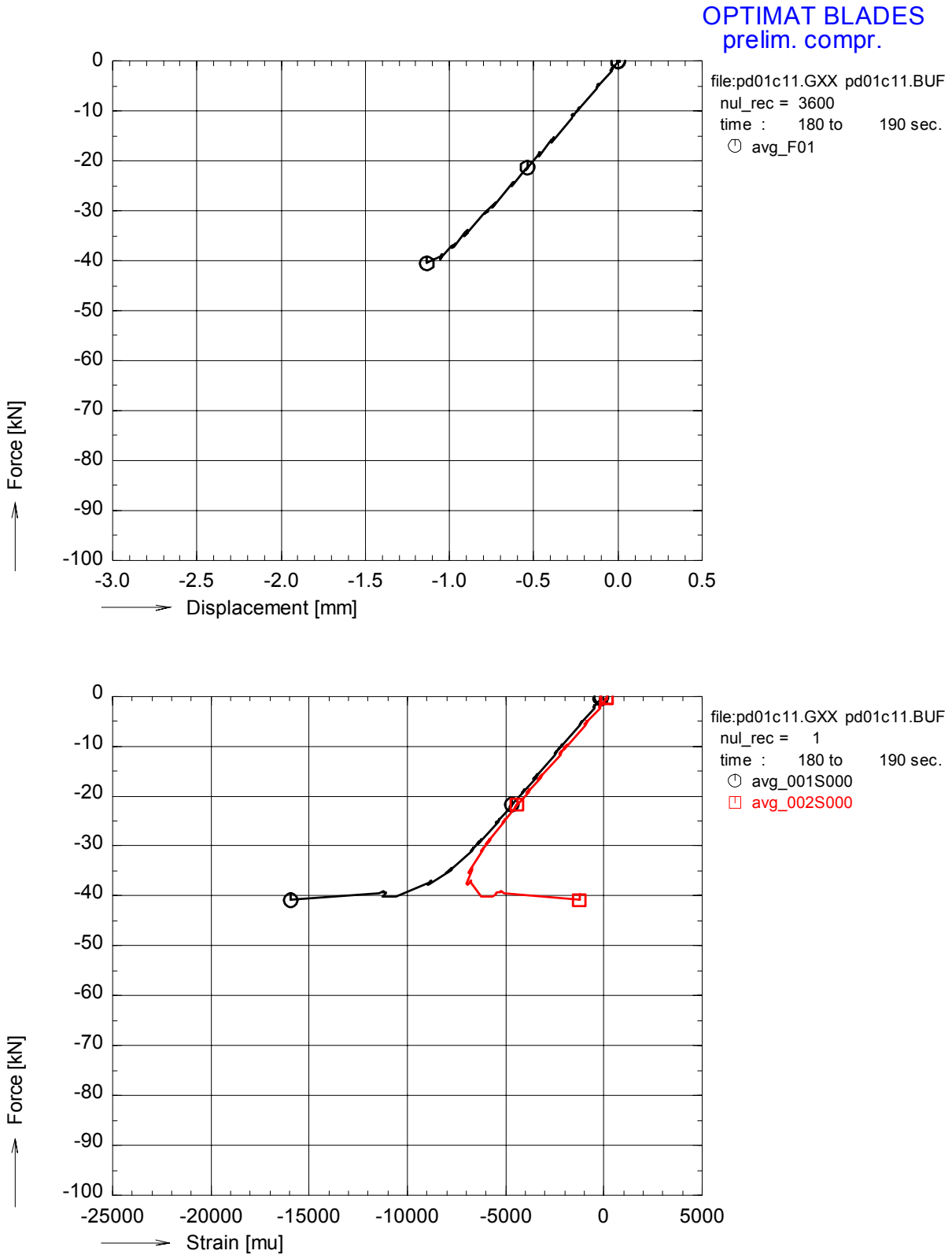

figure A 5: Axial compressive force vs. bench displacement and strains for pd01c11

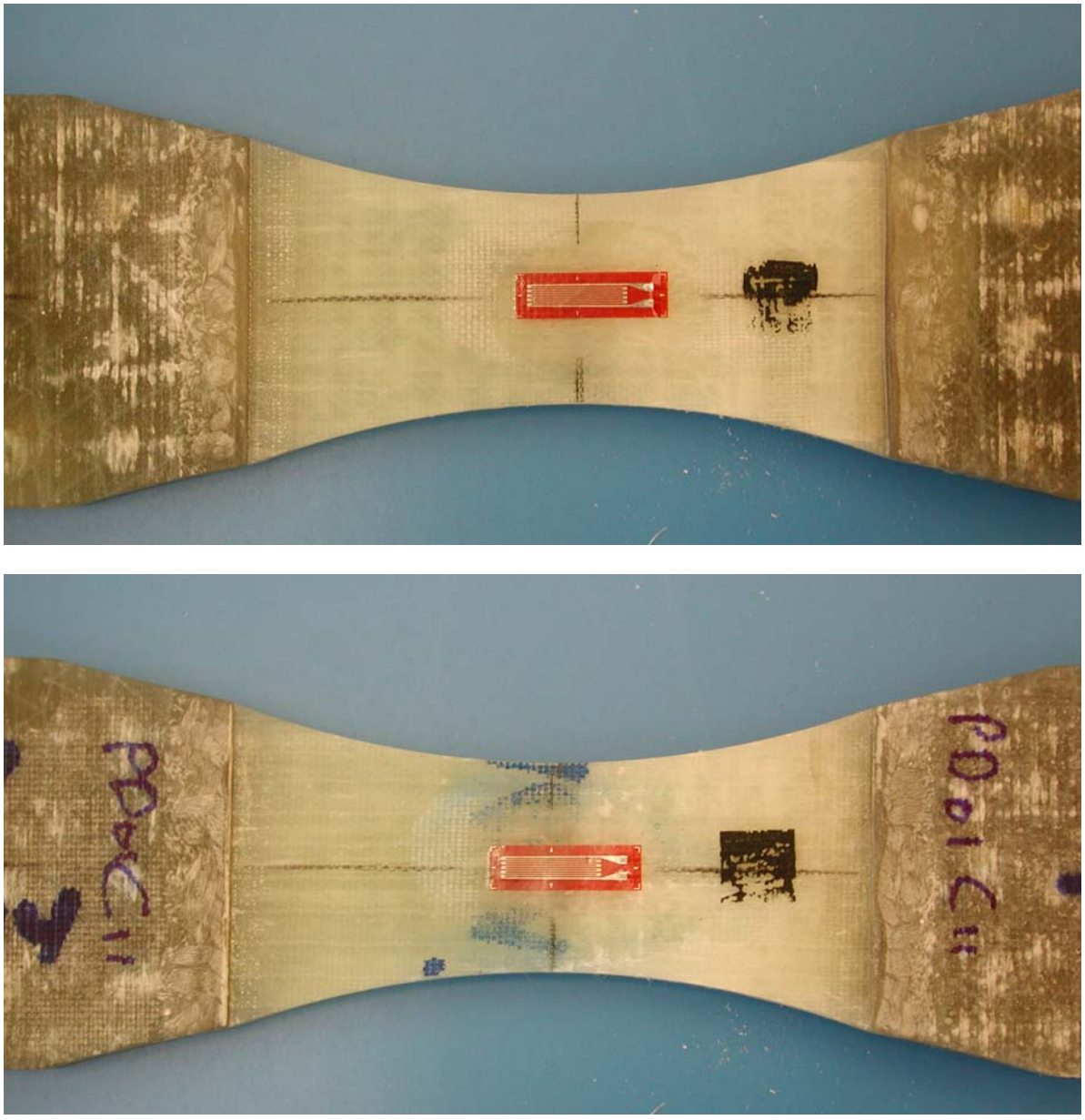

figure A 6: Photographs of failed specimen pd01c11

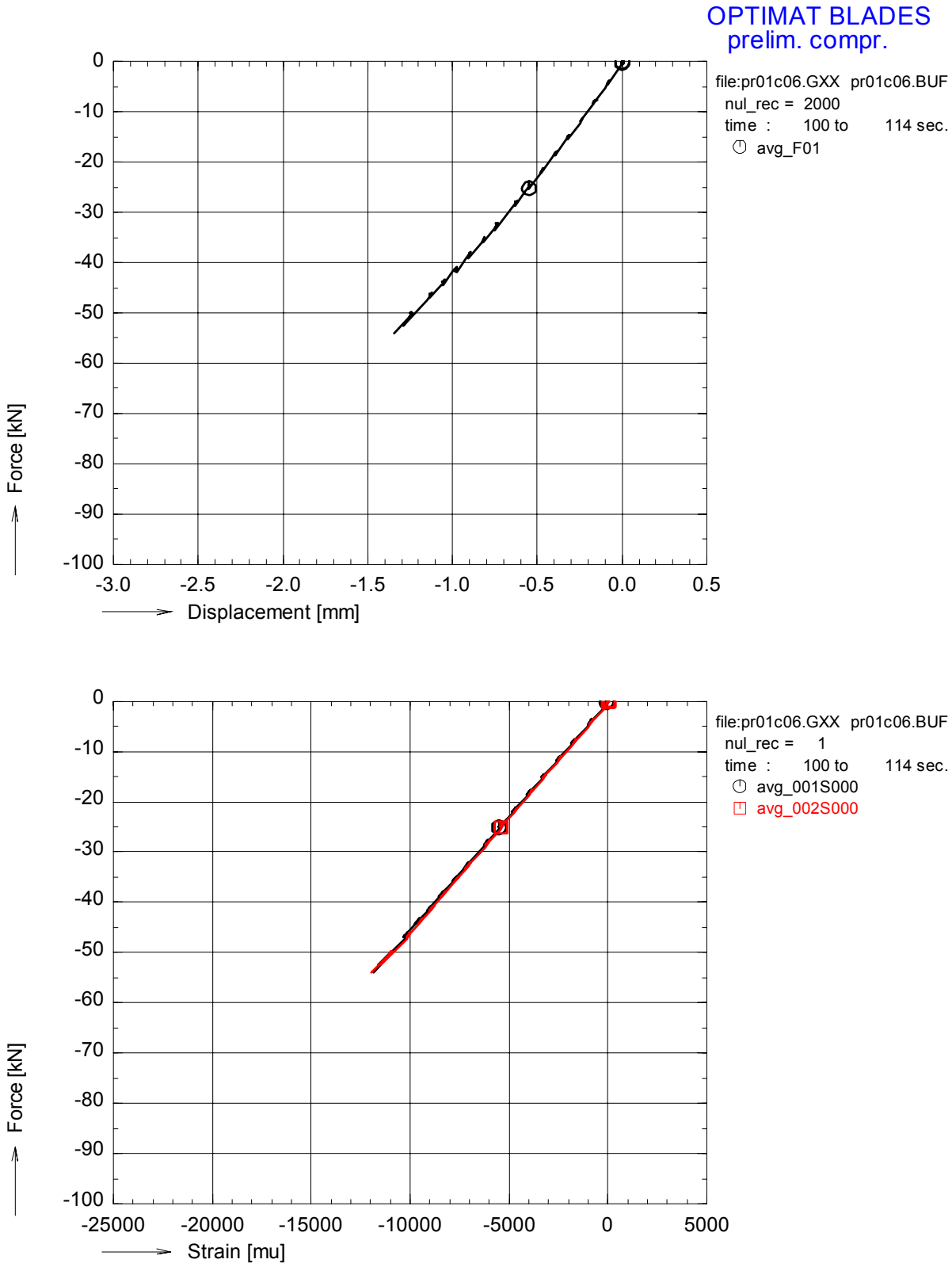

figure A 7: Axial compressive force vs. bench displacement and strains for pr01c06

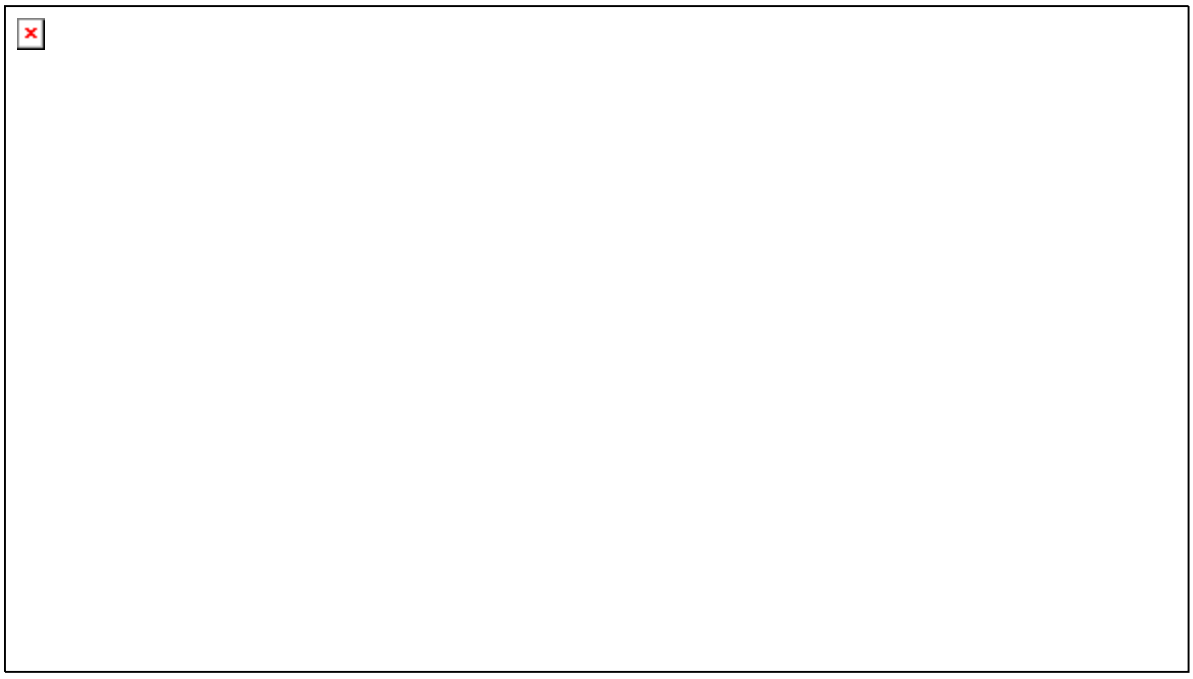

figure A 8: Photographs of failed specimen pr01c06

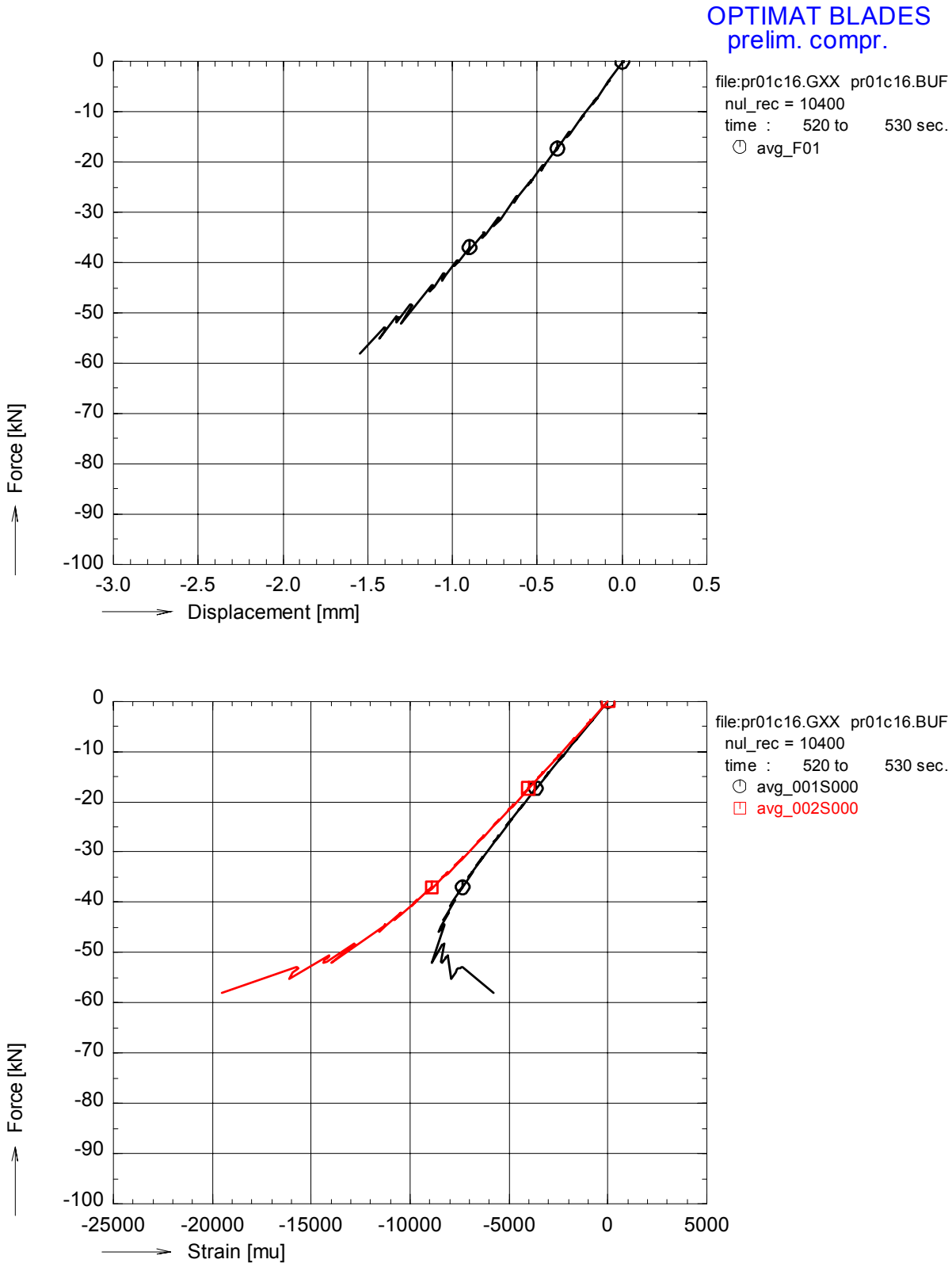

figure A 9: Axial compressive force vs. bench displacement and strains for pr01c16

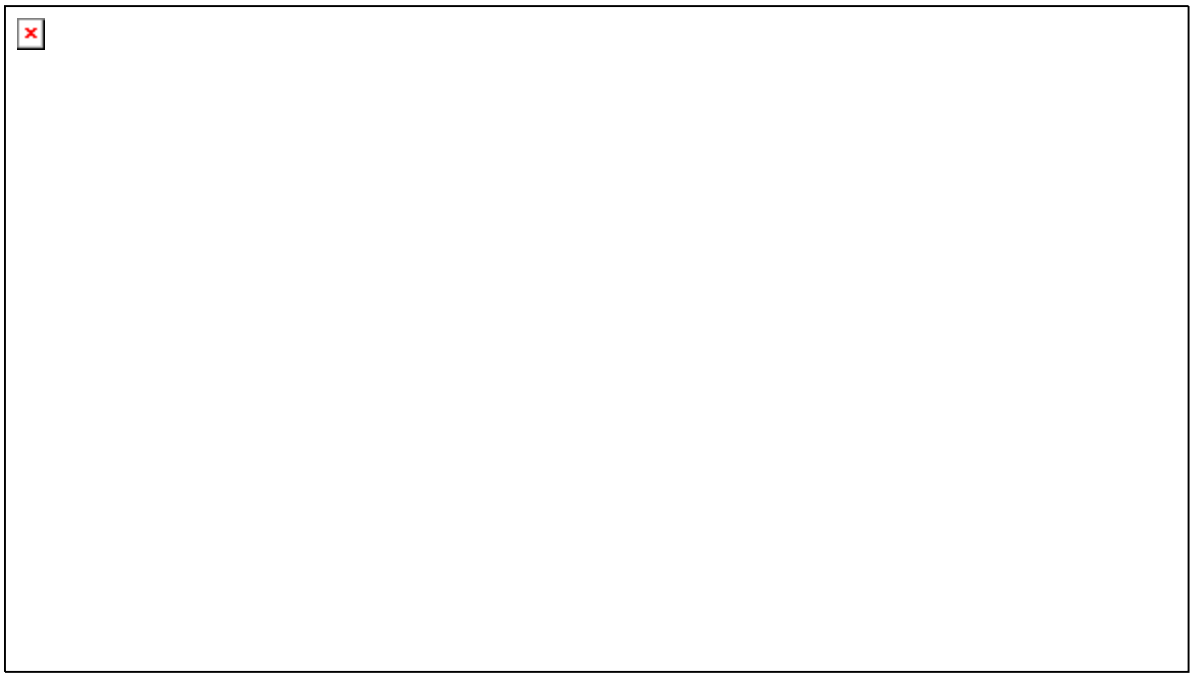

figure A 10: Photographs of failed specimen pr01c16

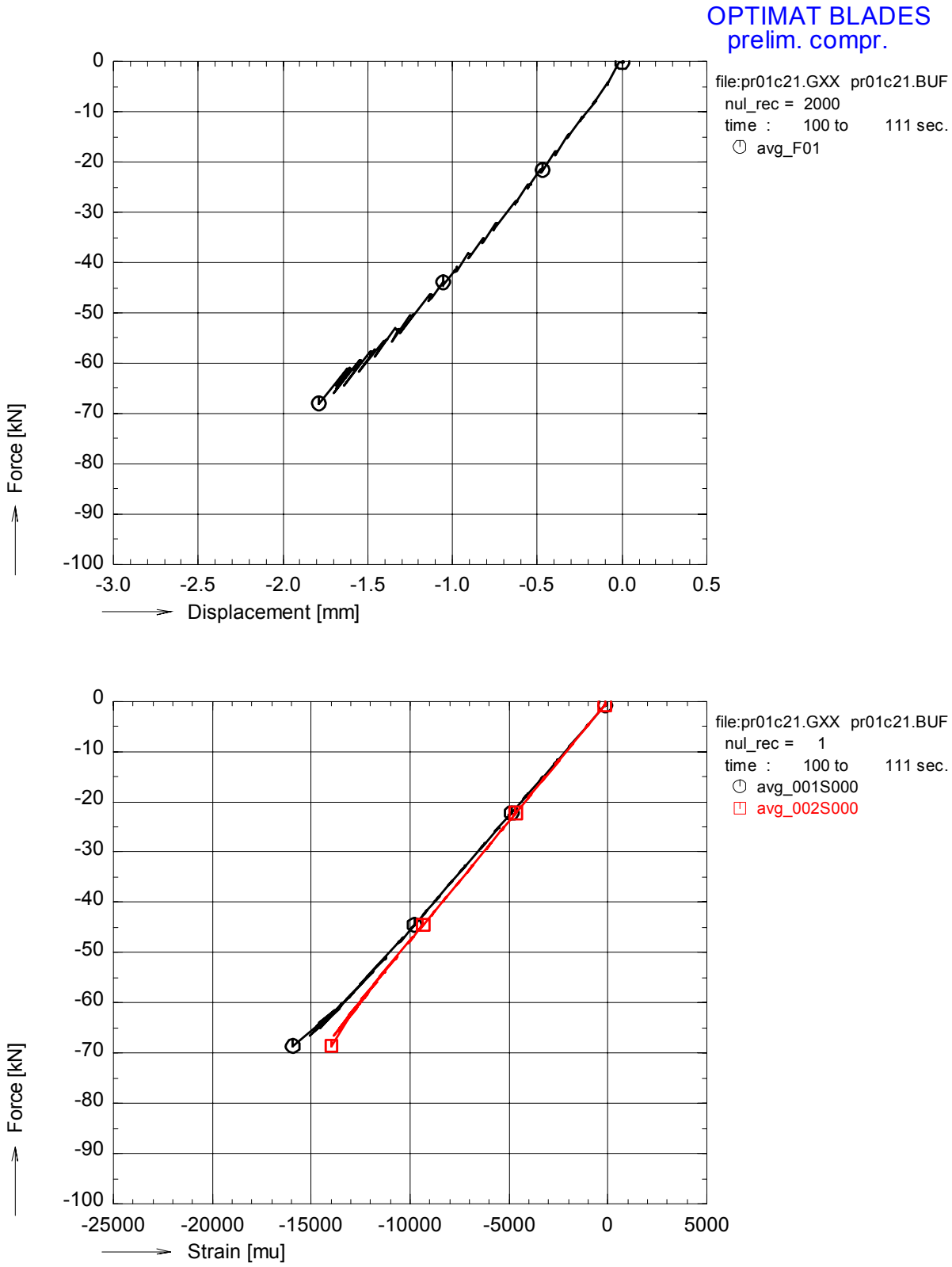

figure A 11: Axial compressive force vs. bench displacement and strains for pr01c21

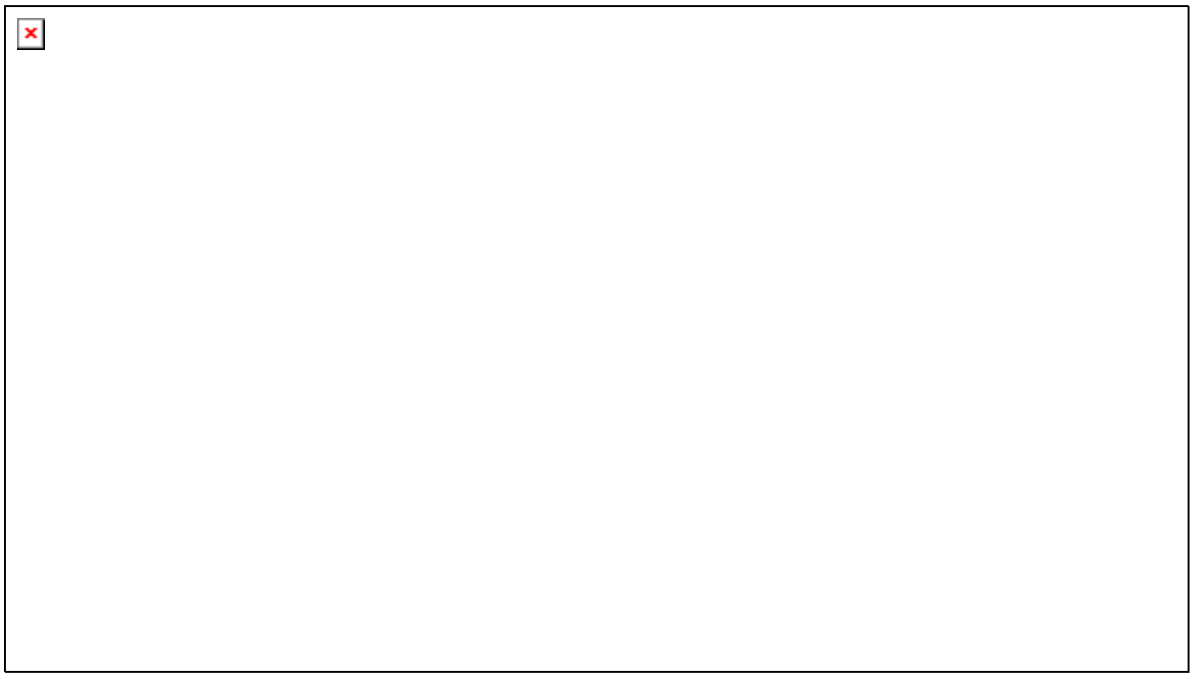

figure A 12: Photographs of failed specimen pr01c21

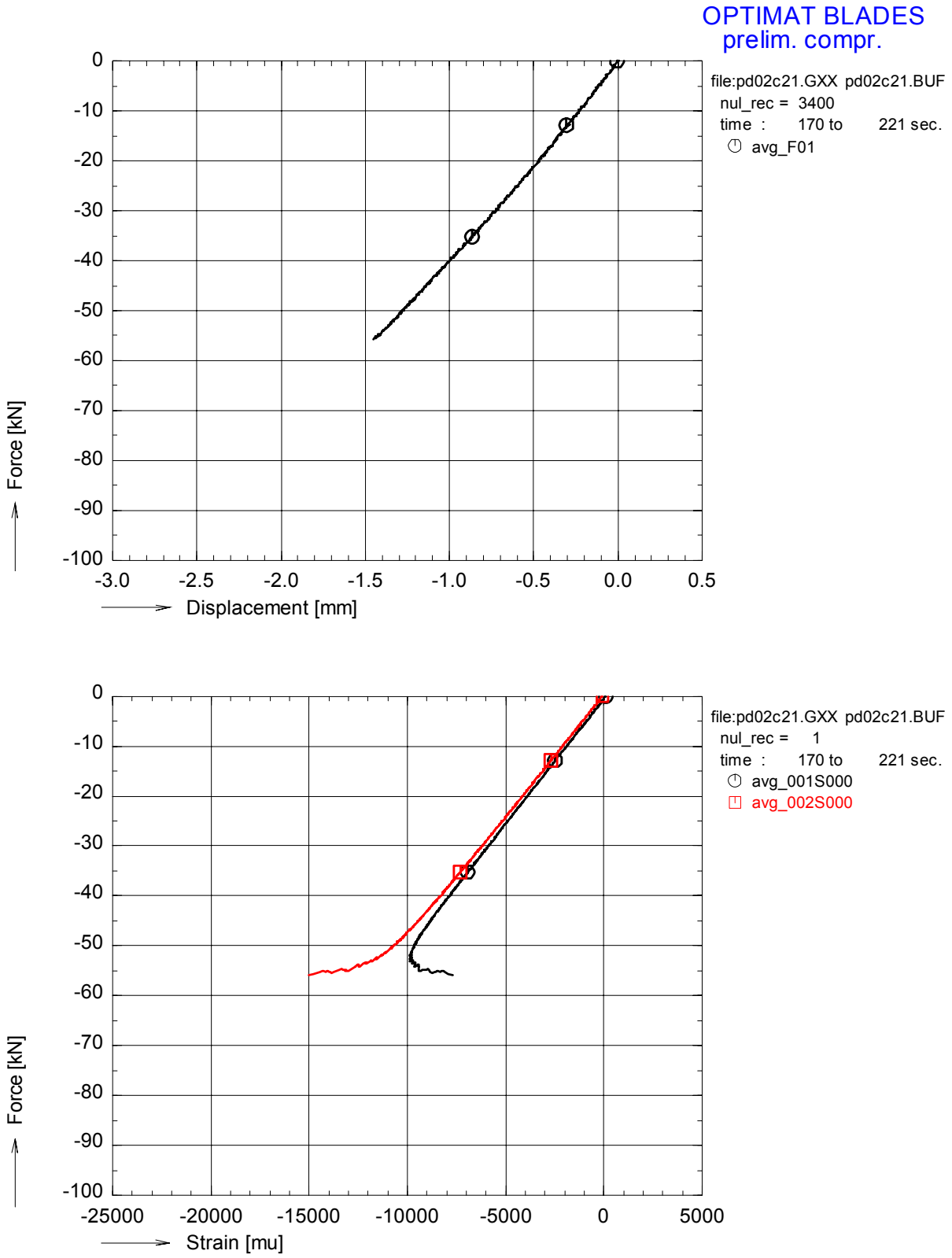

figure A 13: Axial compressive force vs. bench displacement and strains for pd02c21

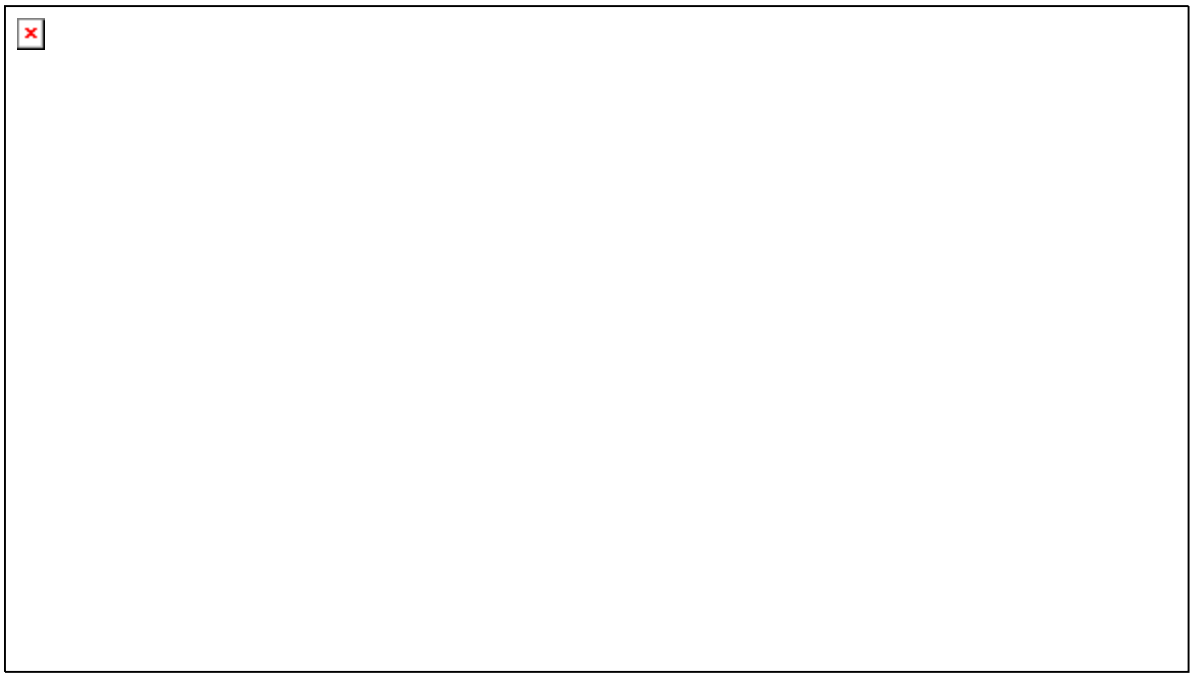

figure A 14: Photographs of failed specimen pd02c21

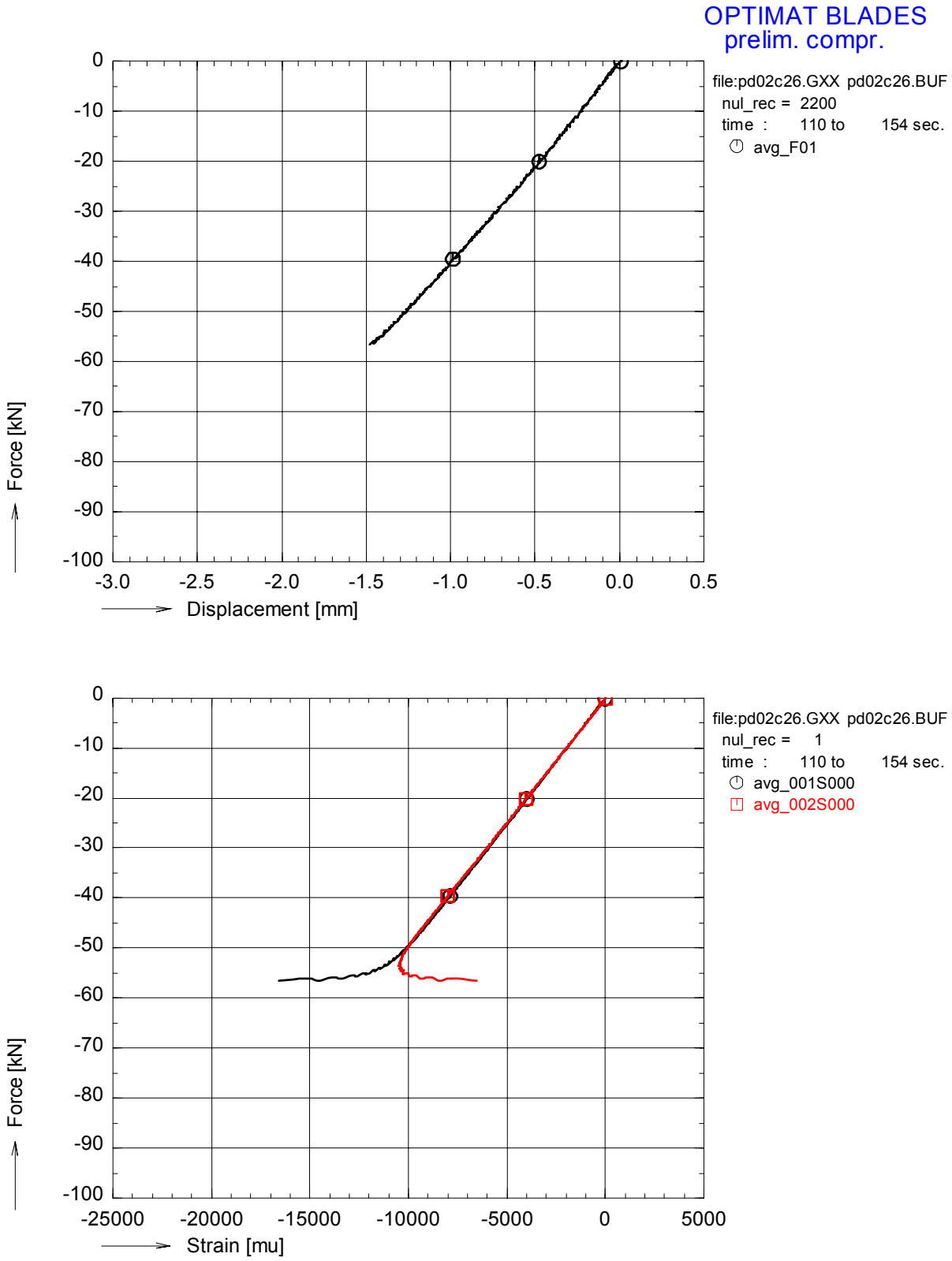

figure A 15: Axial compressive force vs. bench displacement and strains for pd02c26

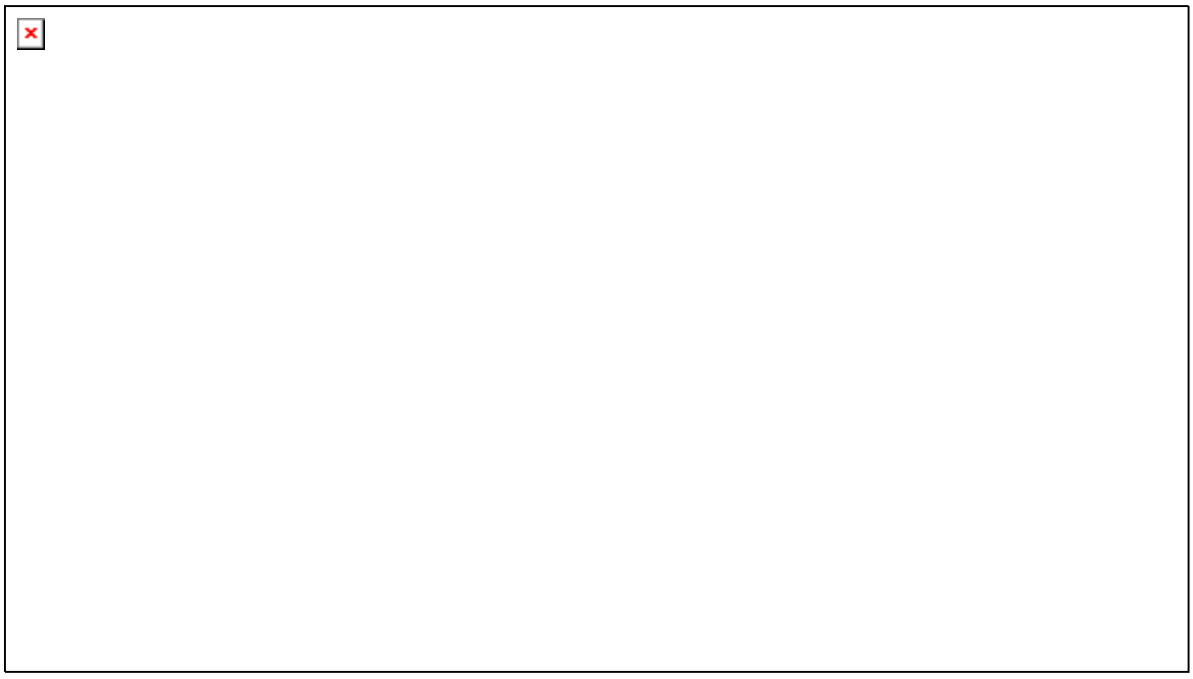

figure A 16: Photographs of failed specimen pd02c26

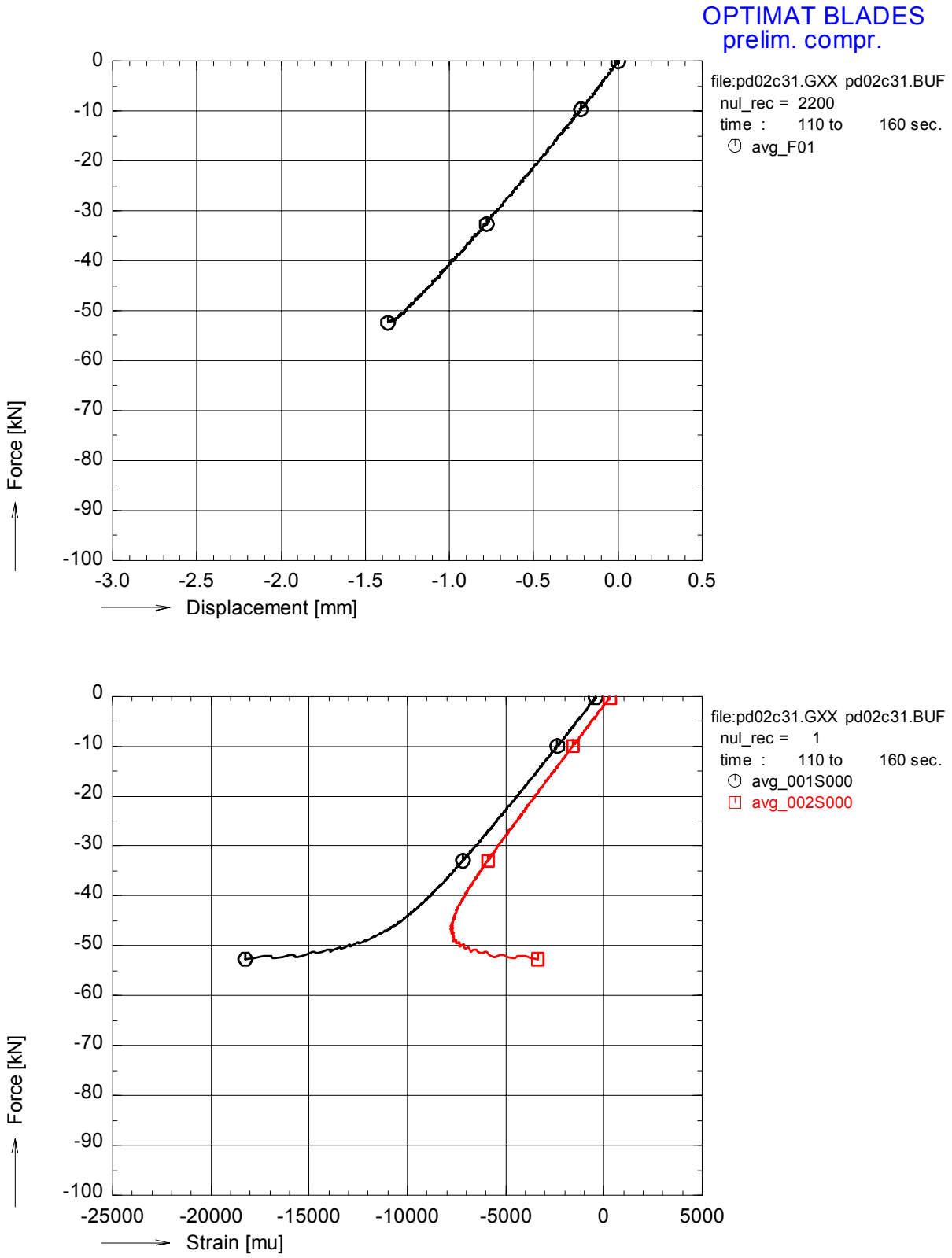

figure A 17: Axial compressive force vs. bench displacement and strains for pd02c31

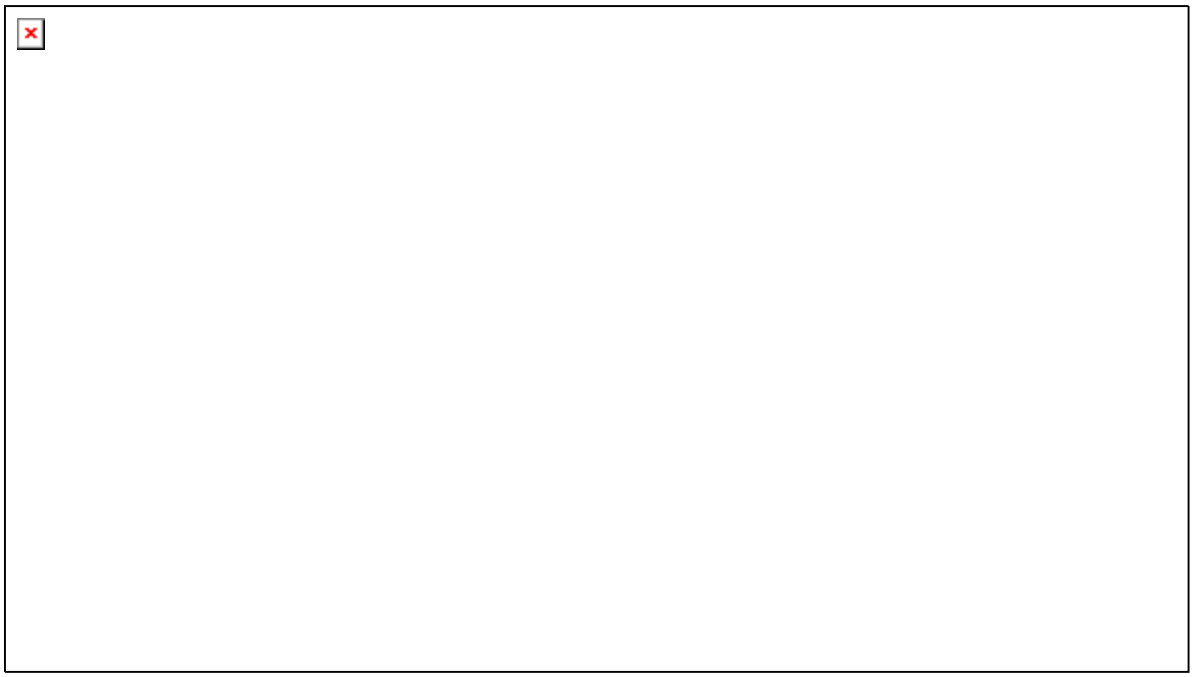

figure A 18: Photographs of failed specimen pd02c31

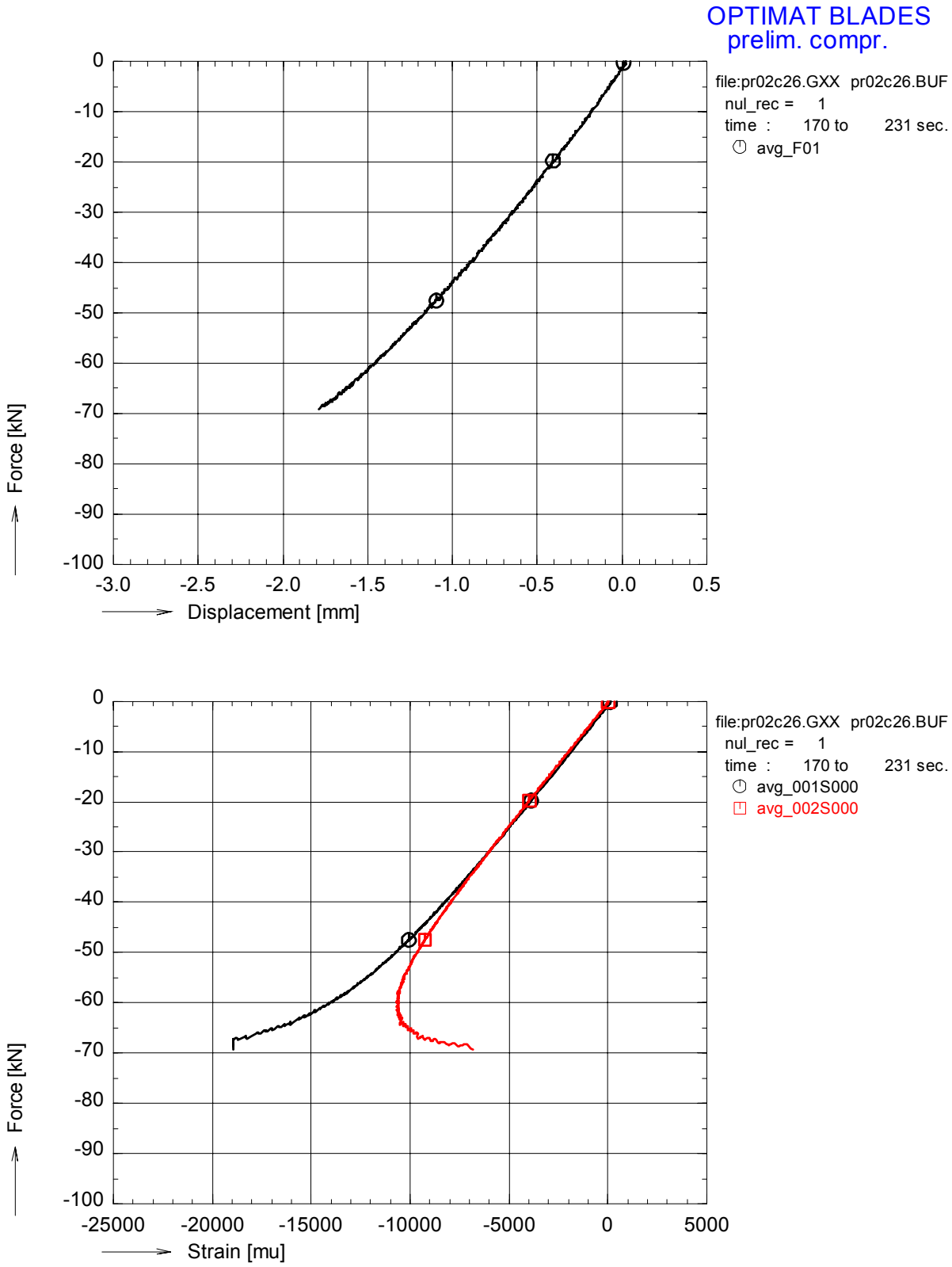

figure A 19: Axial compressive force vs. bench displacement and strains for pr02c26

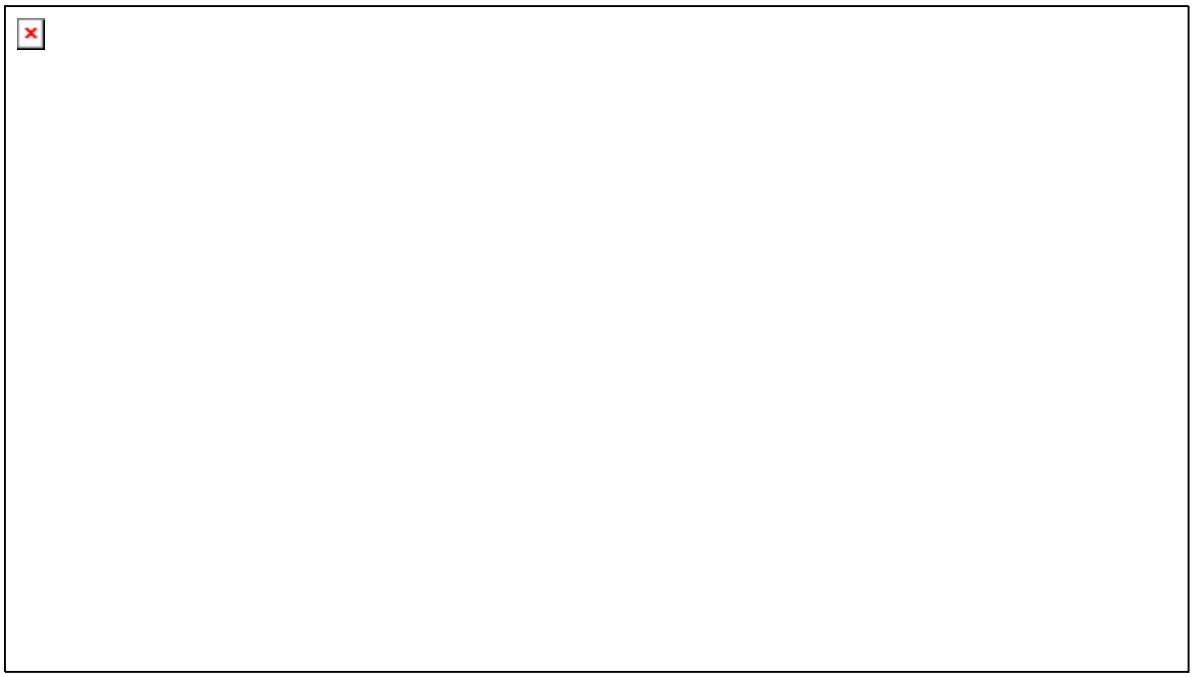

figure A 20: Photographs of failed specimen pr02c26

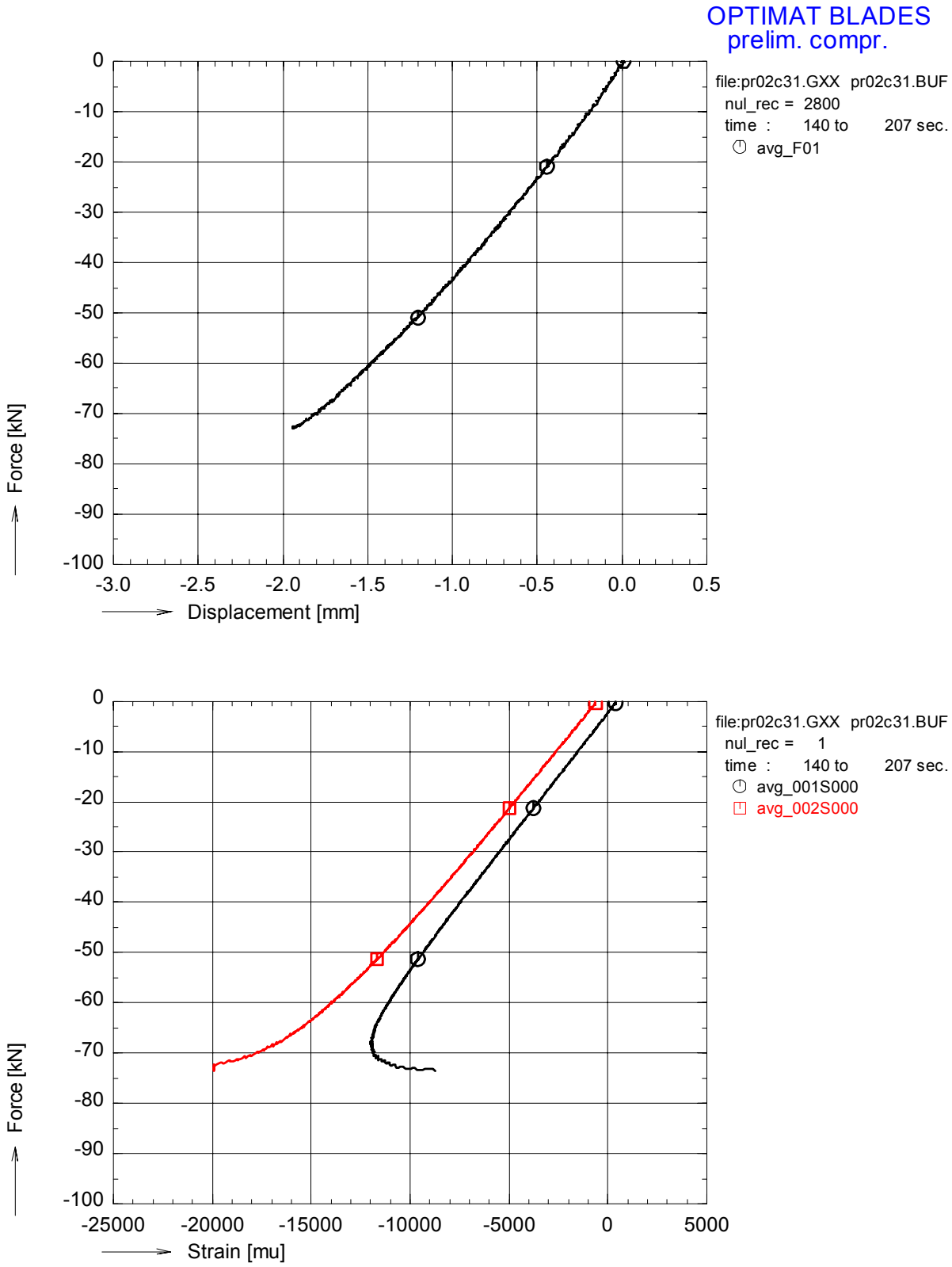

figure A 21: Axial compressive force vs. bench displacement and strains for pr02c31

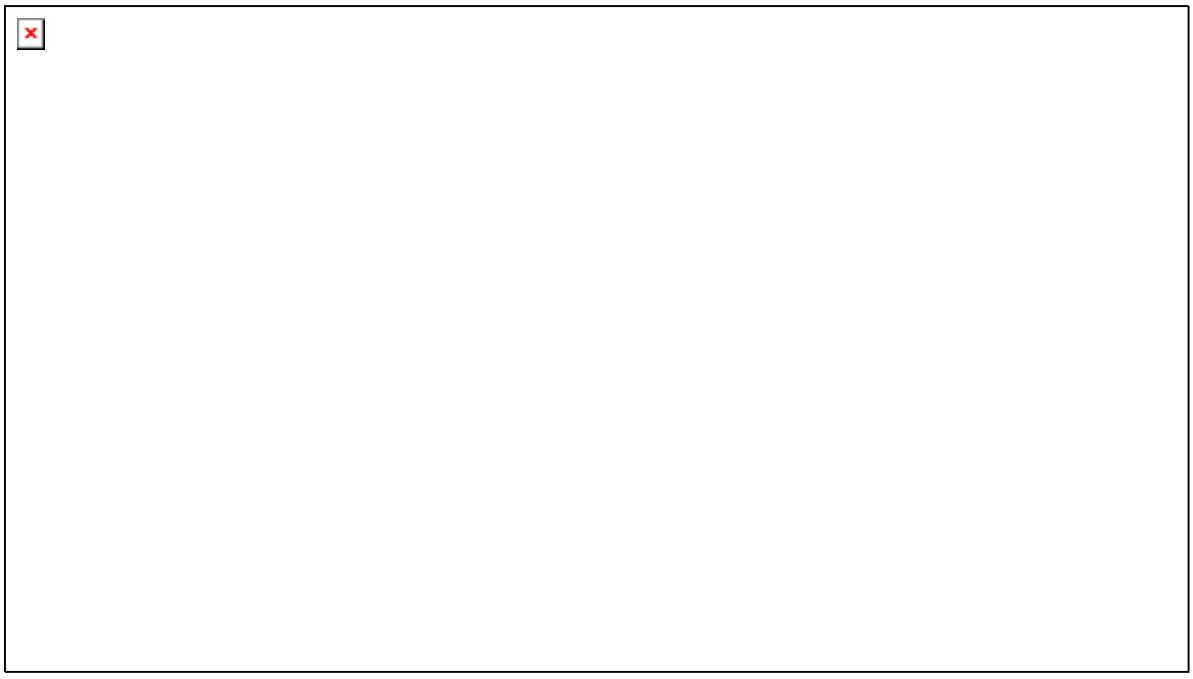

figure A 22: Photographs of failed specimen pr02c31

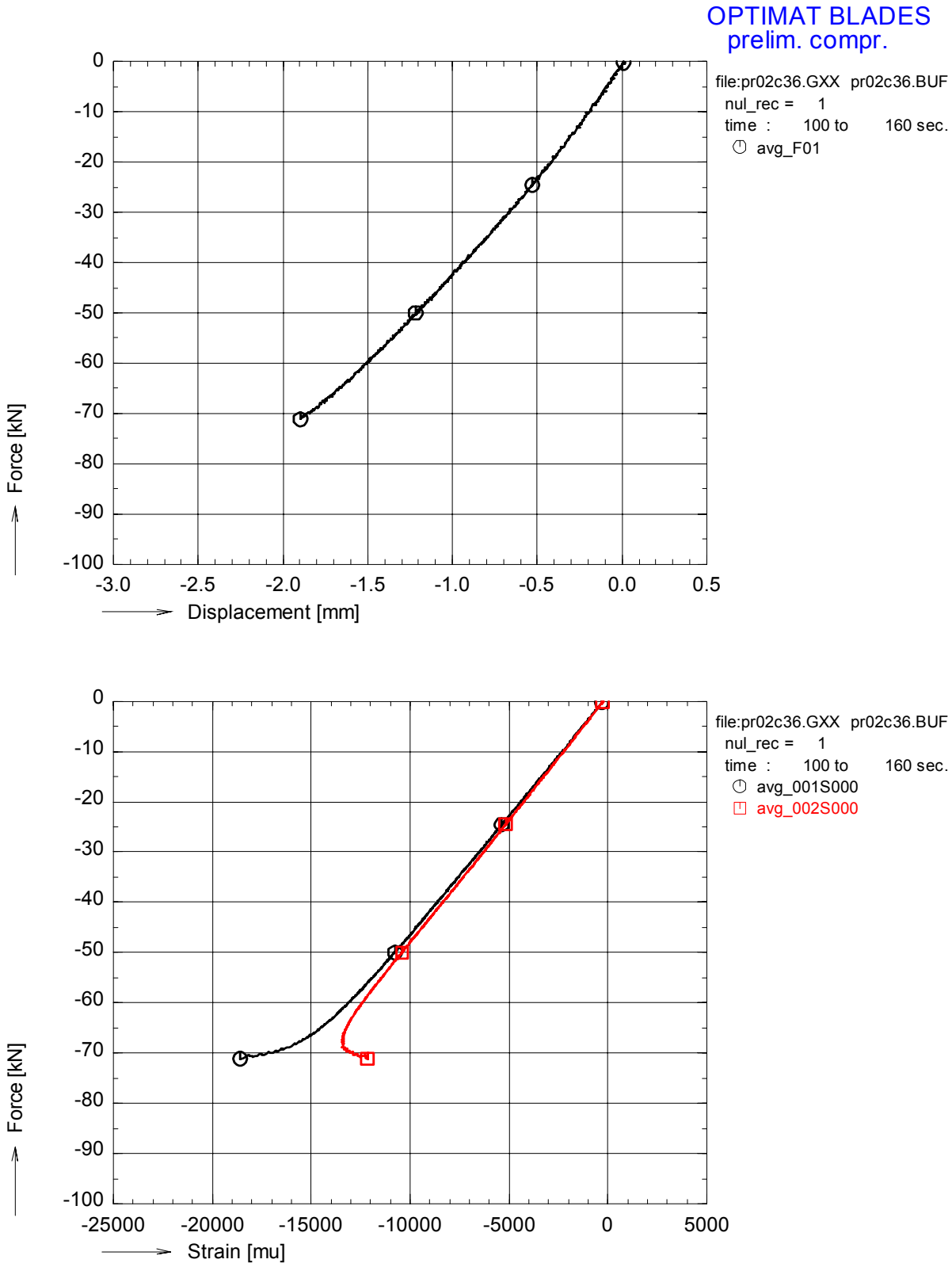

figure A 23: Axial compressive force vs. bench displacement and strains for pr02c36

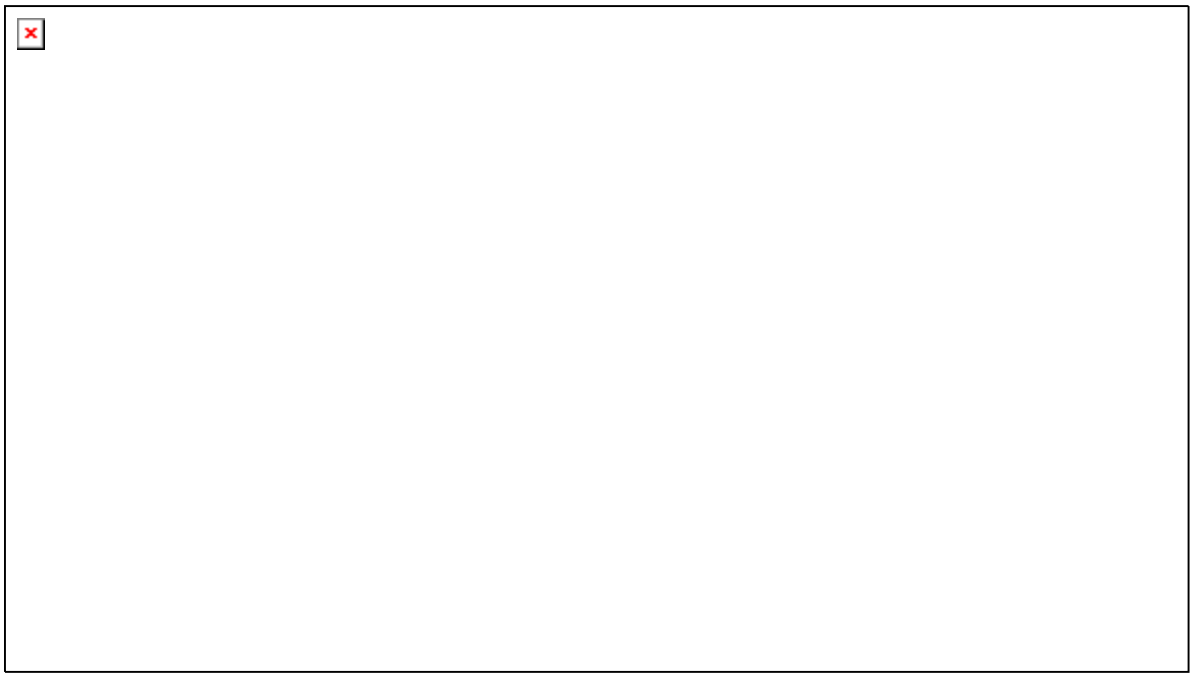

figure A 24: Photographs of failed specimen pr02c36

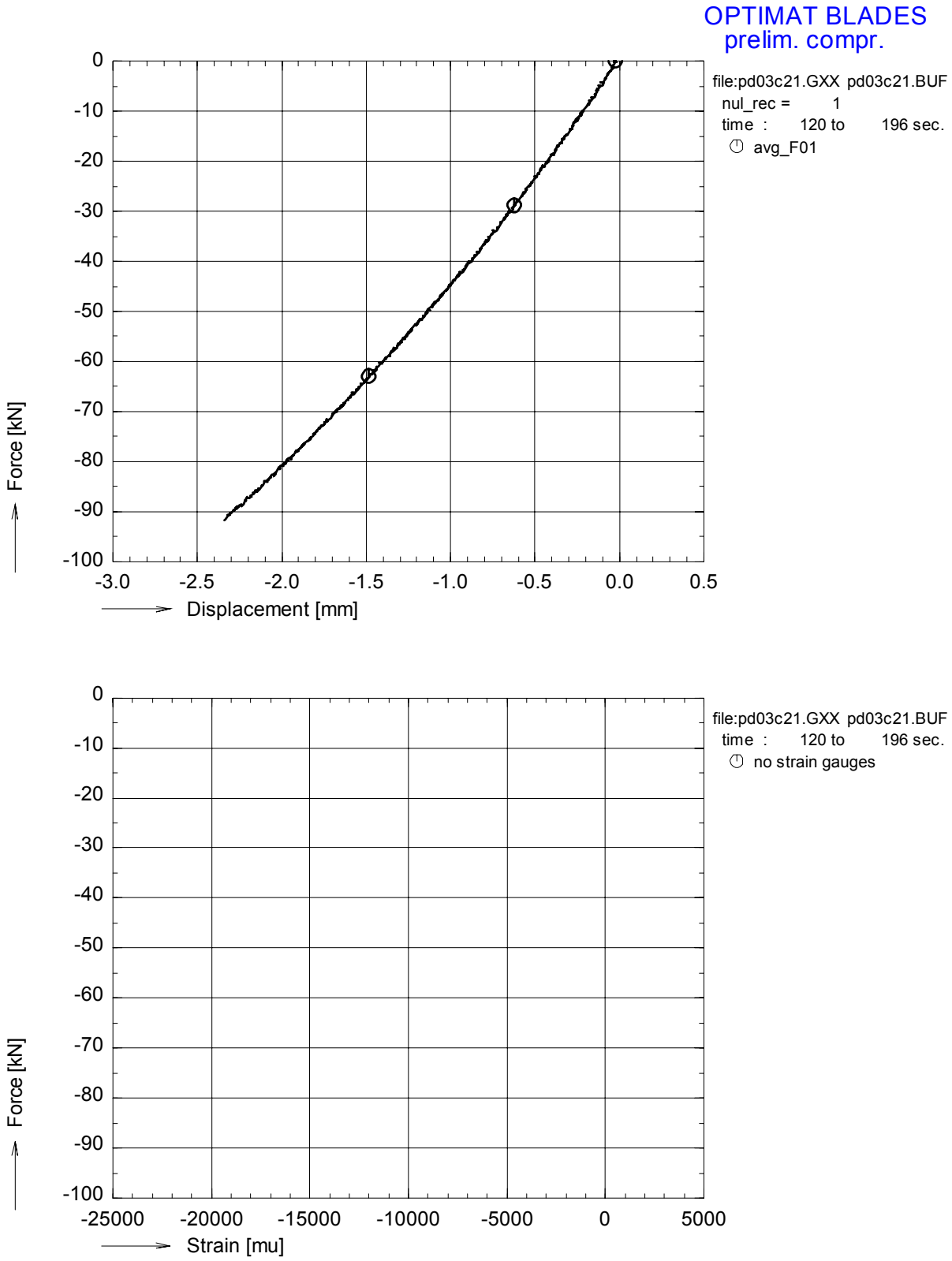

figure A 25: Axial compressive force vs. bench displacement and strains for pd03c21

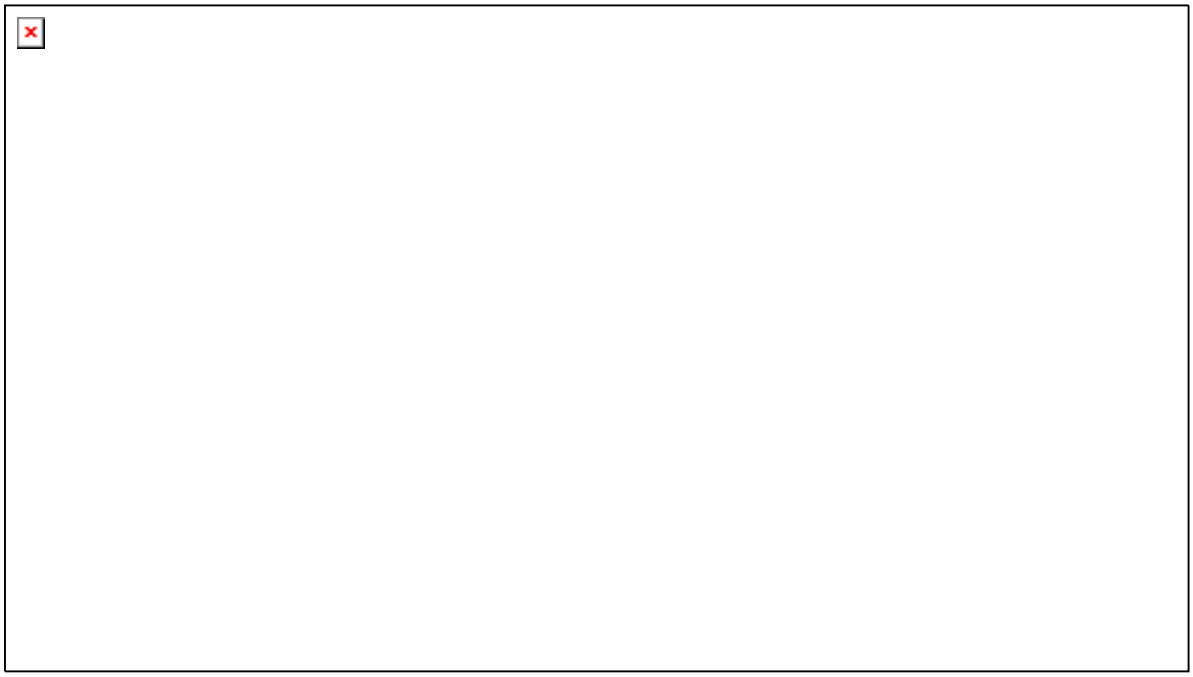

figure A 26: Photographs of failed specimen pd03c21

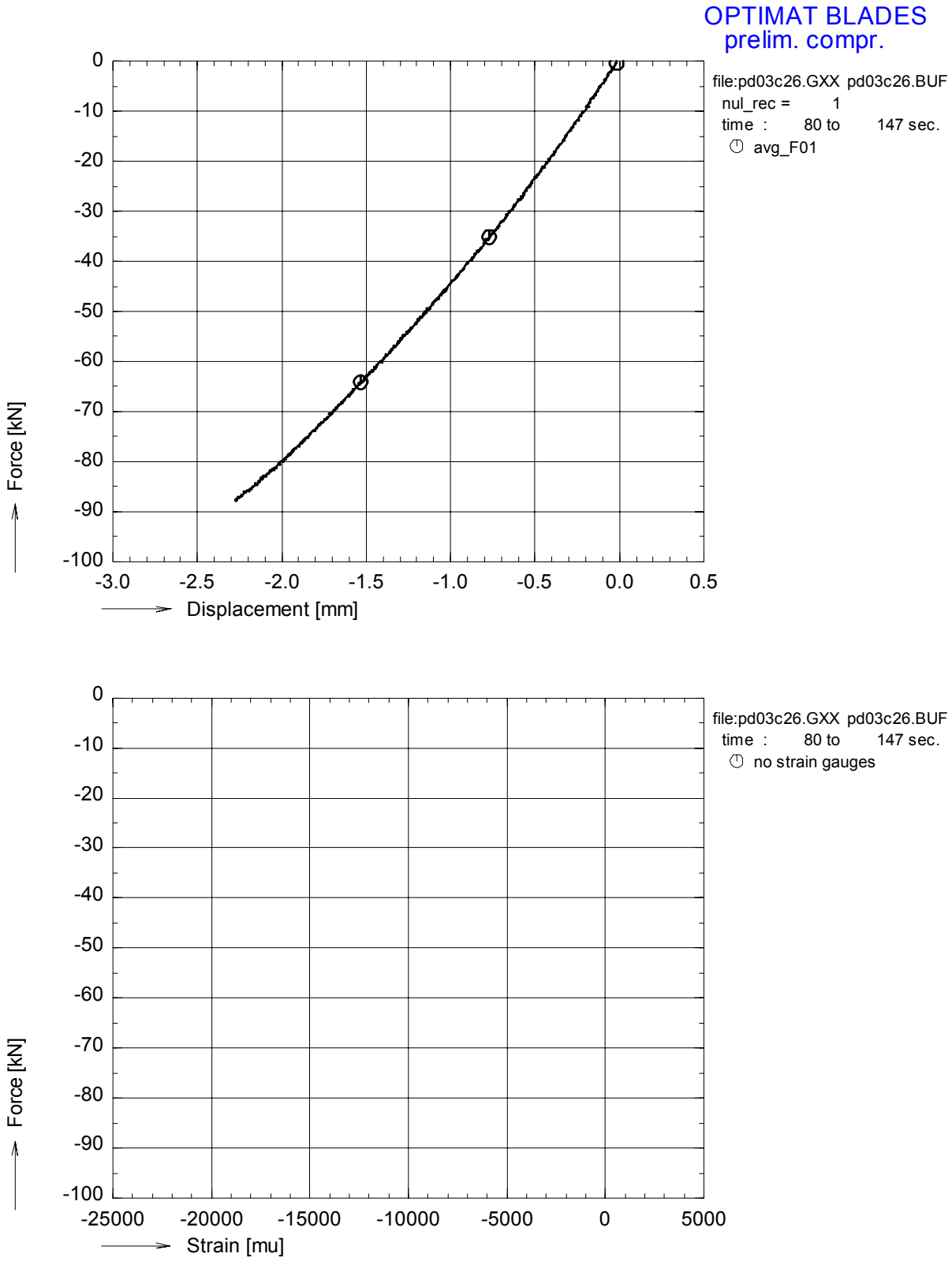

figure A 27: Axial compressive force vs. bench displacement and strains for pd03c26

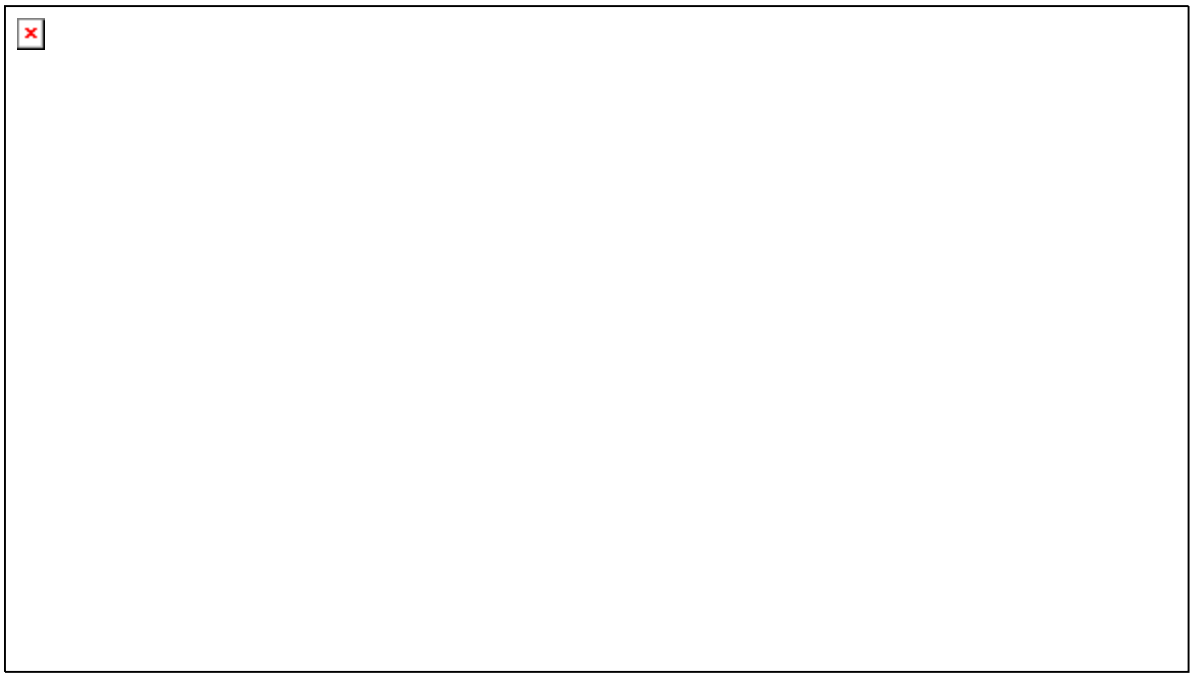

figure A 28: Photographs of failed specimen pd03c26

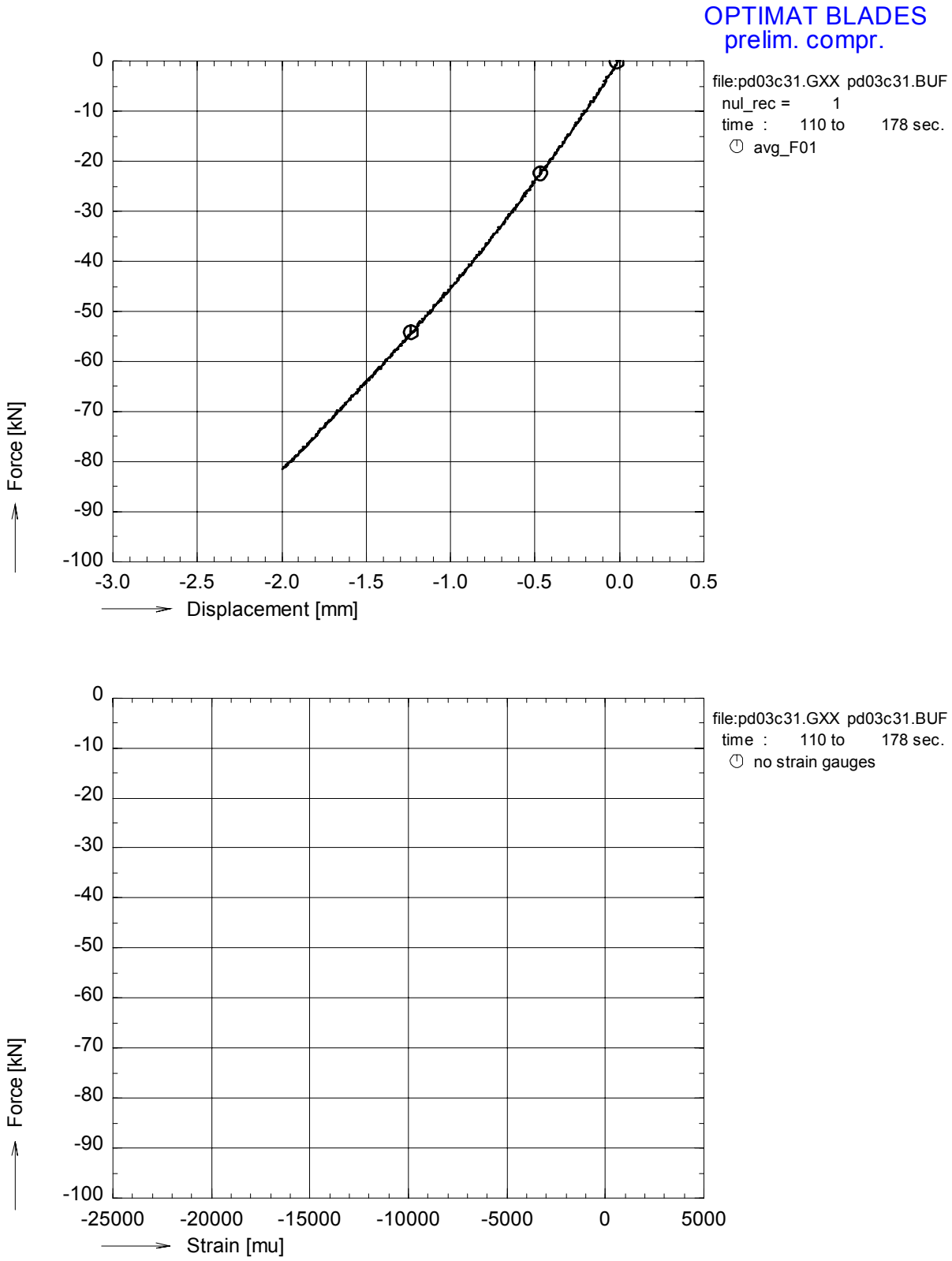

figure A 29: Axial compressive force vs. bench displacement and strains for pd03c31

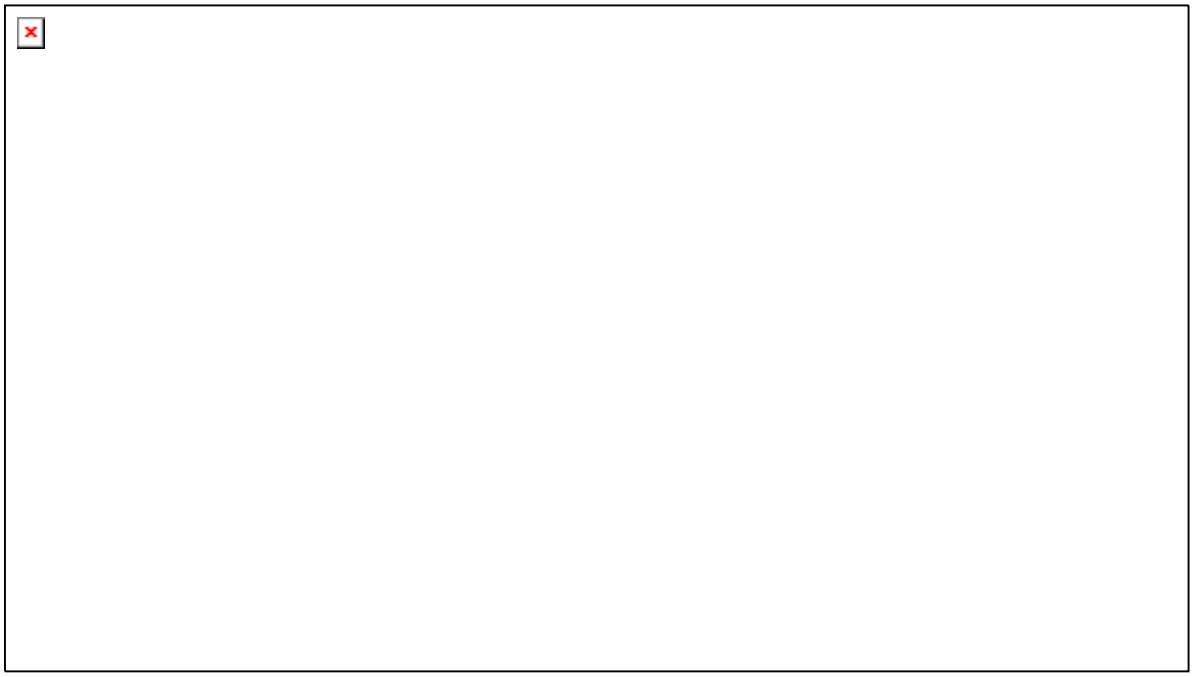

figure A 30: Photographs of failed specimen pd03c31

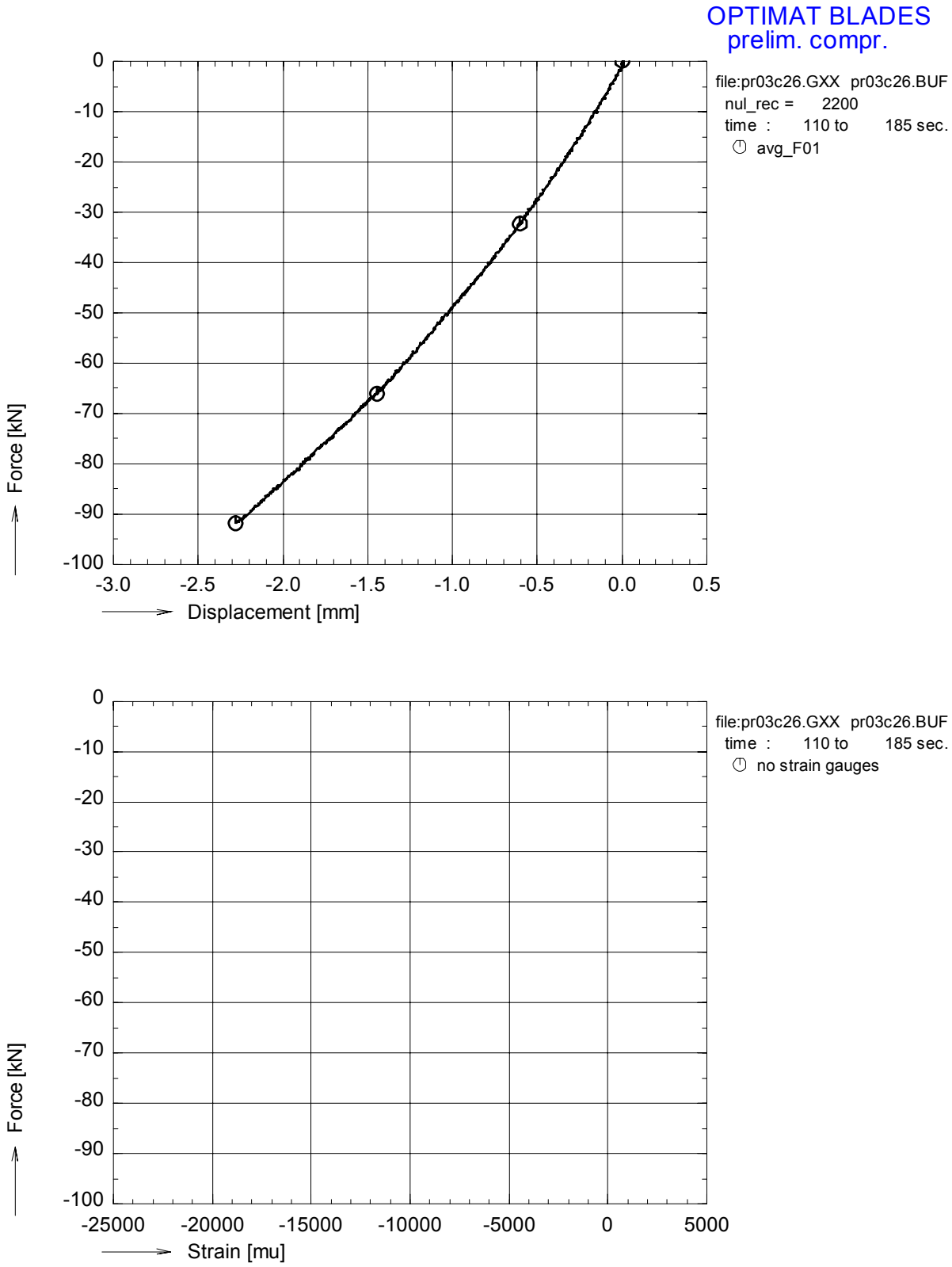

figure A 31: Axial compressive force vs. bench displacement and strains for pr03c26

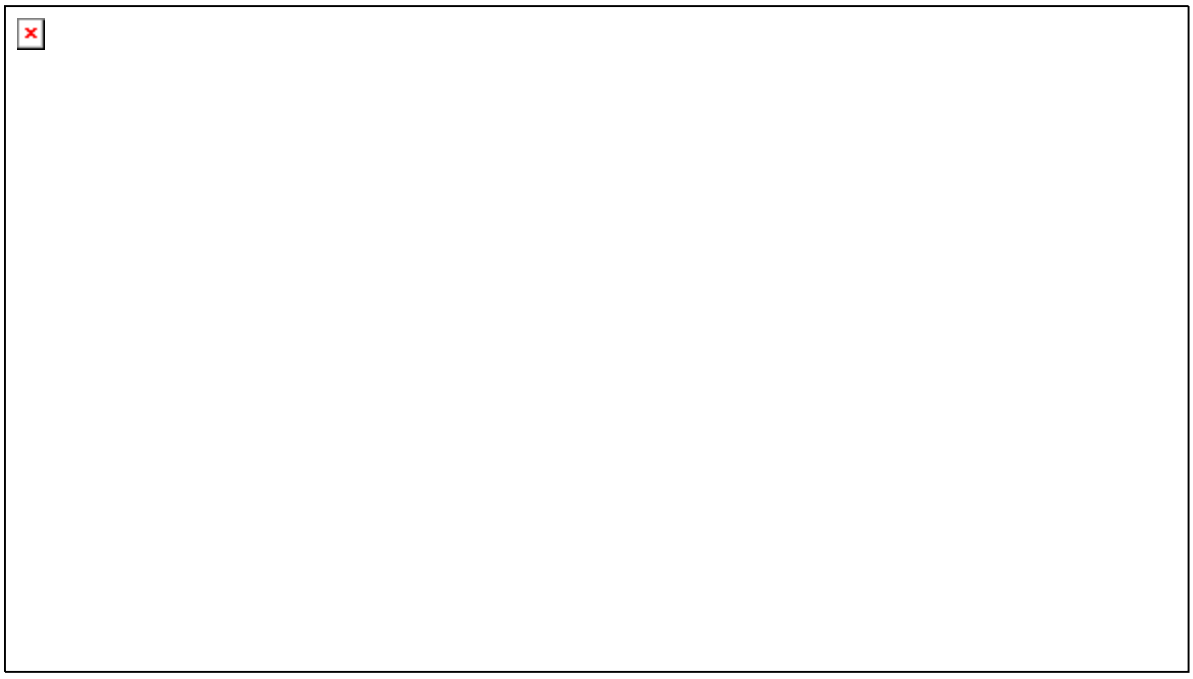

figure A 32: Photographs of failed specimen pr03c26

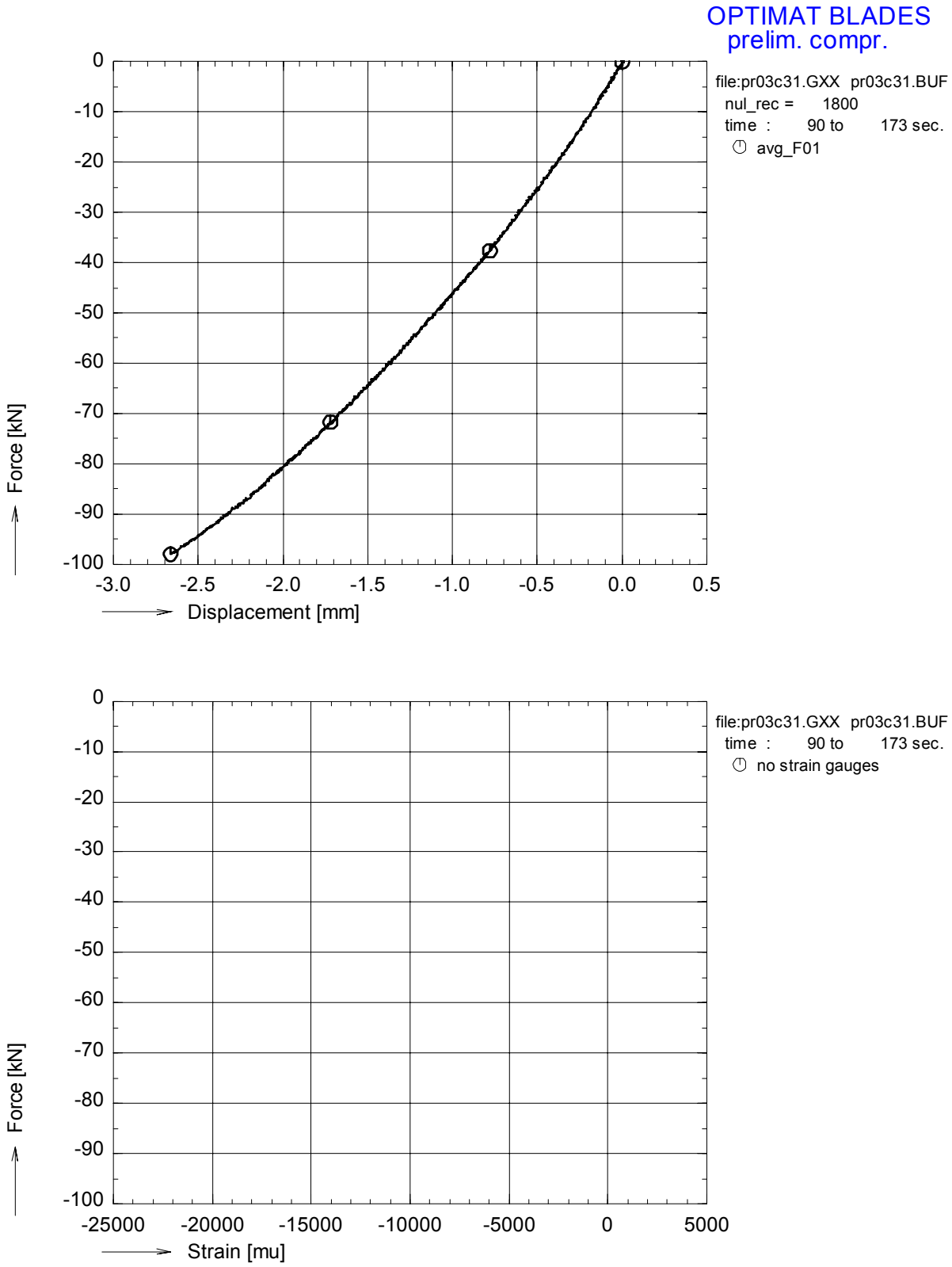

figure A 33: Axial compressive force vs. bench displacement and strains for pr03c31

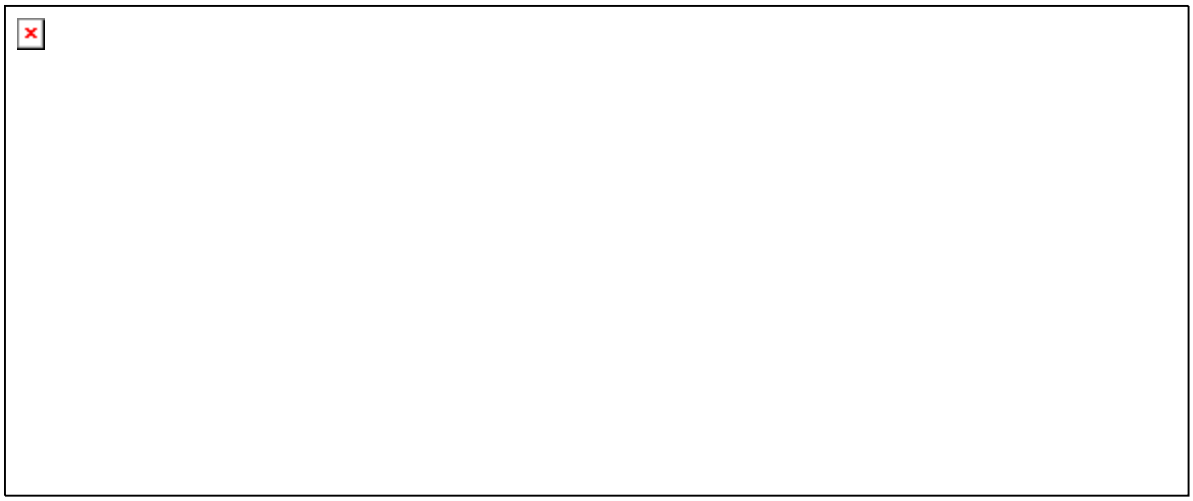

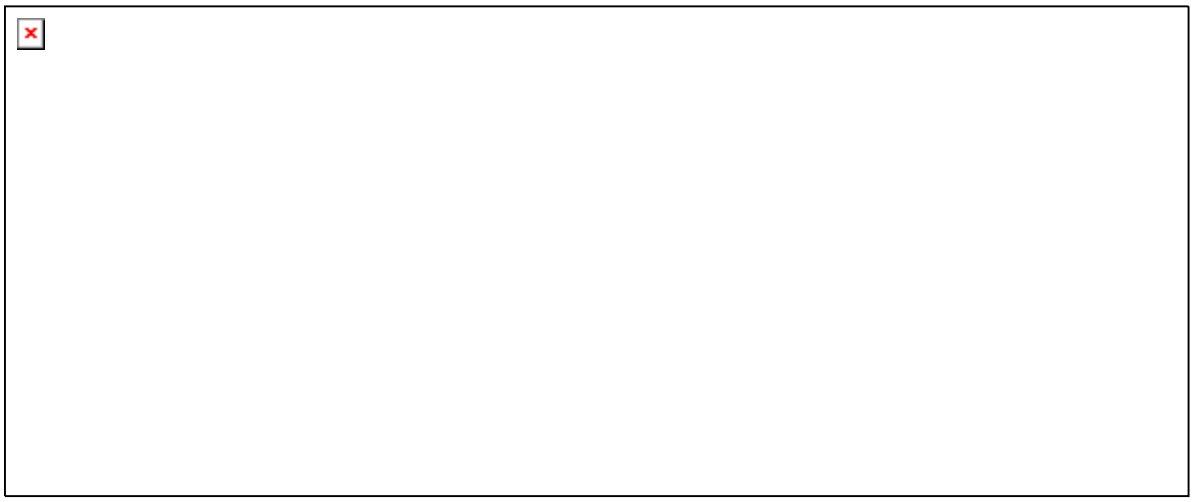

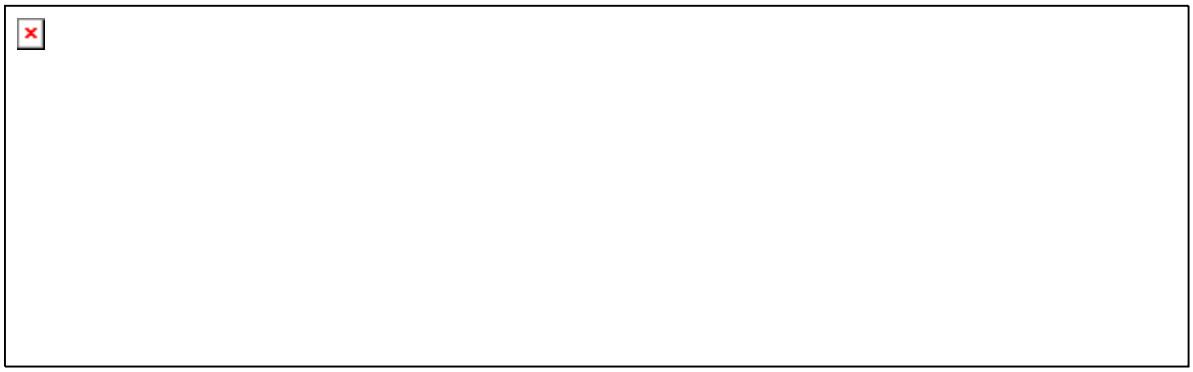

figure A 34: Photographs of failed specimen pr03c31 (resp. back, front and side)

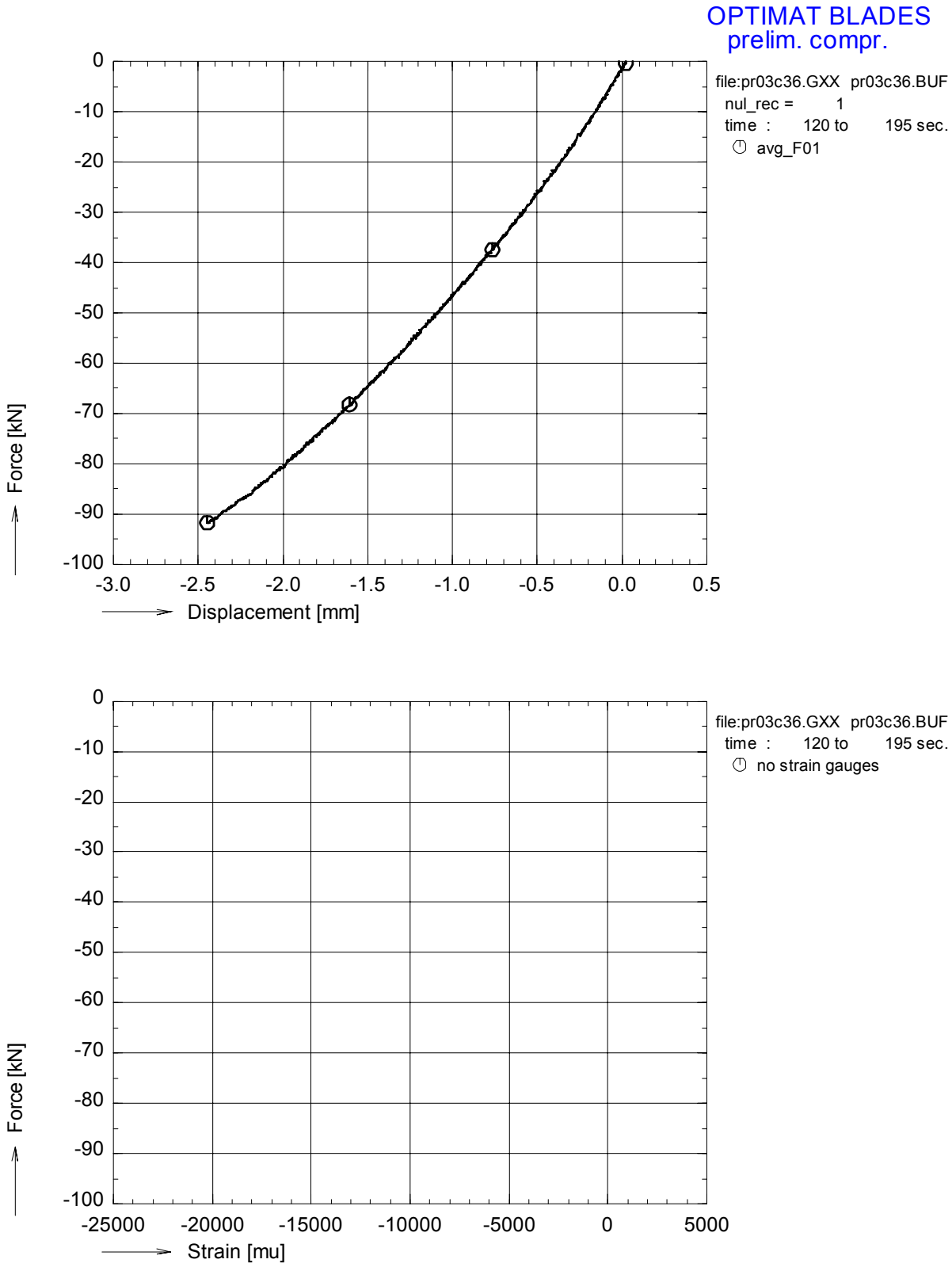

figure A 35: Axial compressive force vs. bench displacement and strains for pr03c36

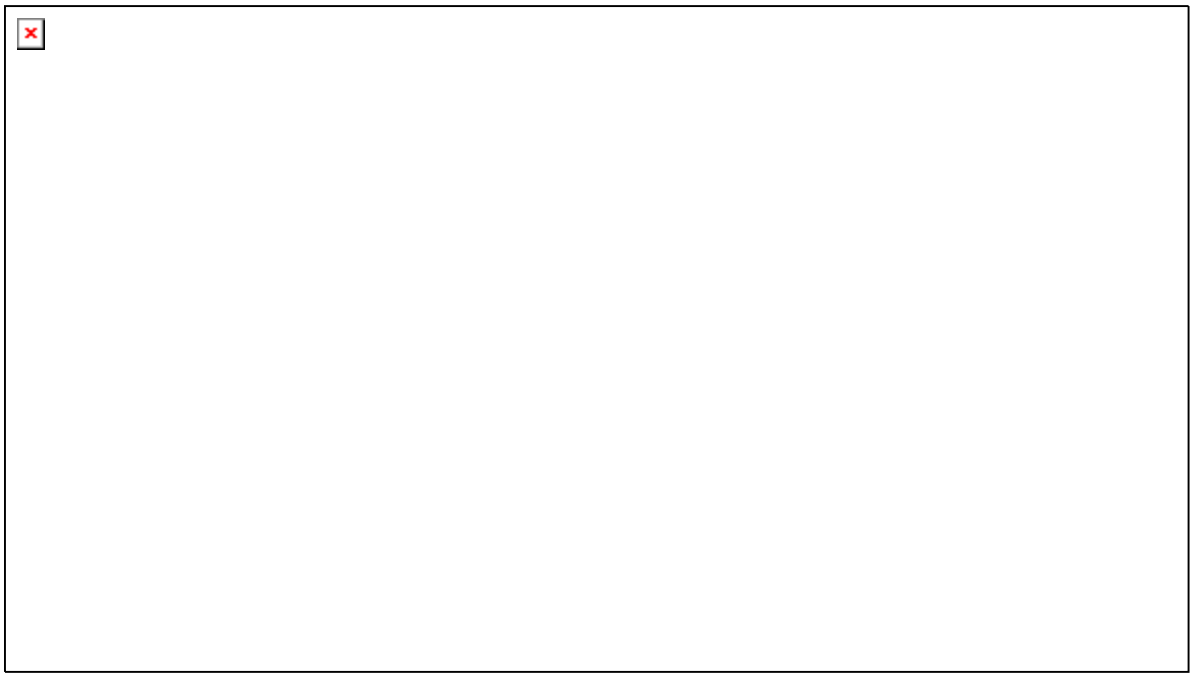

figure A 36: Photographs of failed specimen pr03c36

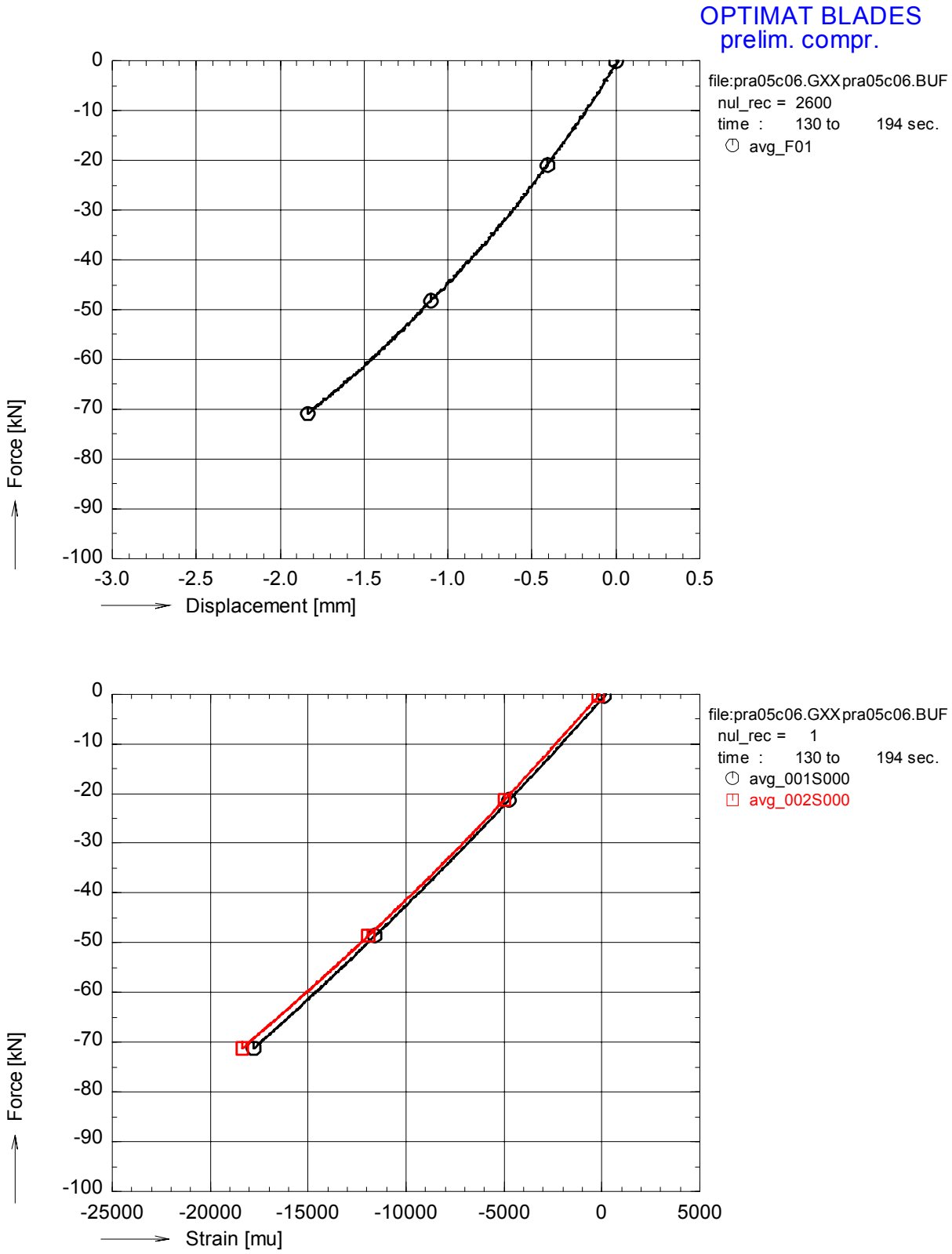

figure A 37: Axial compressive force vs. bench displacement and strains for pra05c06

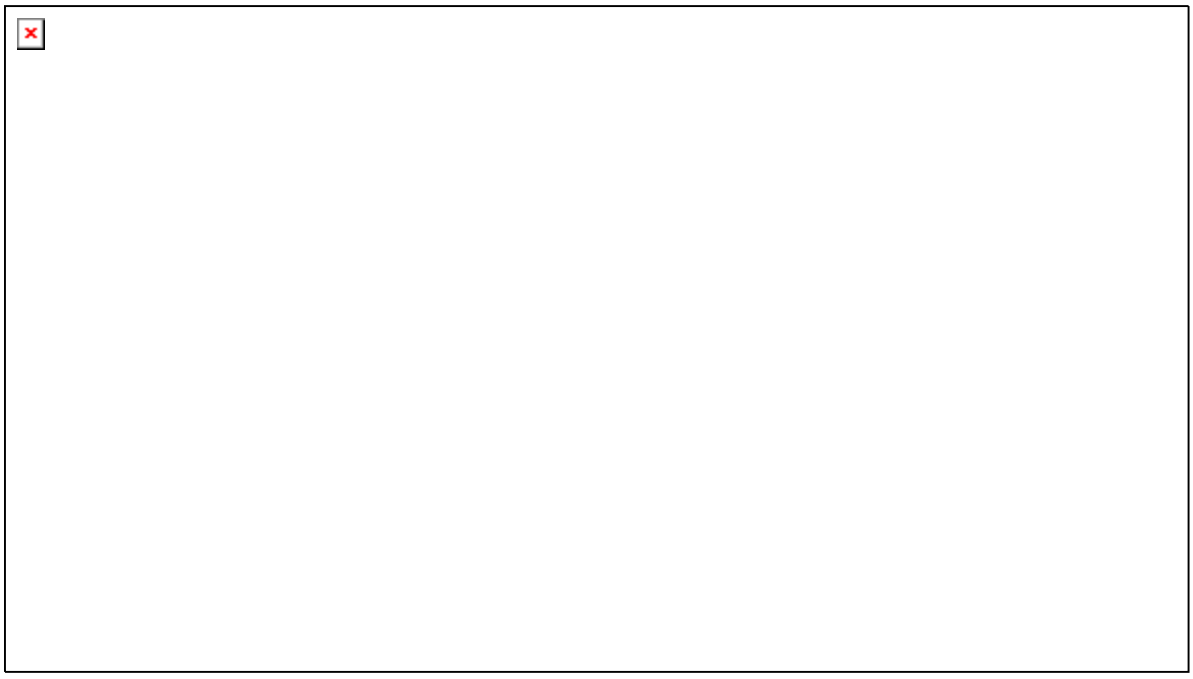

figure A 38: Photographs of failed specimen pra05c06

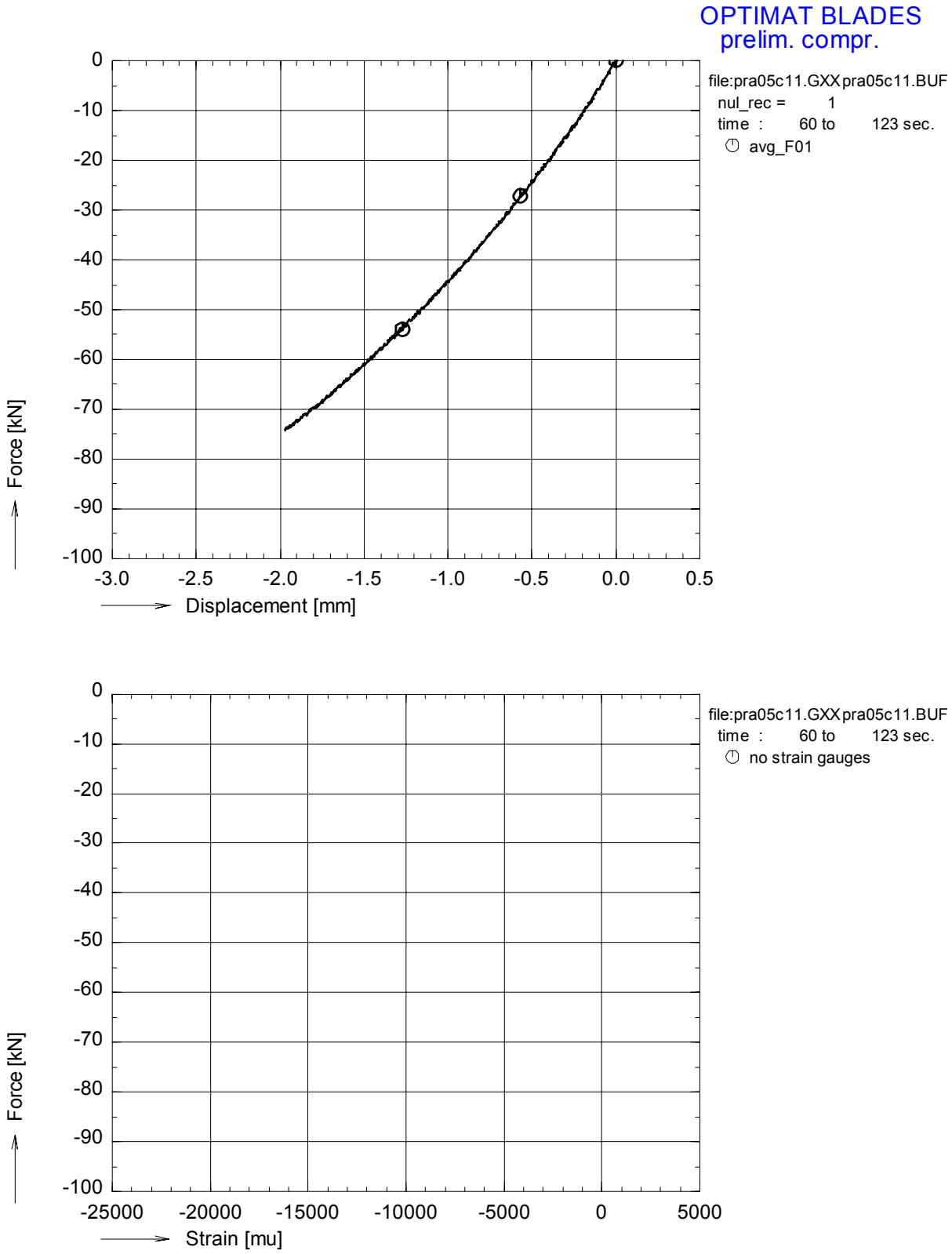

figure A 39: Axial compressive force vs. bench displacement and strains for pra05c11

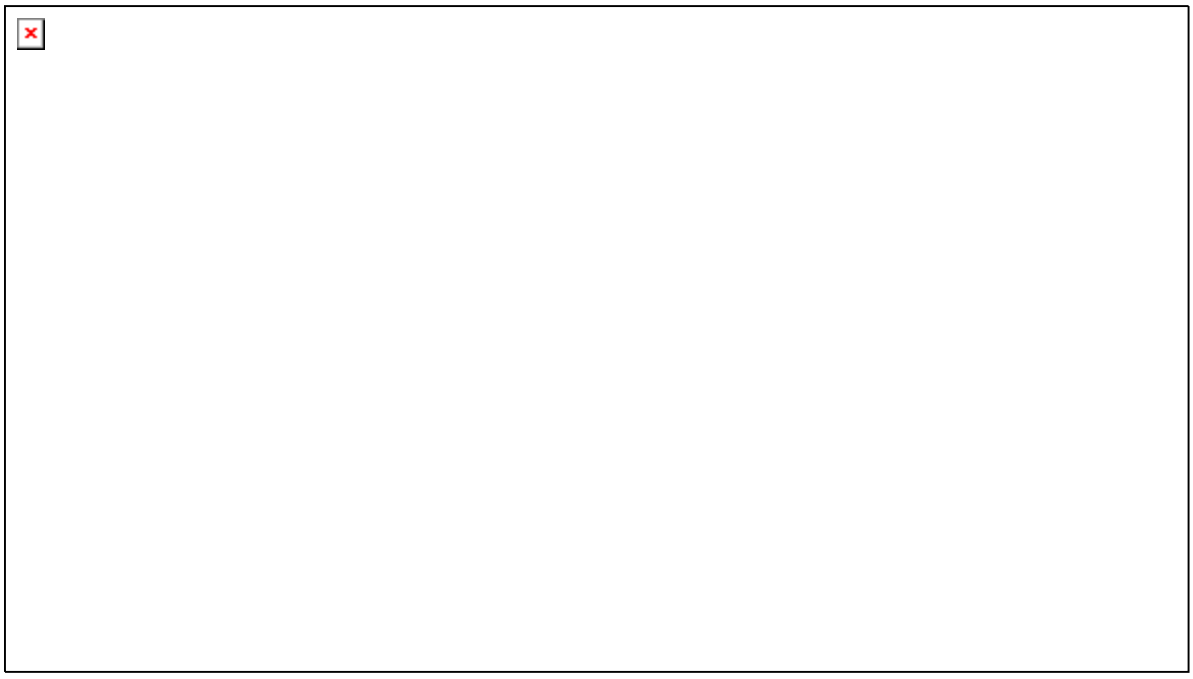

figure A 40: Photographs of failed specimen pra05c11

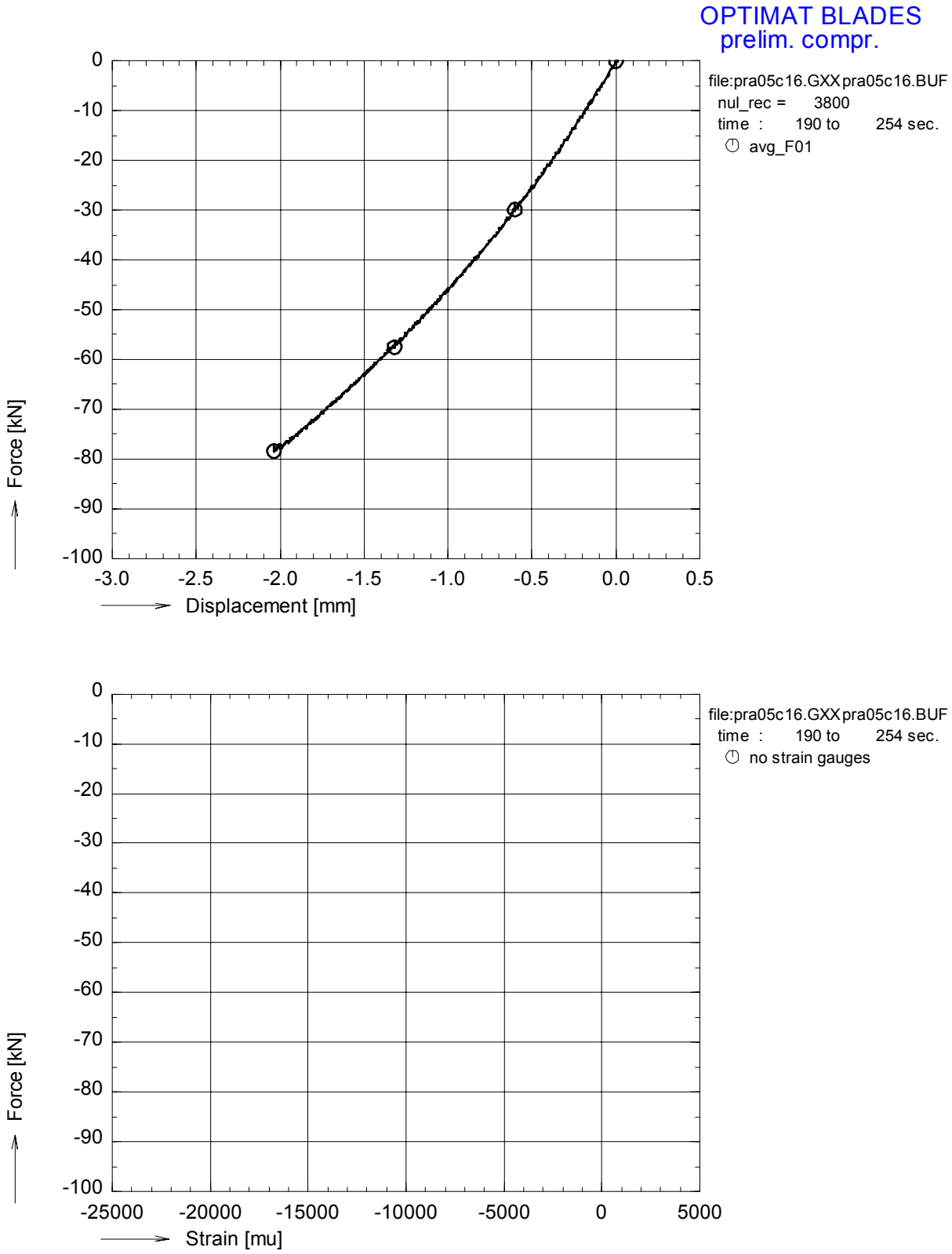

figure A 41: Axial compressive force vs. bench displacement and strains for pra05c16

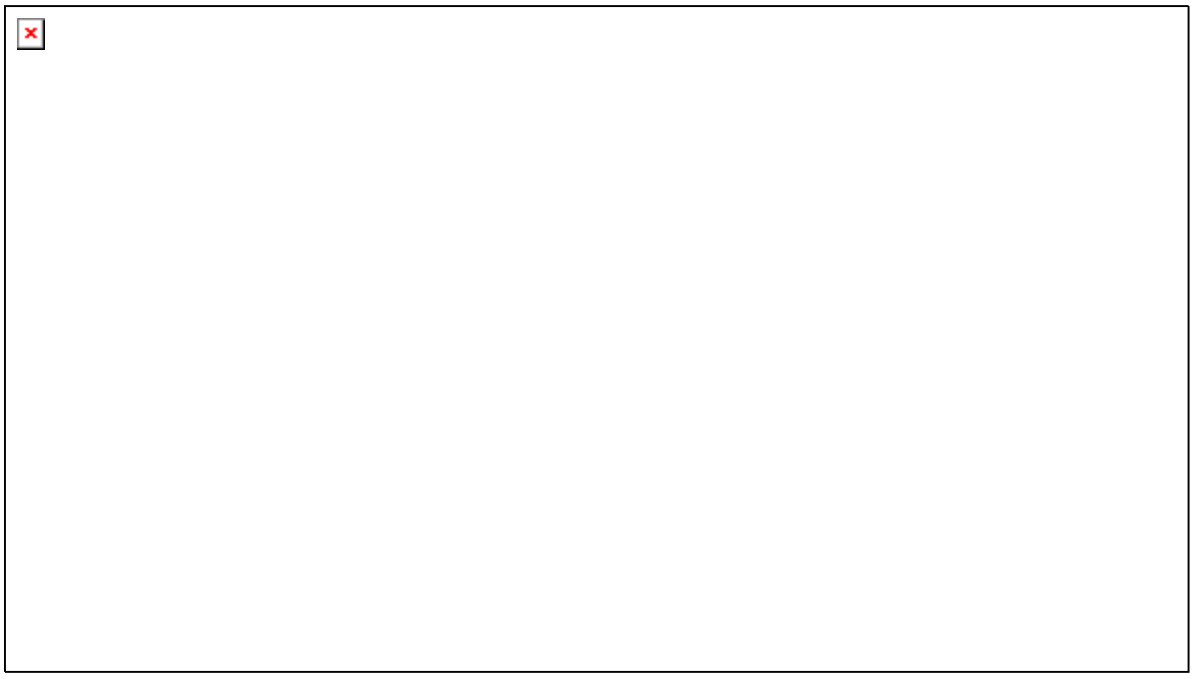

figure A 42: Photographs of failed specimen pra05c16

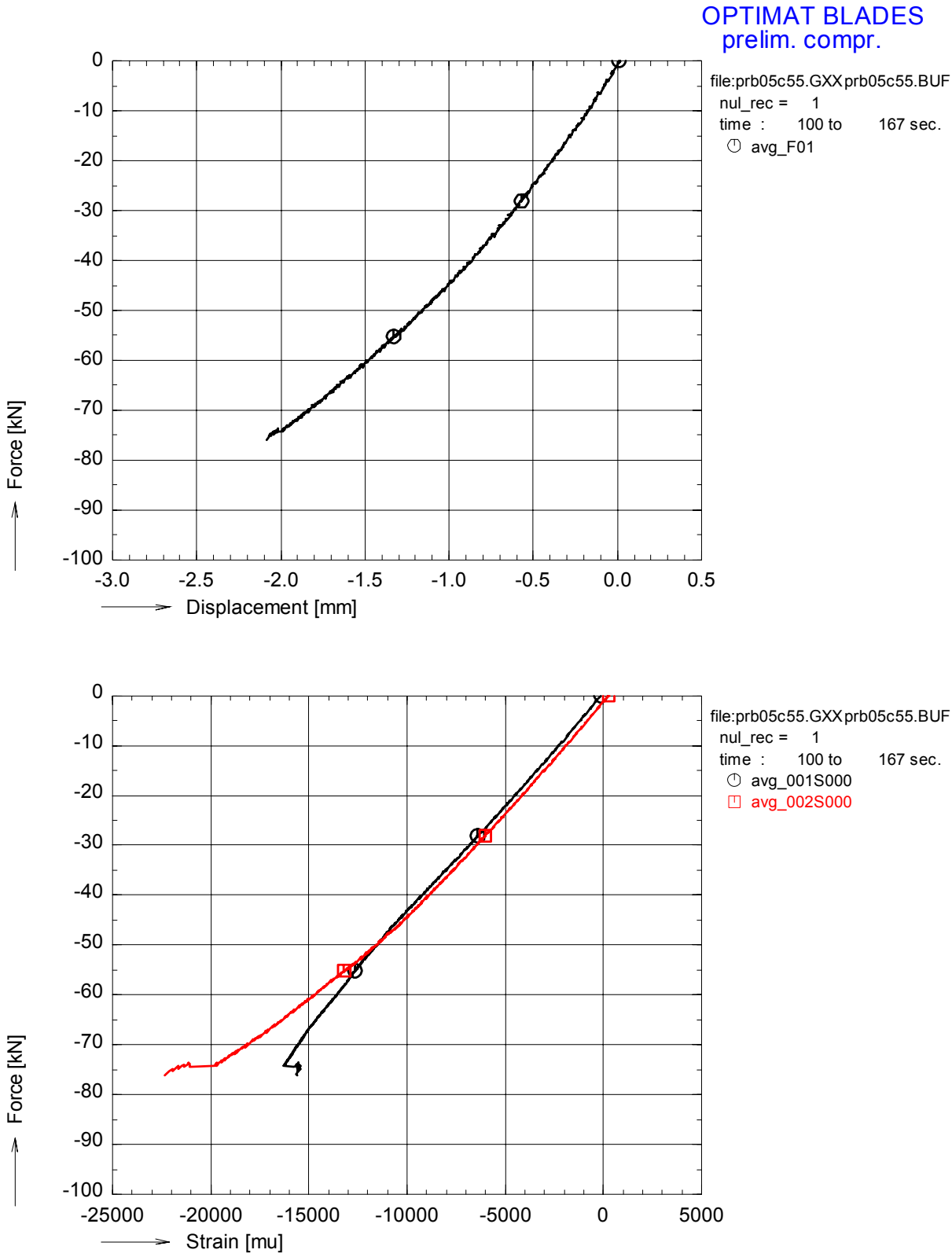

figure A 43: Axial compressive force vs. bench displacement and strains for prb05c55

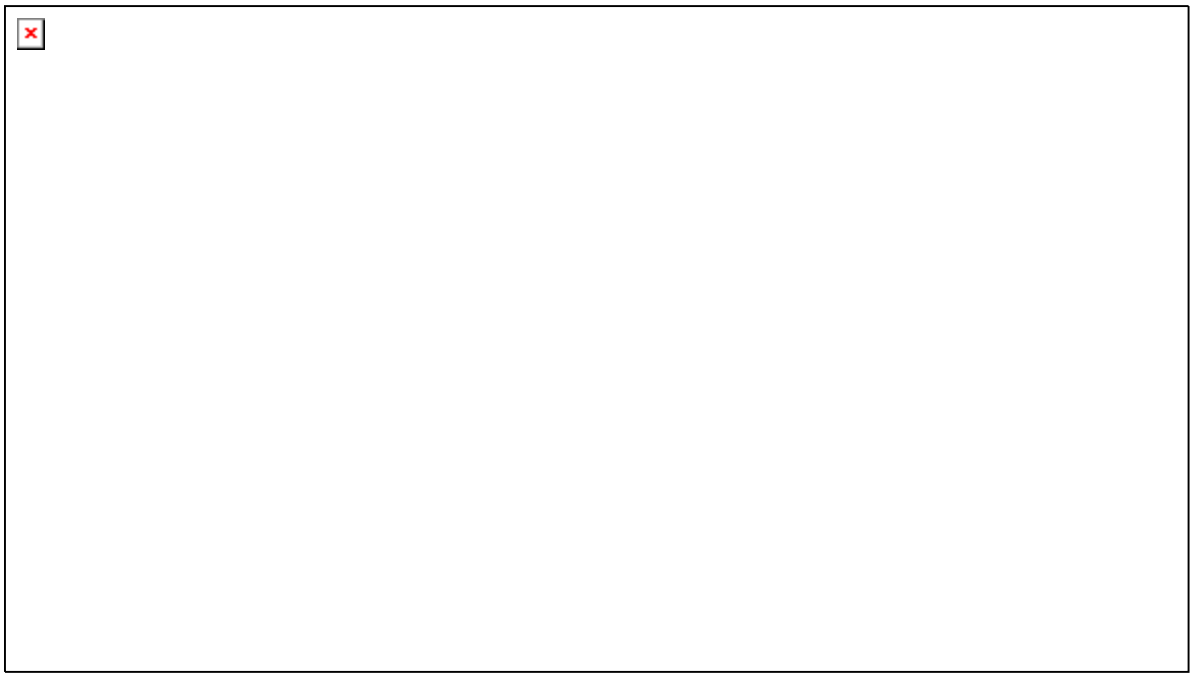

figure A 44: Photographs of failed specimen prb05c55

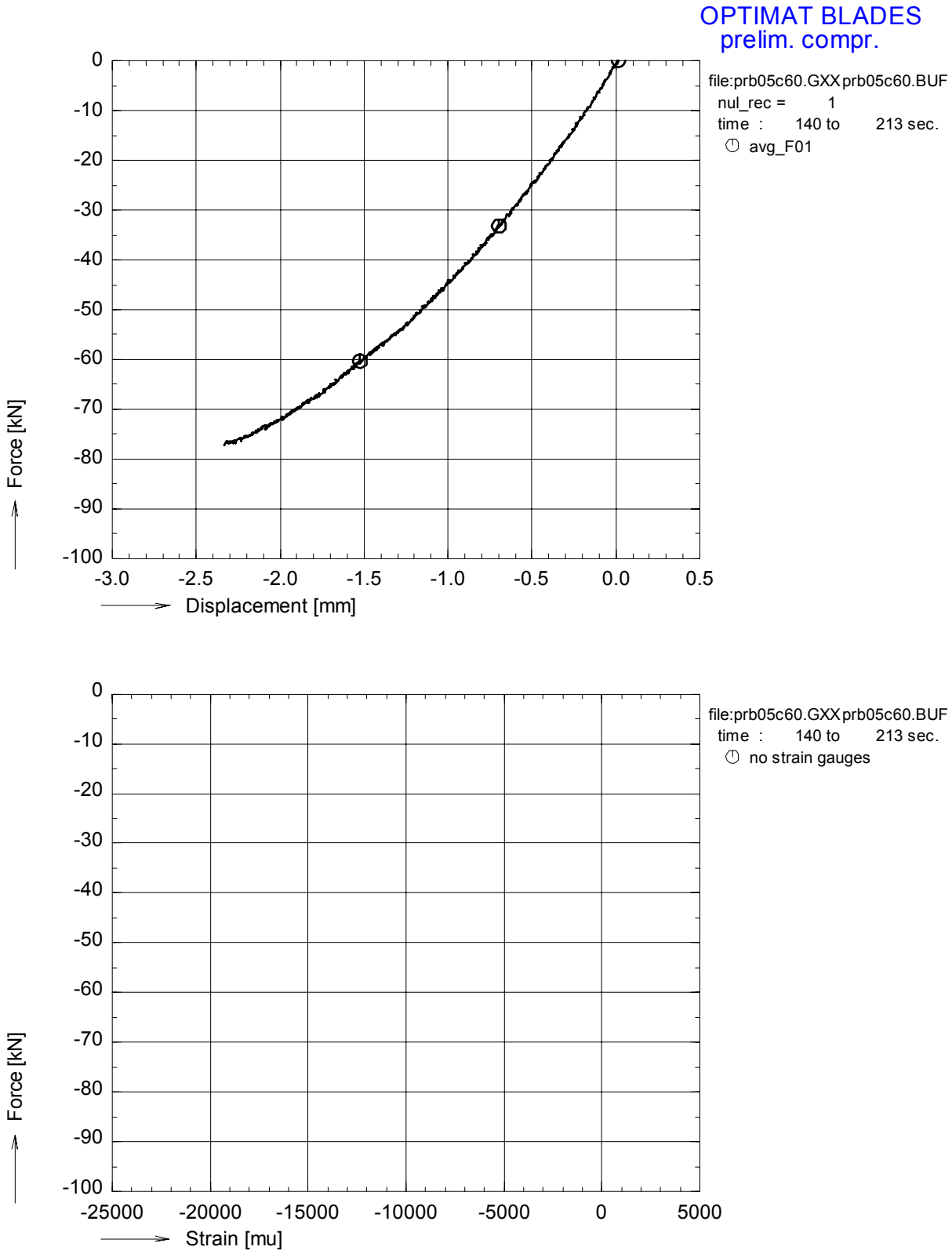

figure A 45: Axial compressive force vs. bench displacement and strains for prb05c60

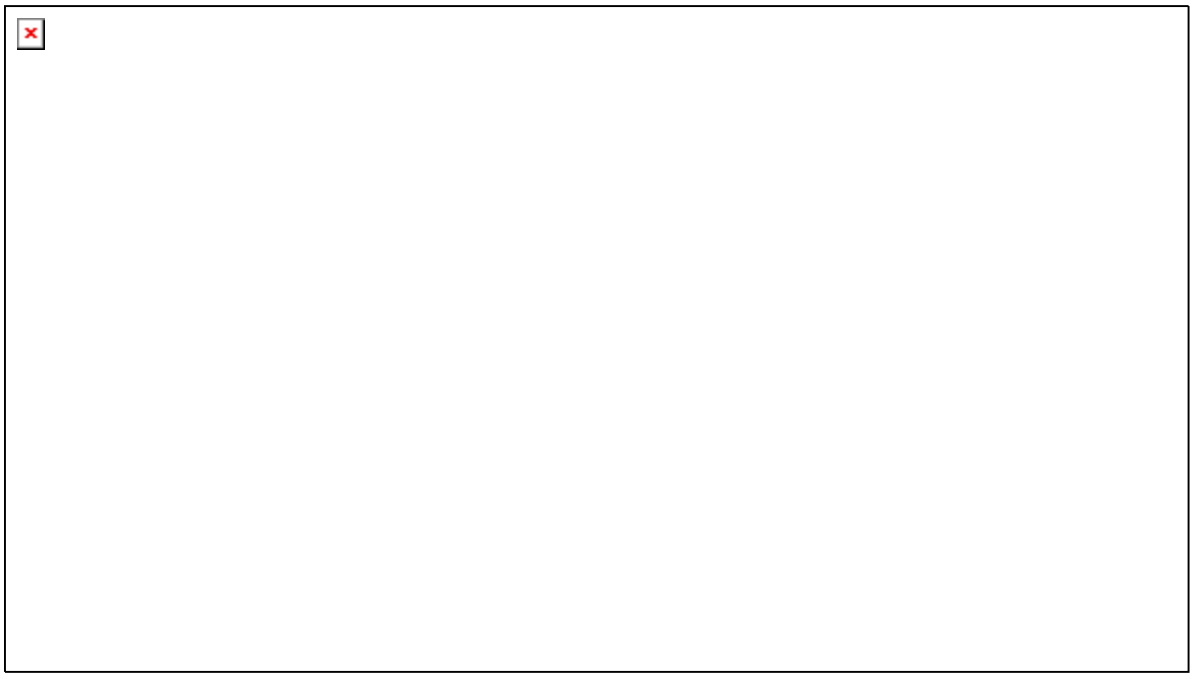

figure A 46: Photographs of failed specimen prb05c60

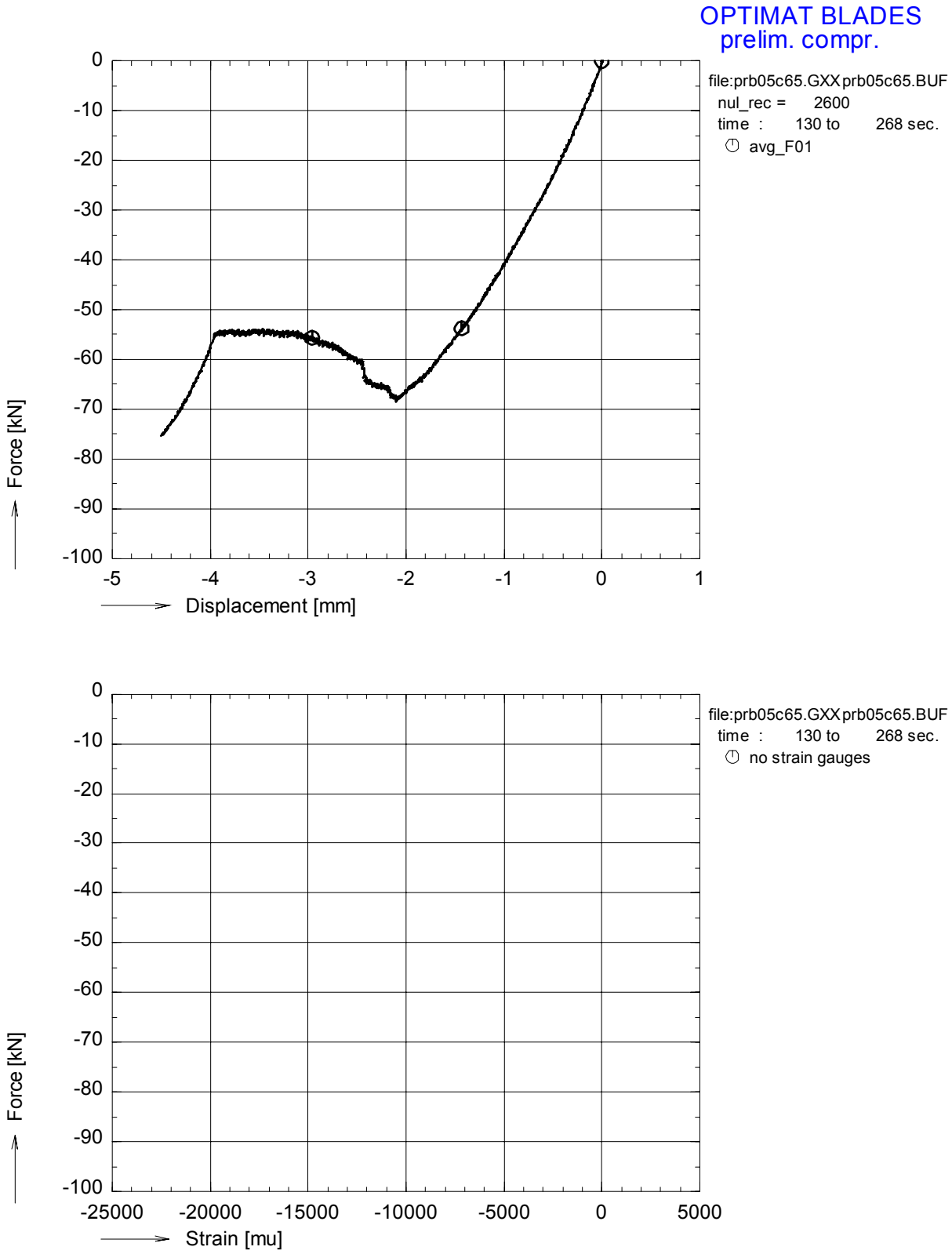

figure A 47: Axial compressive force vs. bench displacement and strains for prb05c65

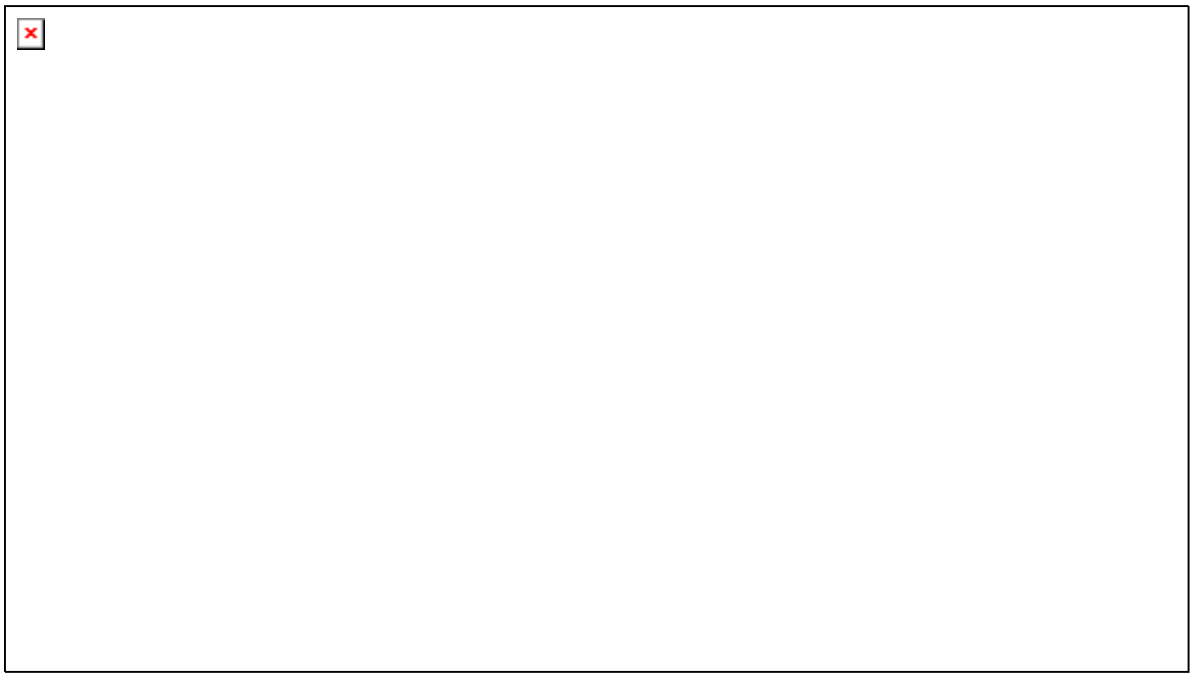

figure A 48: Photographs of failed specimen prb05c65

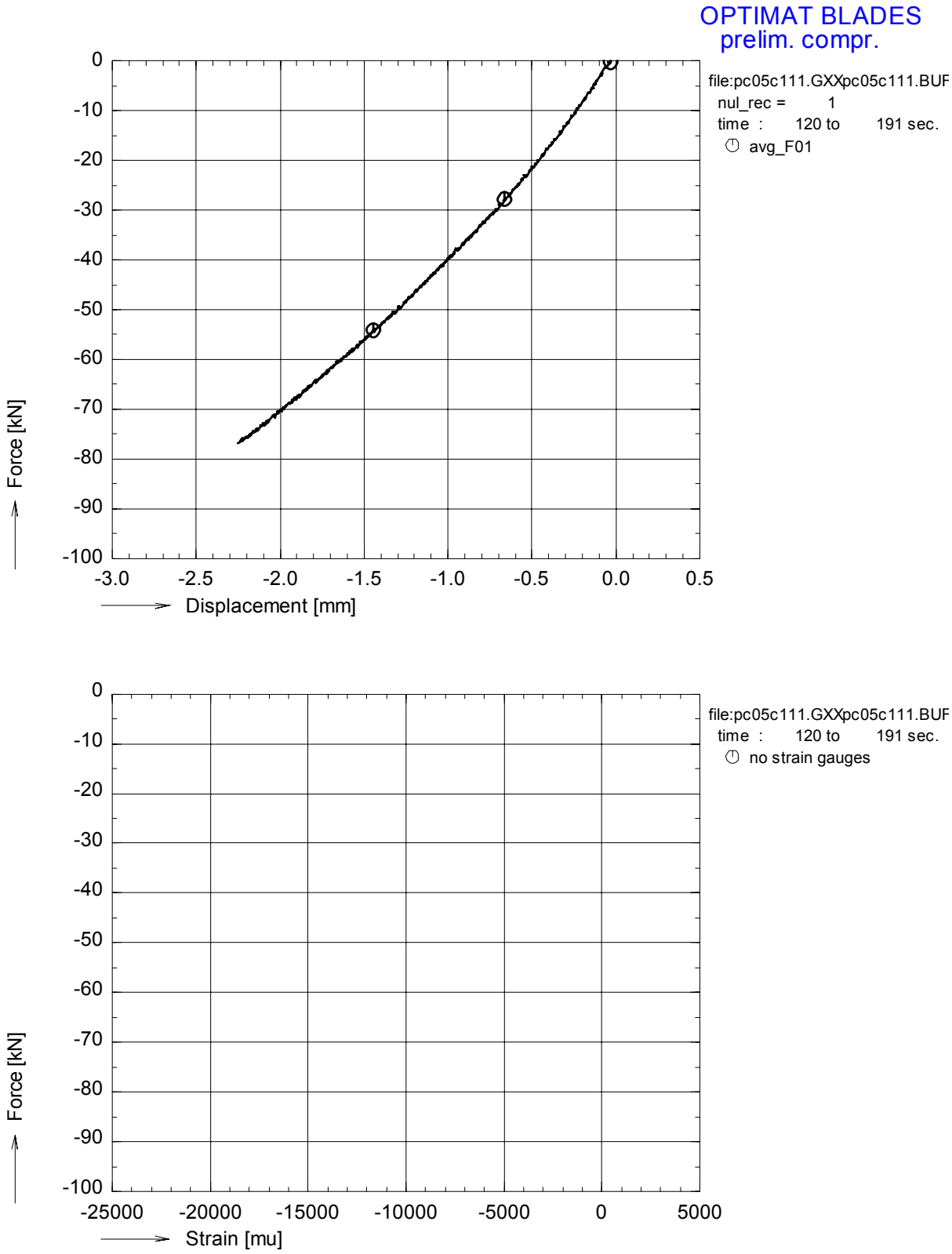

figure A 49: Axial compressive force vs. bench displacement and strains for prc05c111

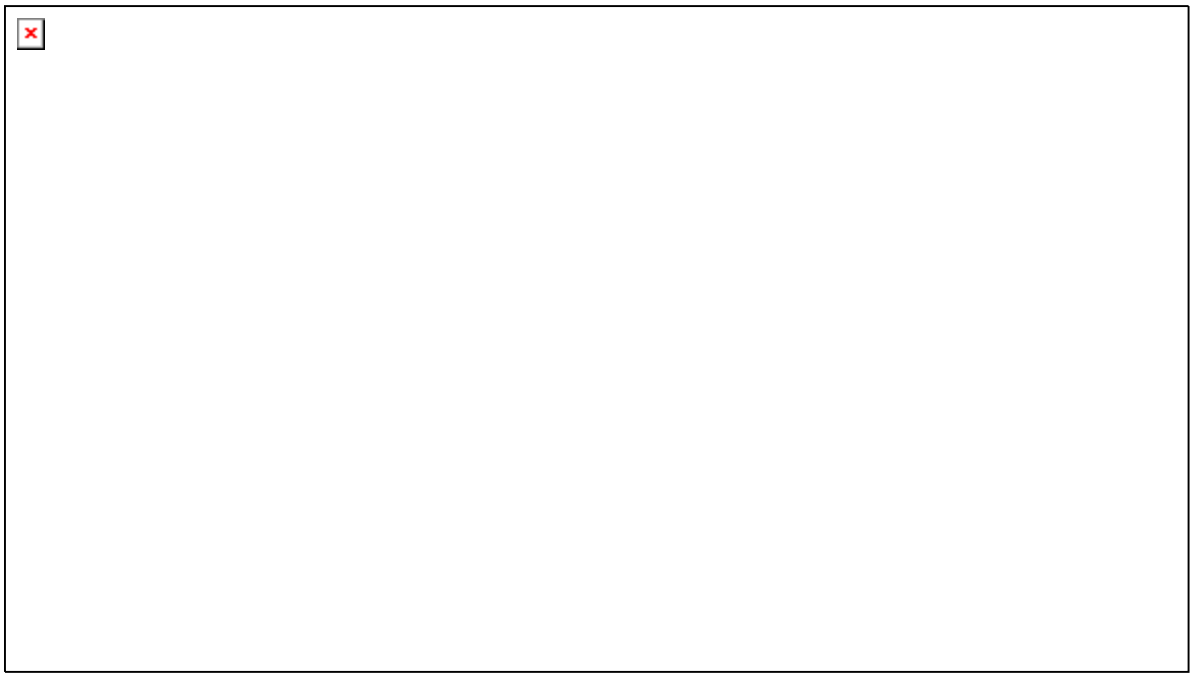

figure A 50: Photographs of failed specimen prc05c111

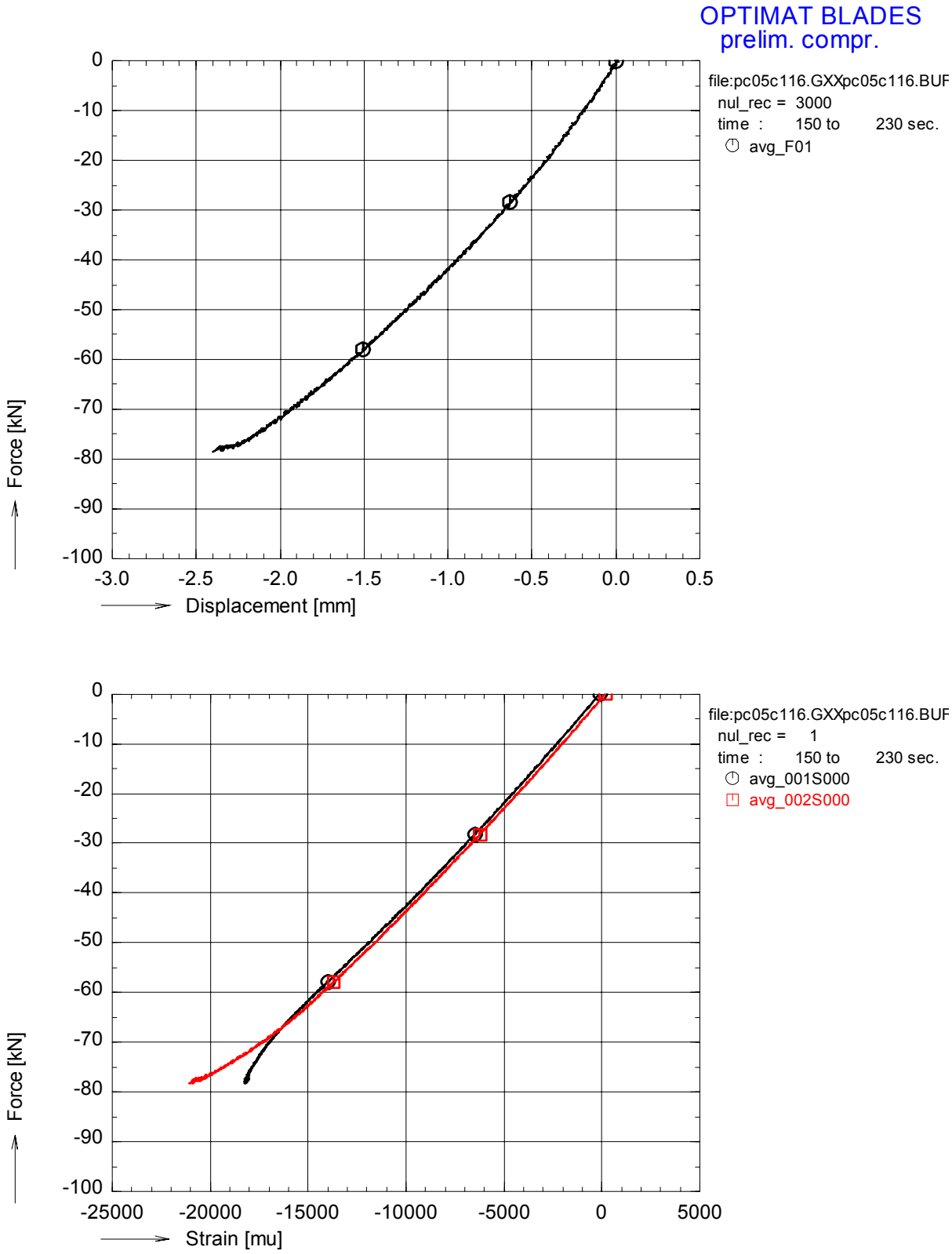

figure A 51: Axial compressive force vs. bench displacement and strains for prc05c116

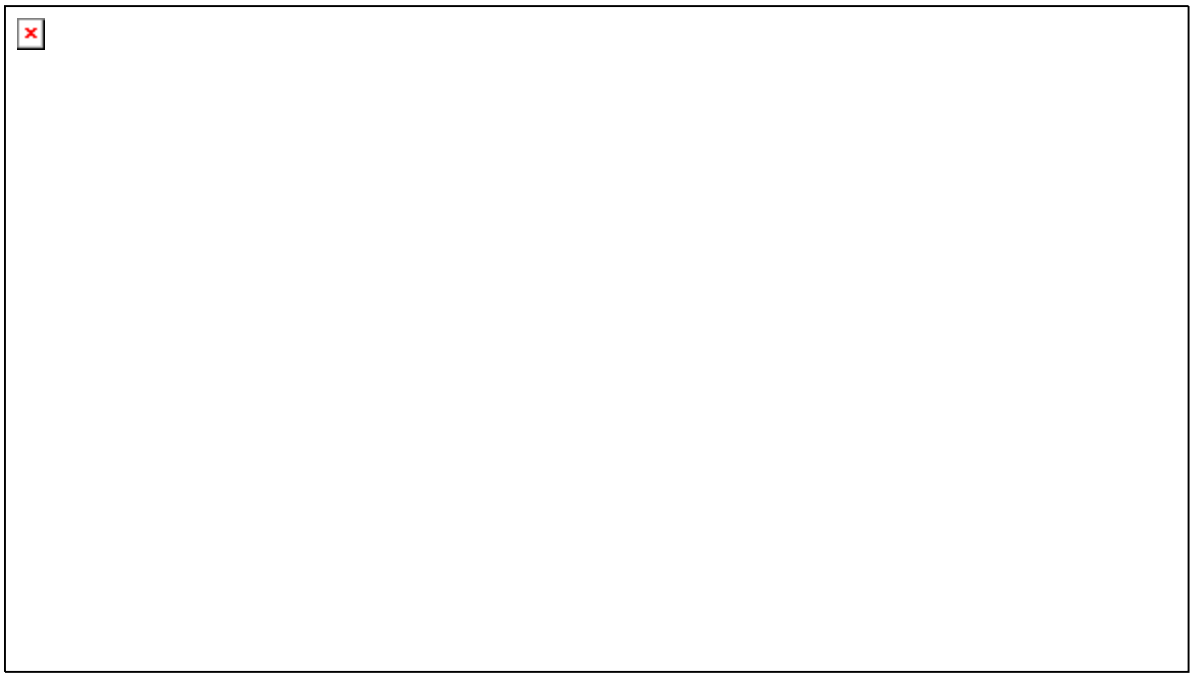

figure A 52: Photographs of failed specimen prc05c116

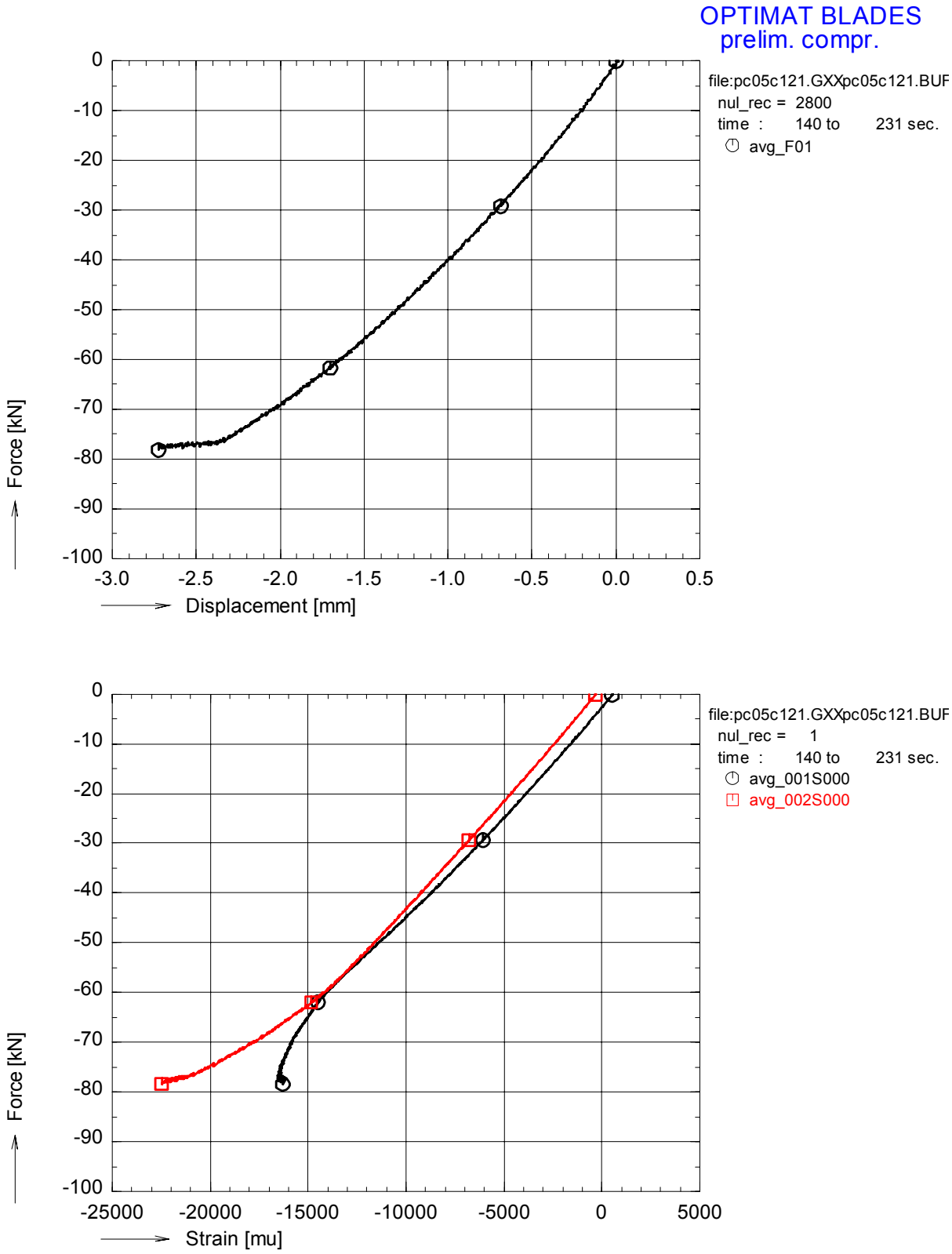

figure A 53: Axial compressive force vs. bench displacement and strains for prc05c121

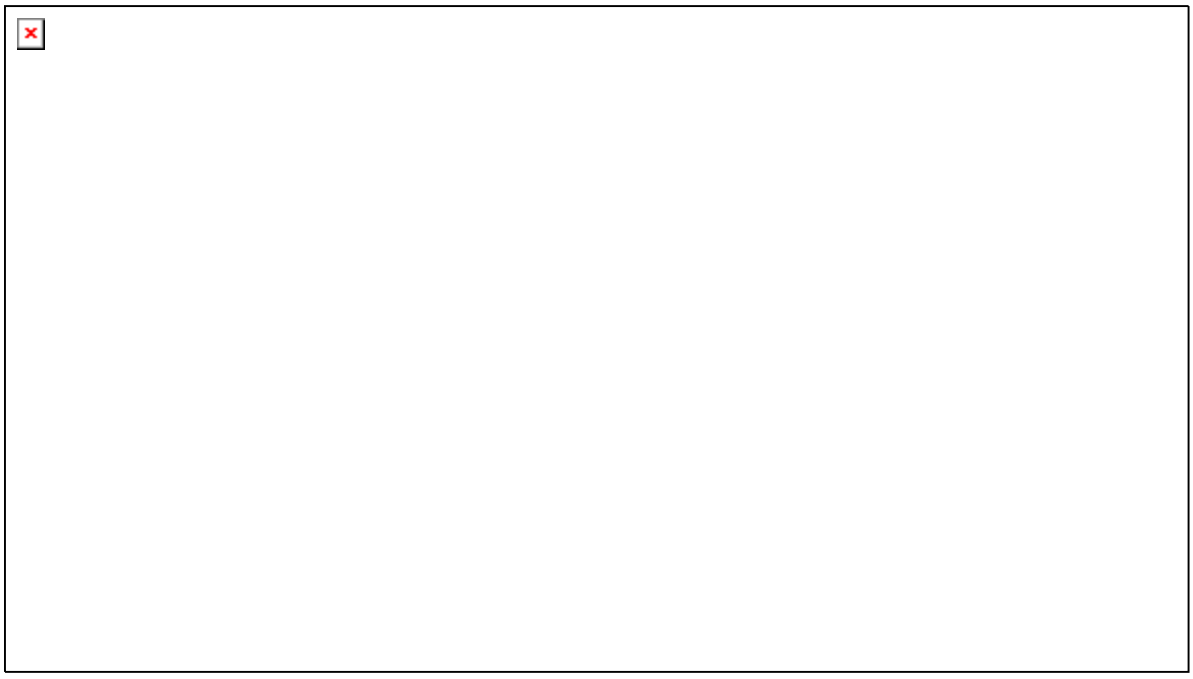

figure A 54: Photographs of failed specimen prc05c121

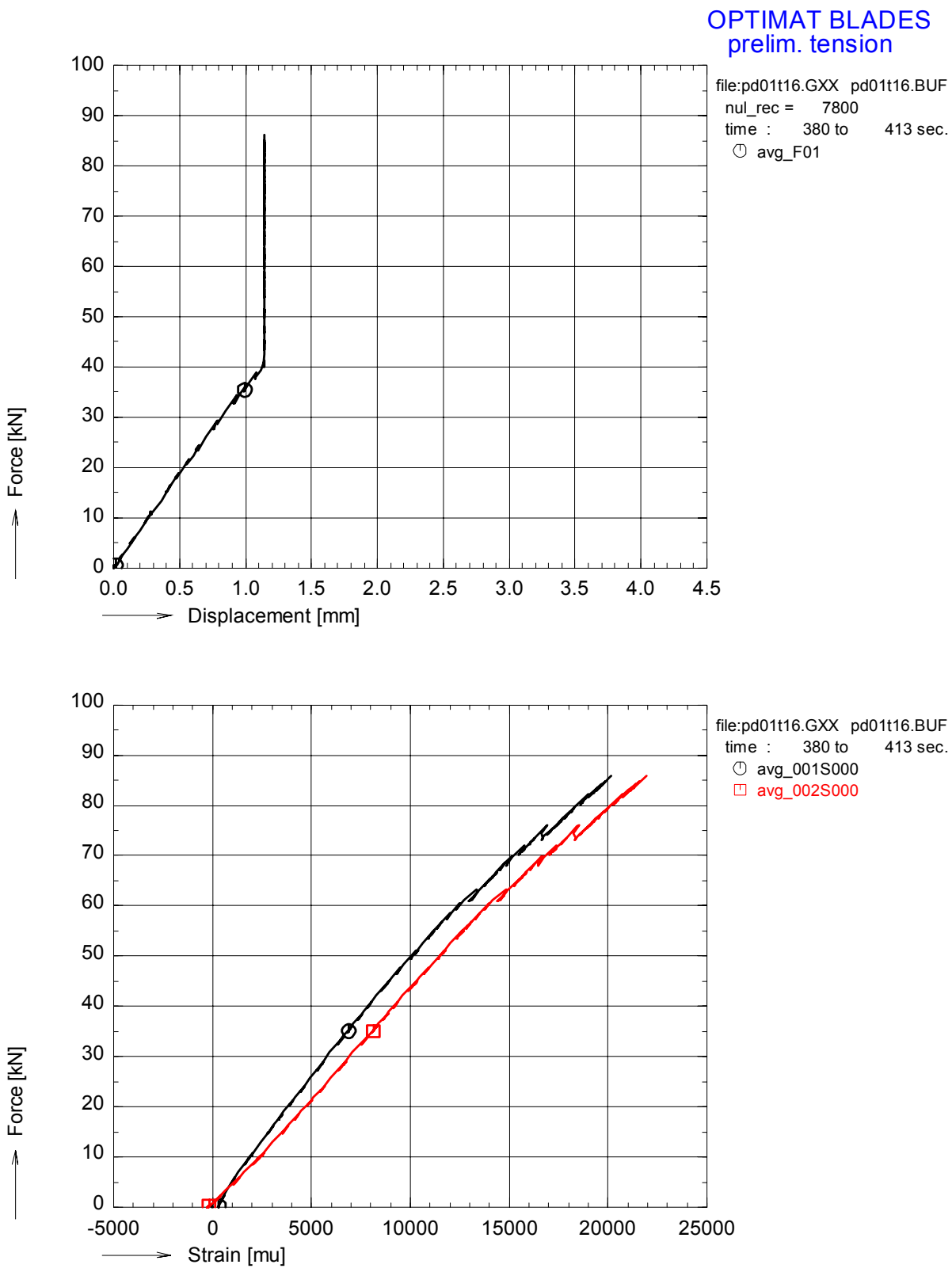

figure A 55: Axial tensile force vs. bench displacement and strains for pd01t16

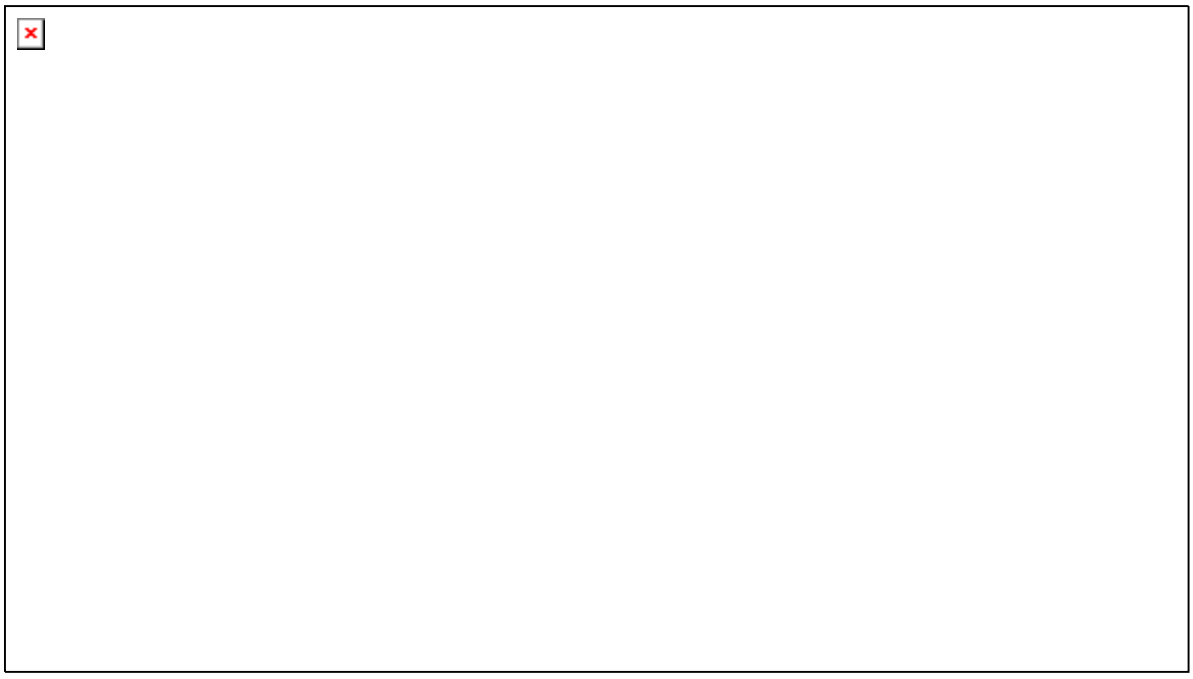

figure A 56: Photographs of failed specimen pd01t16 (top photograph: back side)

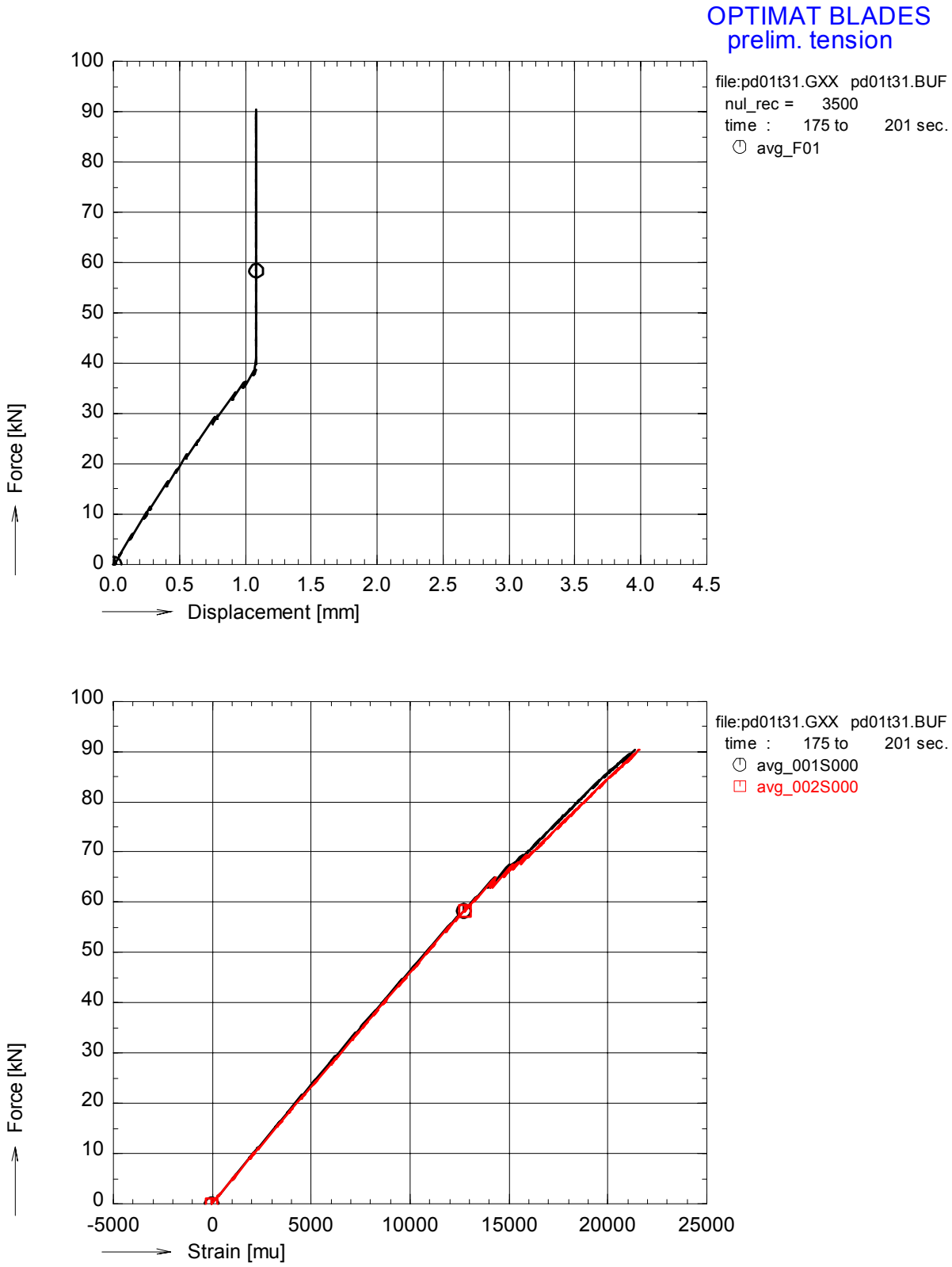

figure A 57: Axial tensile force vs. bench displacement and strains for pd01t31

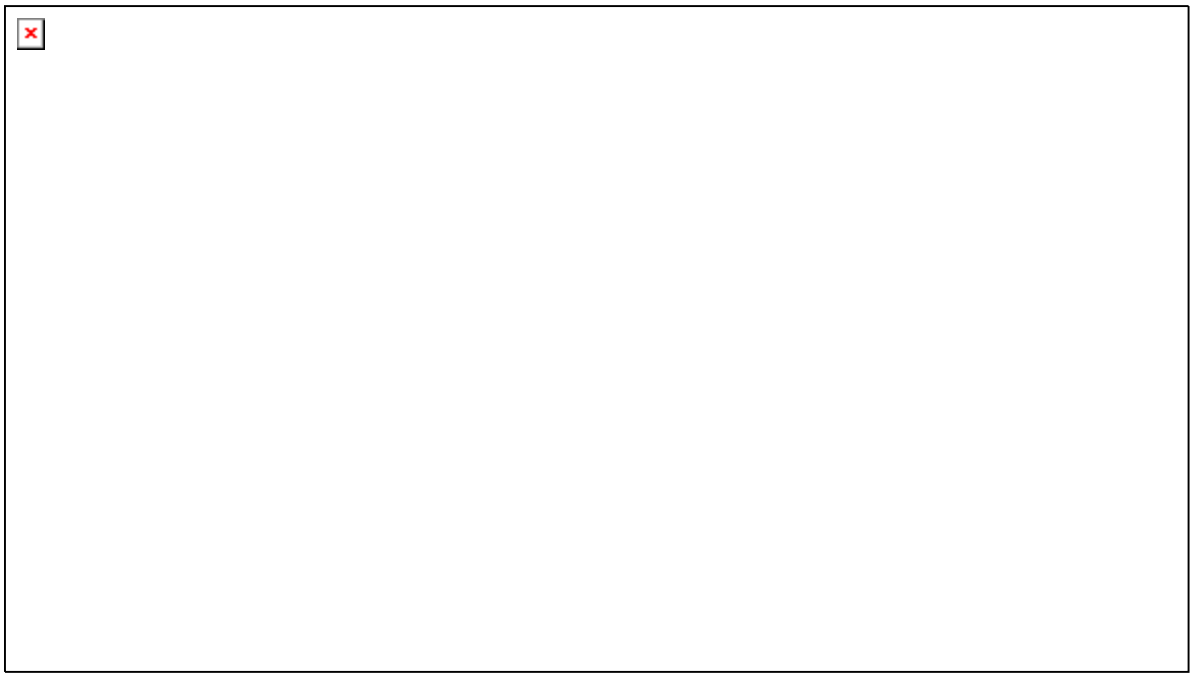

figure A 58: Photographs of failed specimen pd01t31

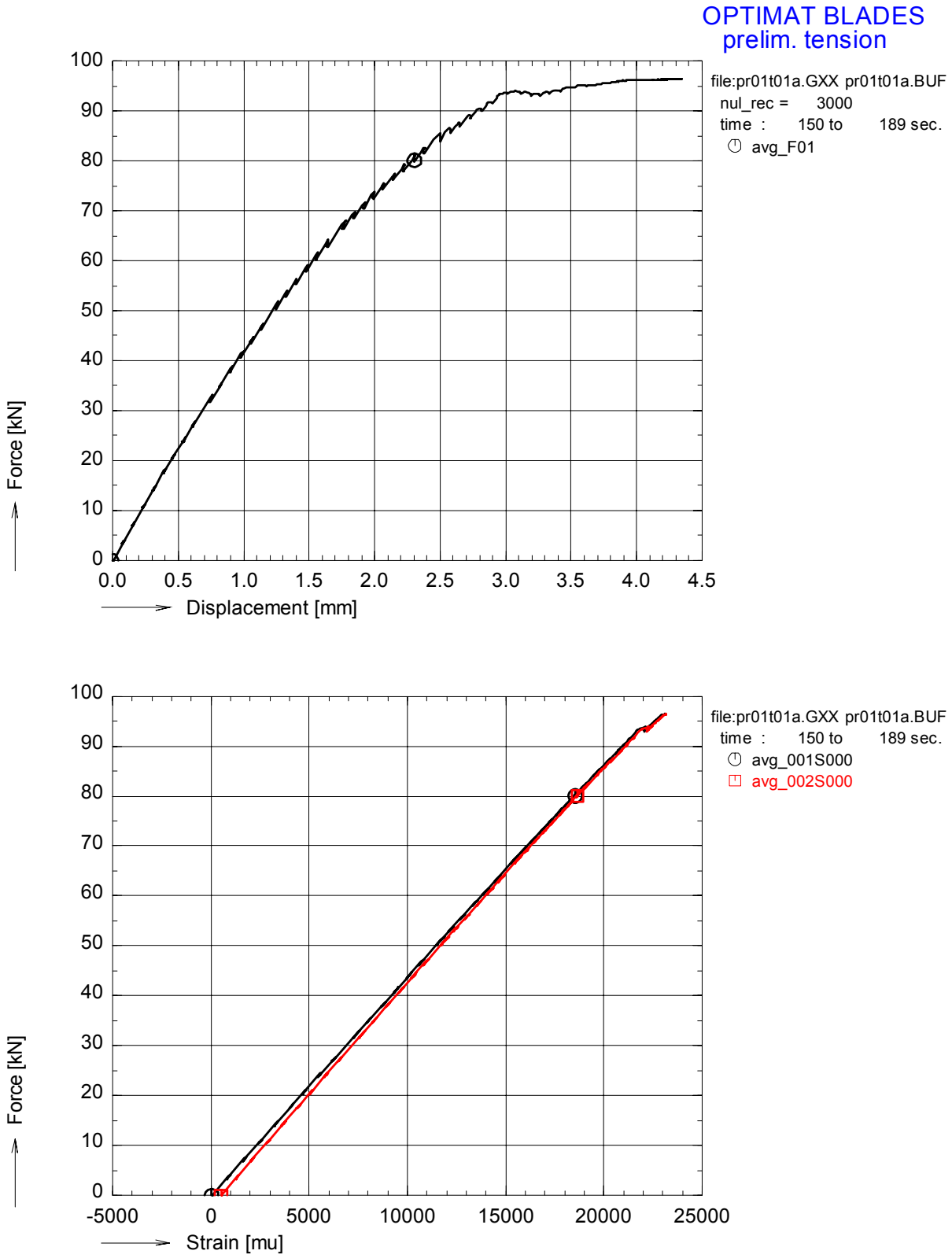

figure A 59: Axial tensile force vs. bench displacement and strains for pr01t01

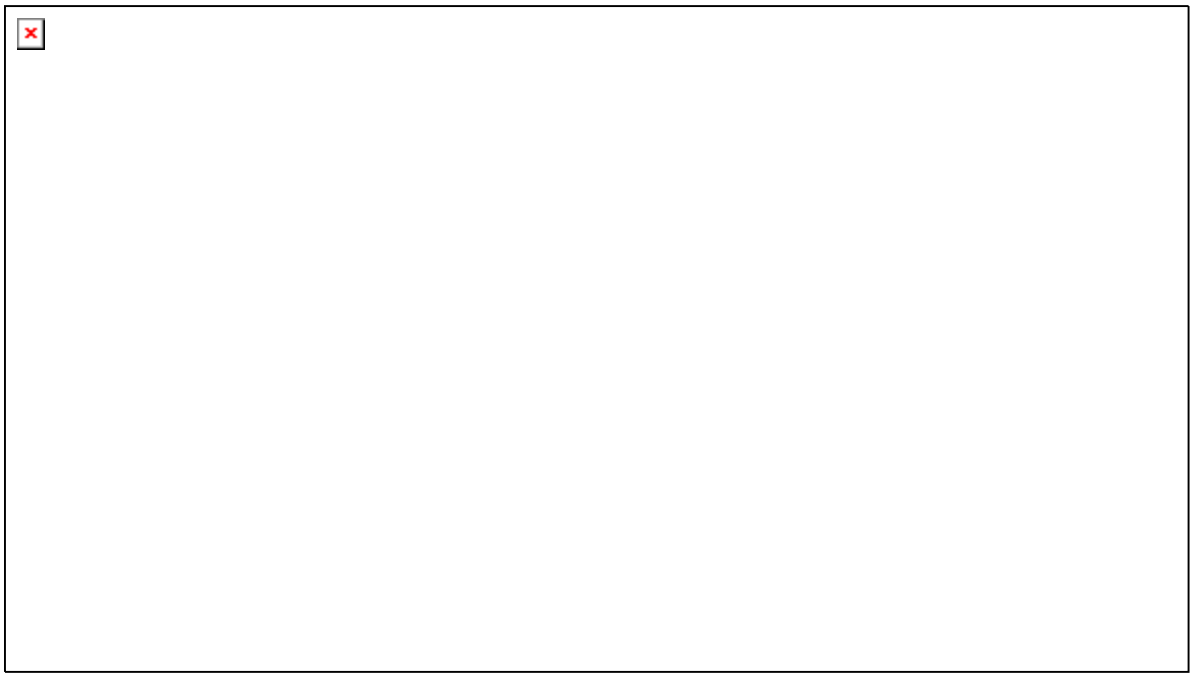

figure A 60: Photographs of failed specimen pr01t01

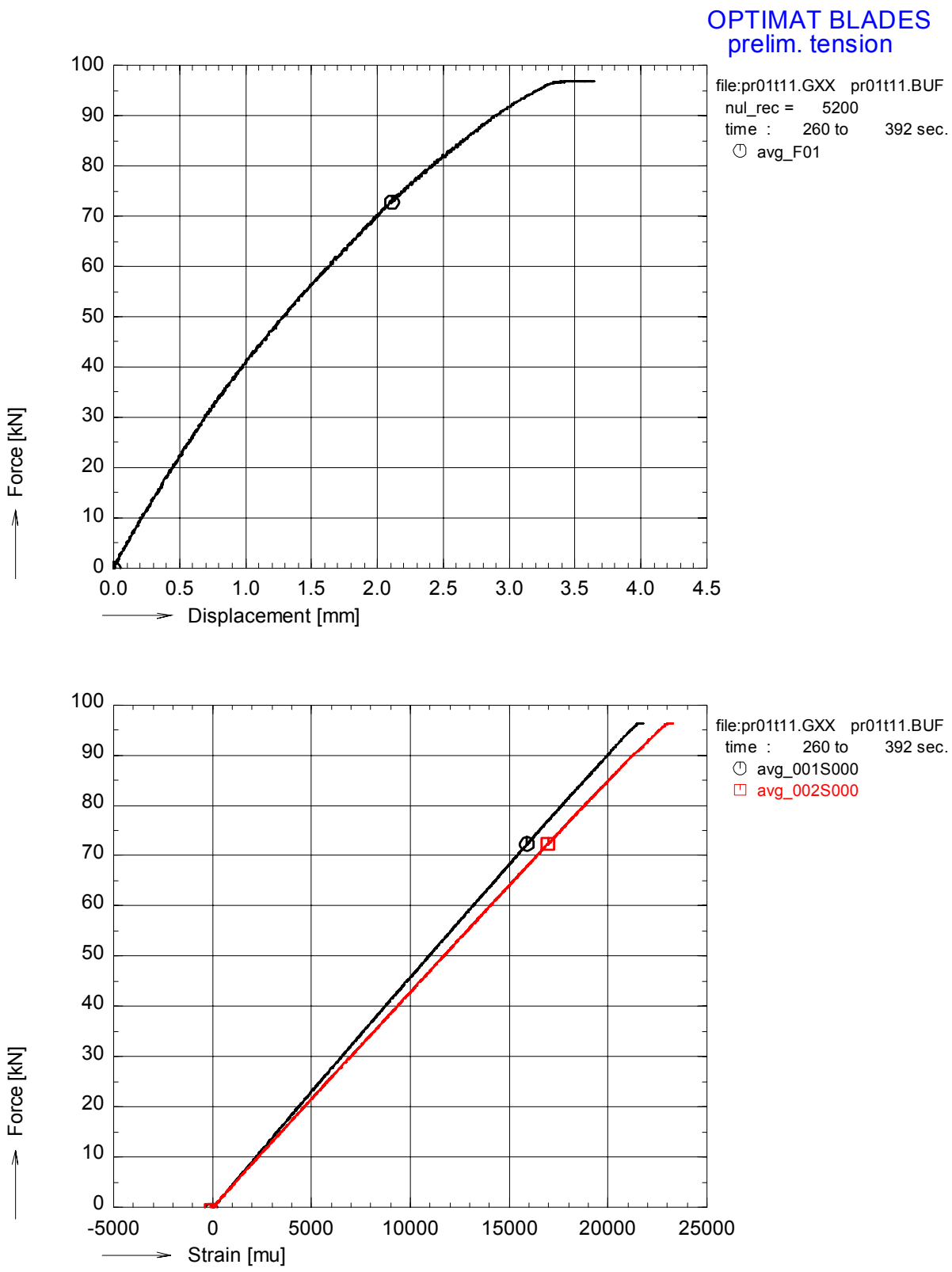

figure A 61: Axial tensile force vs. bench displacement and strains for pr01t11

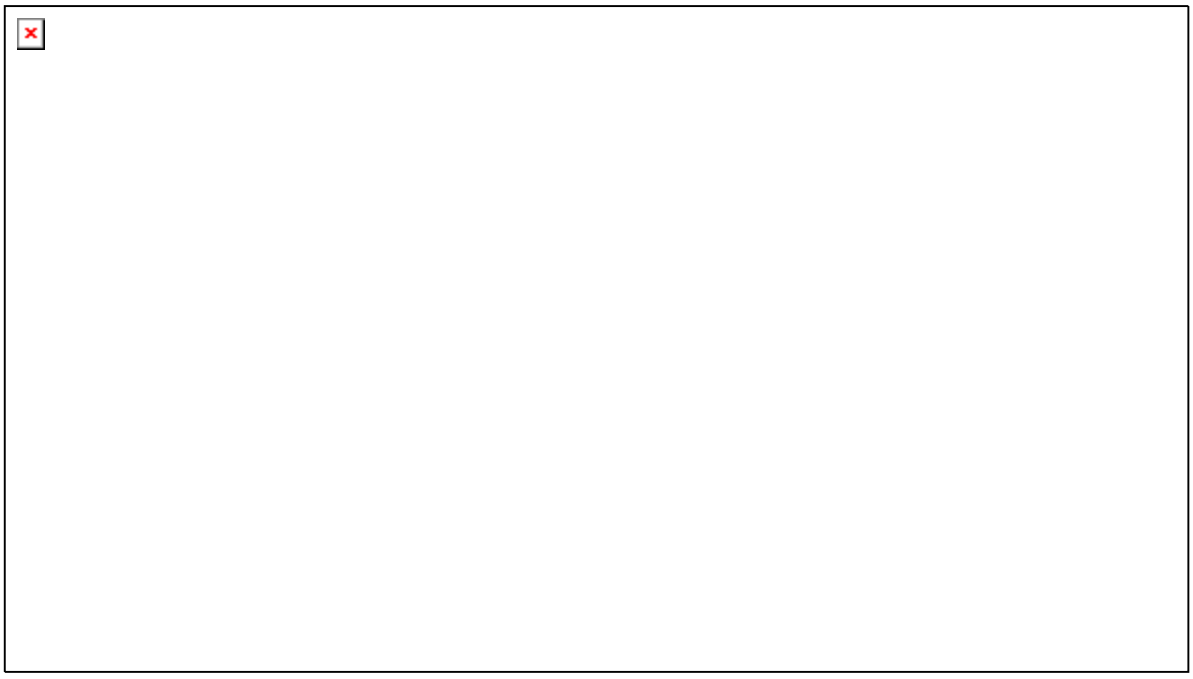

figure A 62: Photographs of failed specimen pr01t11

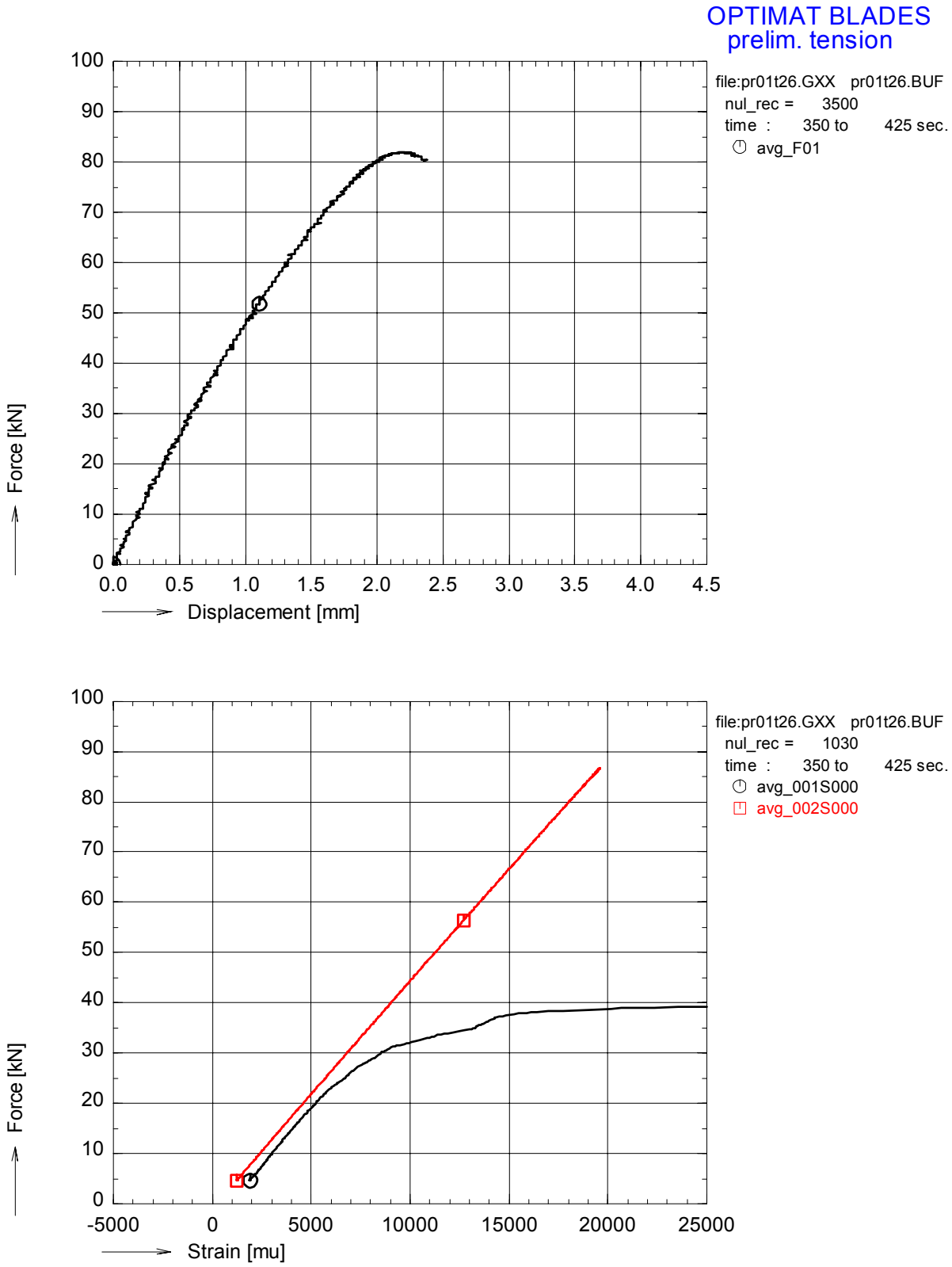

figure A 63: Axial tensile force vs. bench displacement and strains for pr01t26

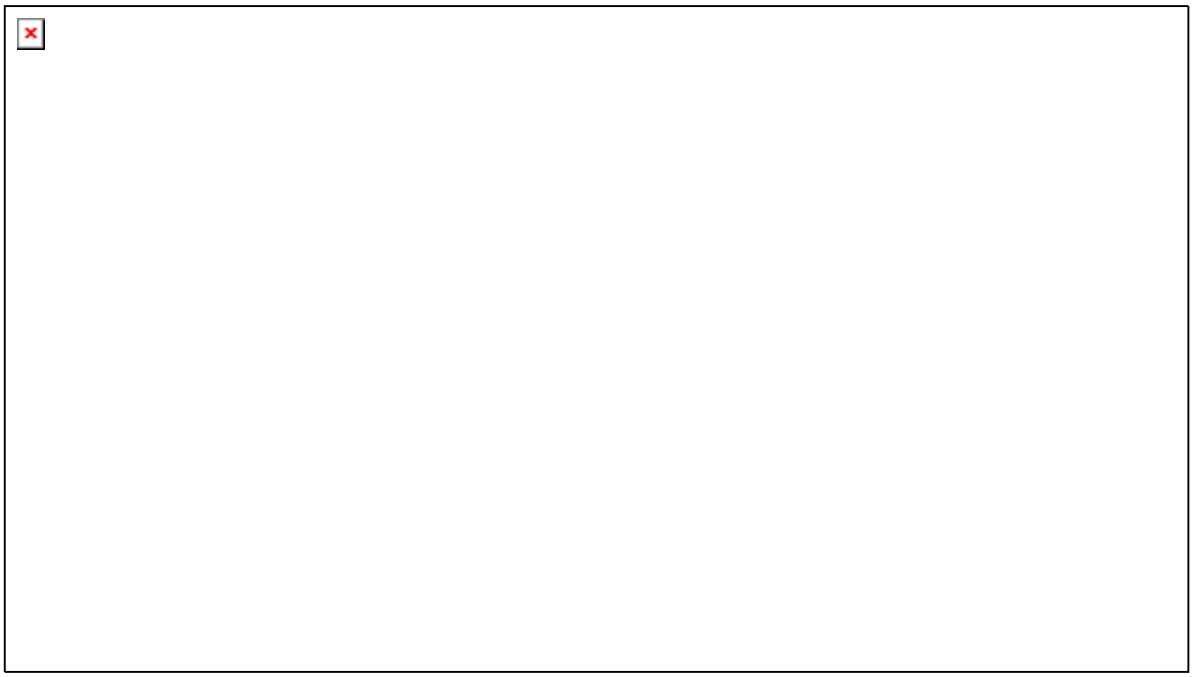

figure A 64: Photographs of failed specimen pr01t26

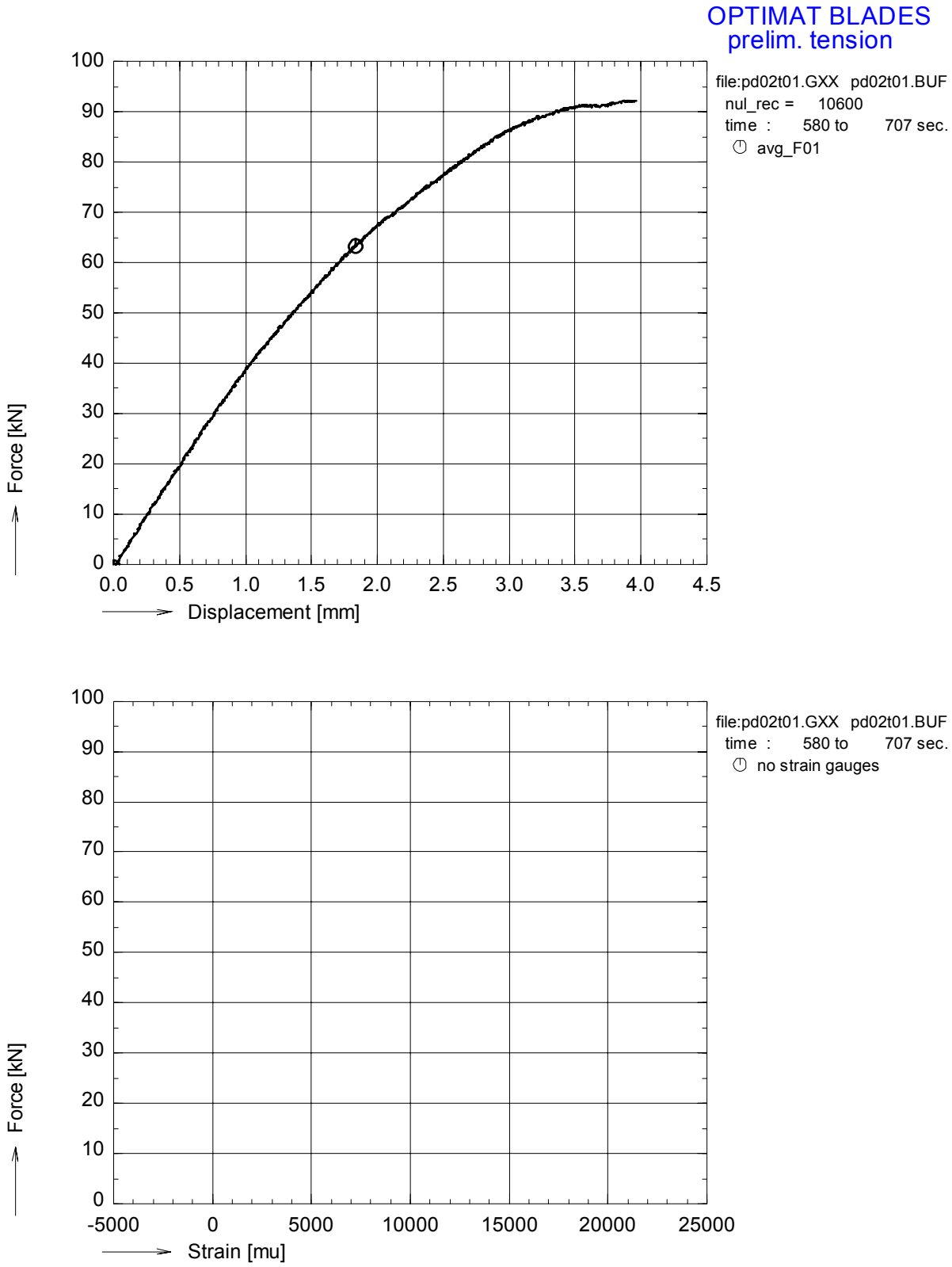

figure A 65: Axial tensile force vs. bench displacement and strains for pd02t01

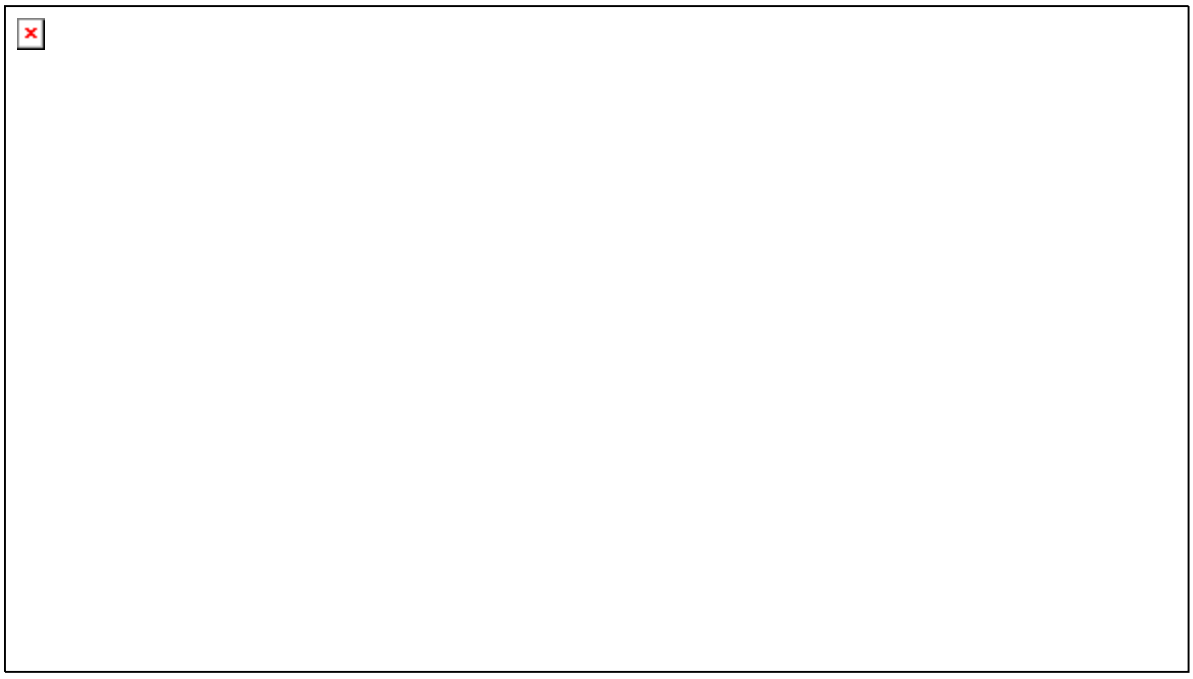

figure A 66: Photographs of failed specimen pd02t01

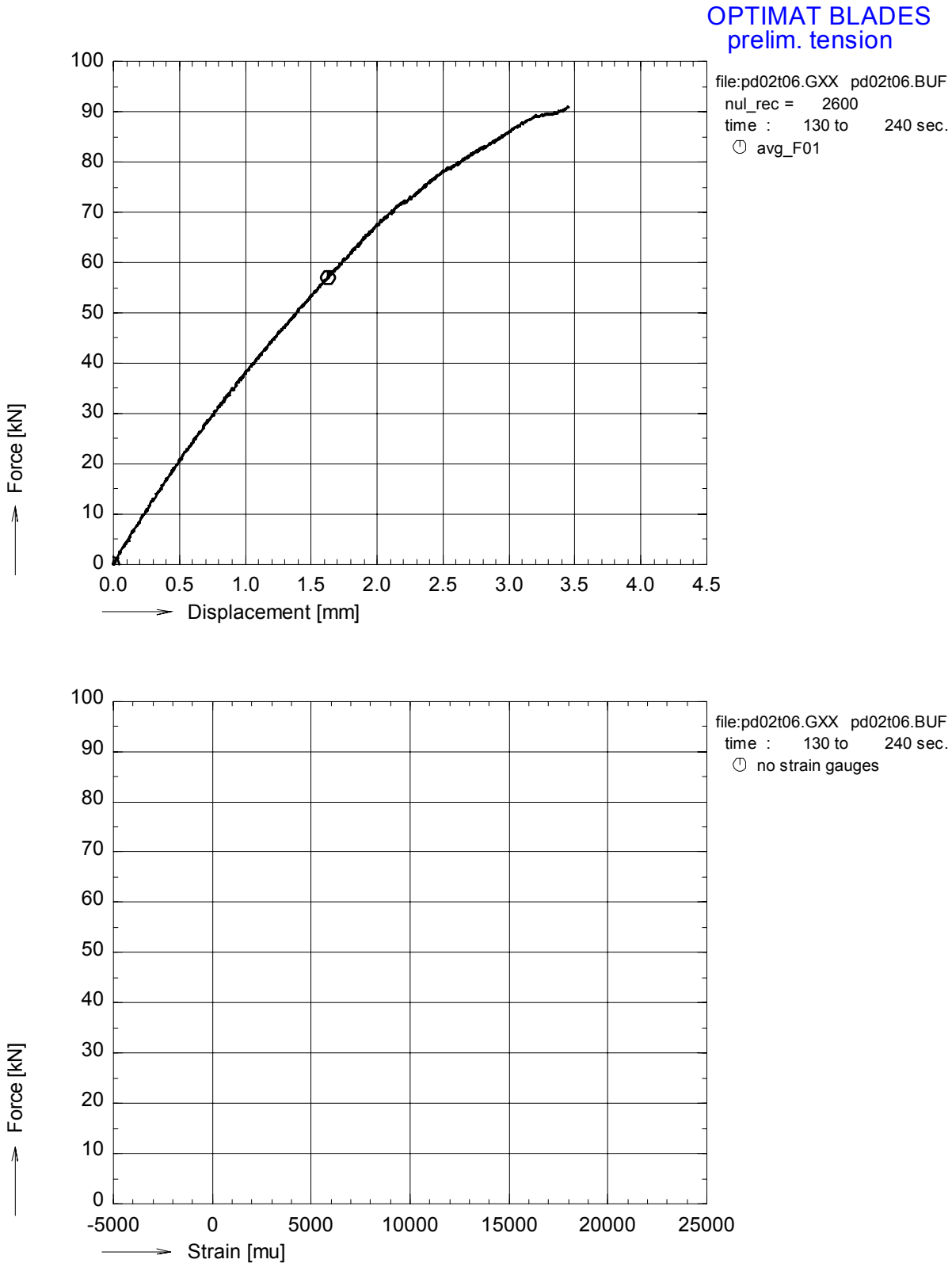

figure A 67: Axial tensile force vs. bench displacement and strains for pd02t06

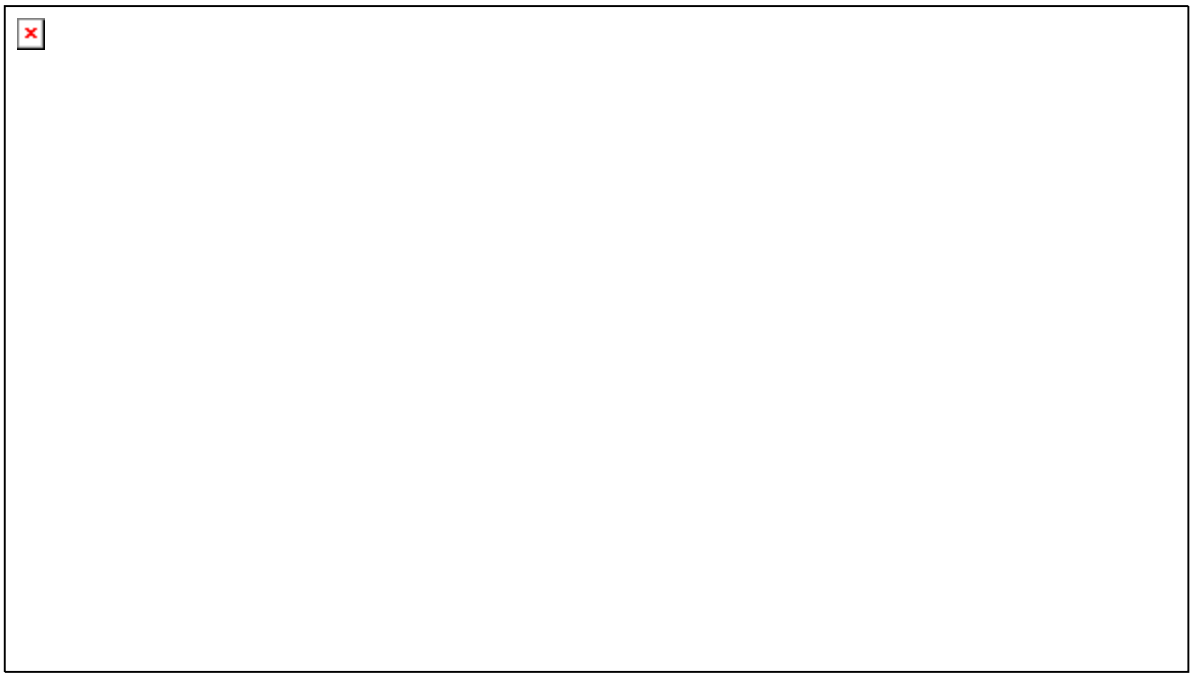

figure A 68: Photographs of failed specimen pd02t06

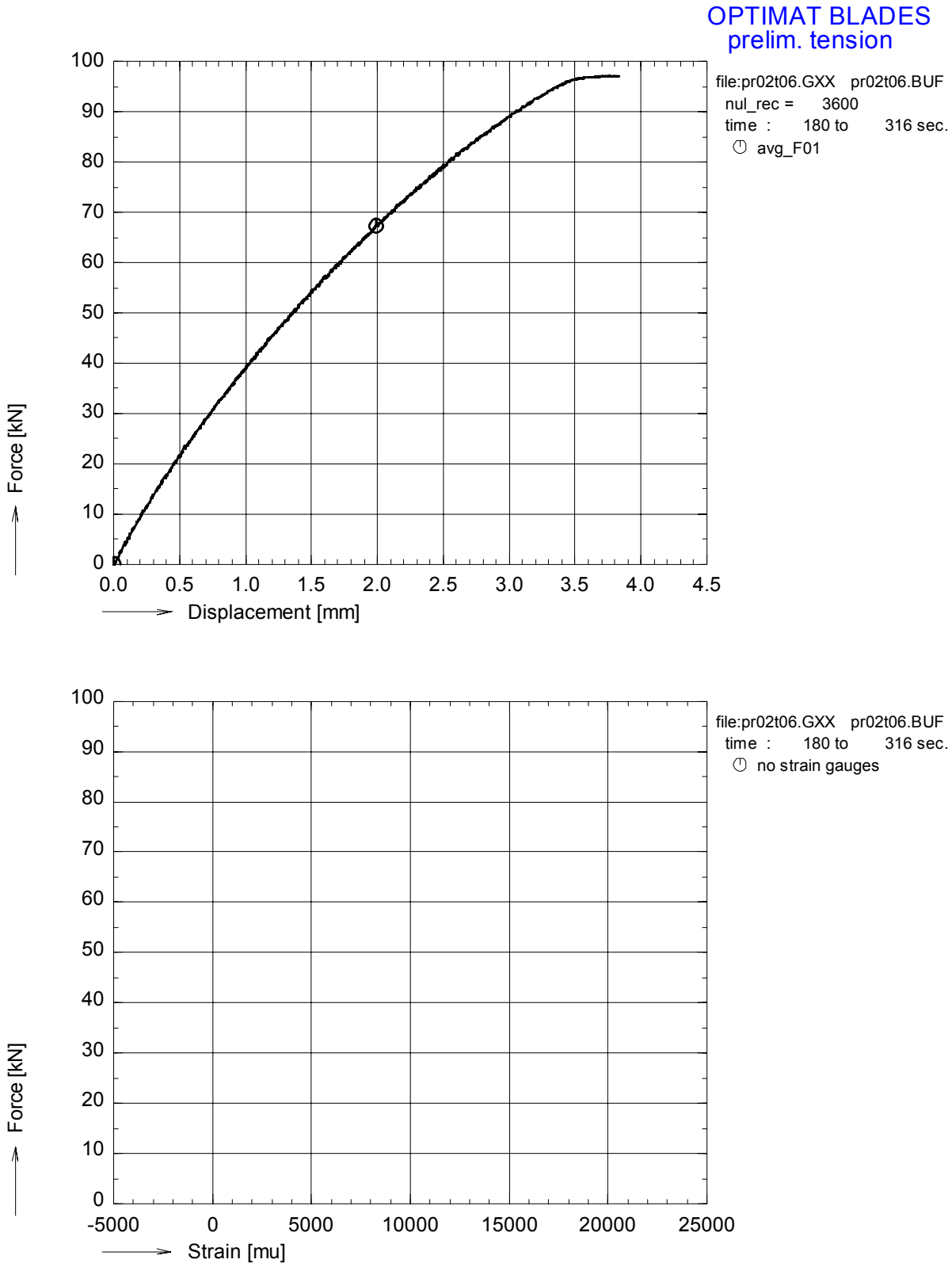

figure A 69: Axial tensile force vs. bench displacement and strains for pr02t06

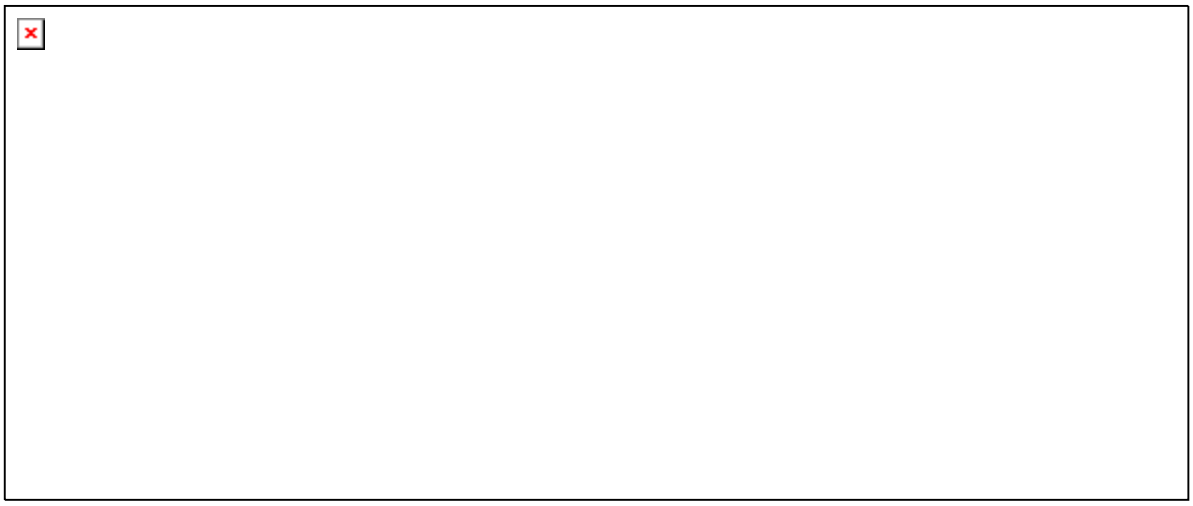

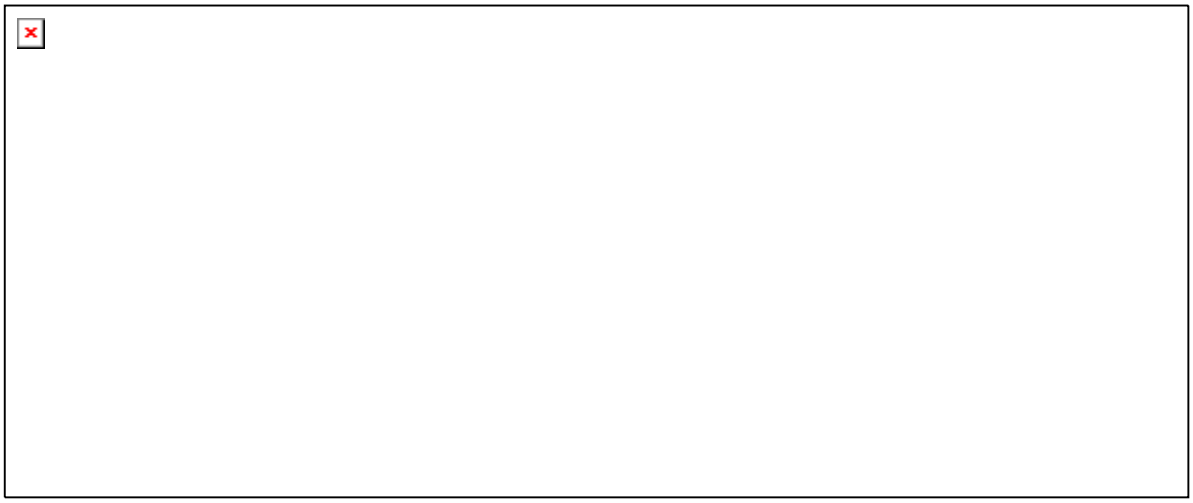

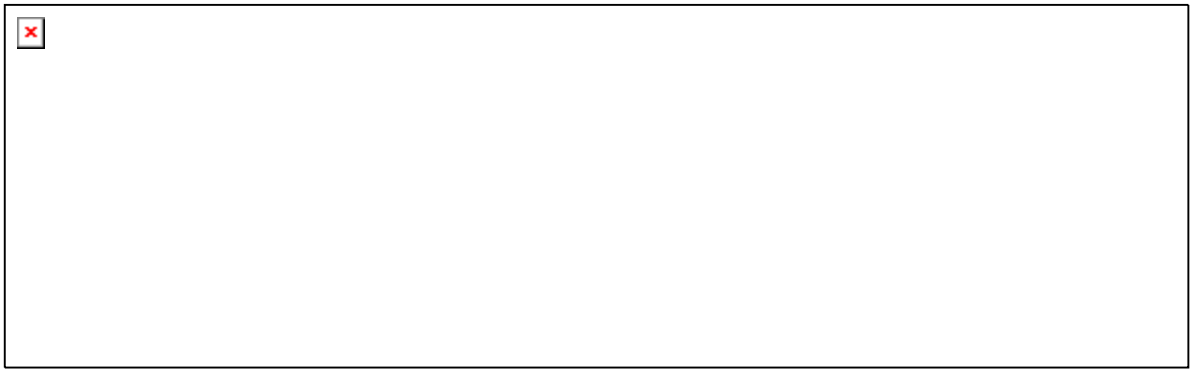

figure A 70: Photographs of failed specimen pr02t06 (resp. back, front, side)

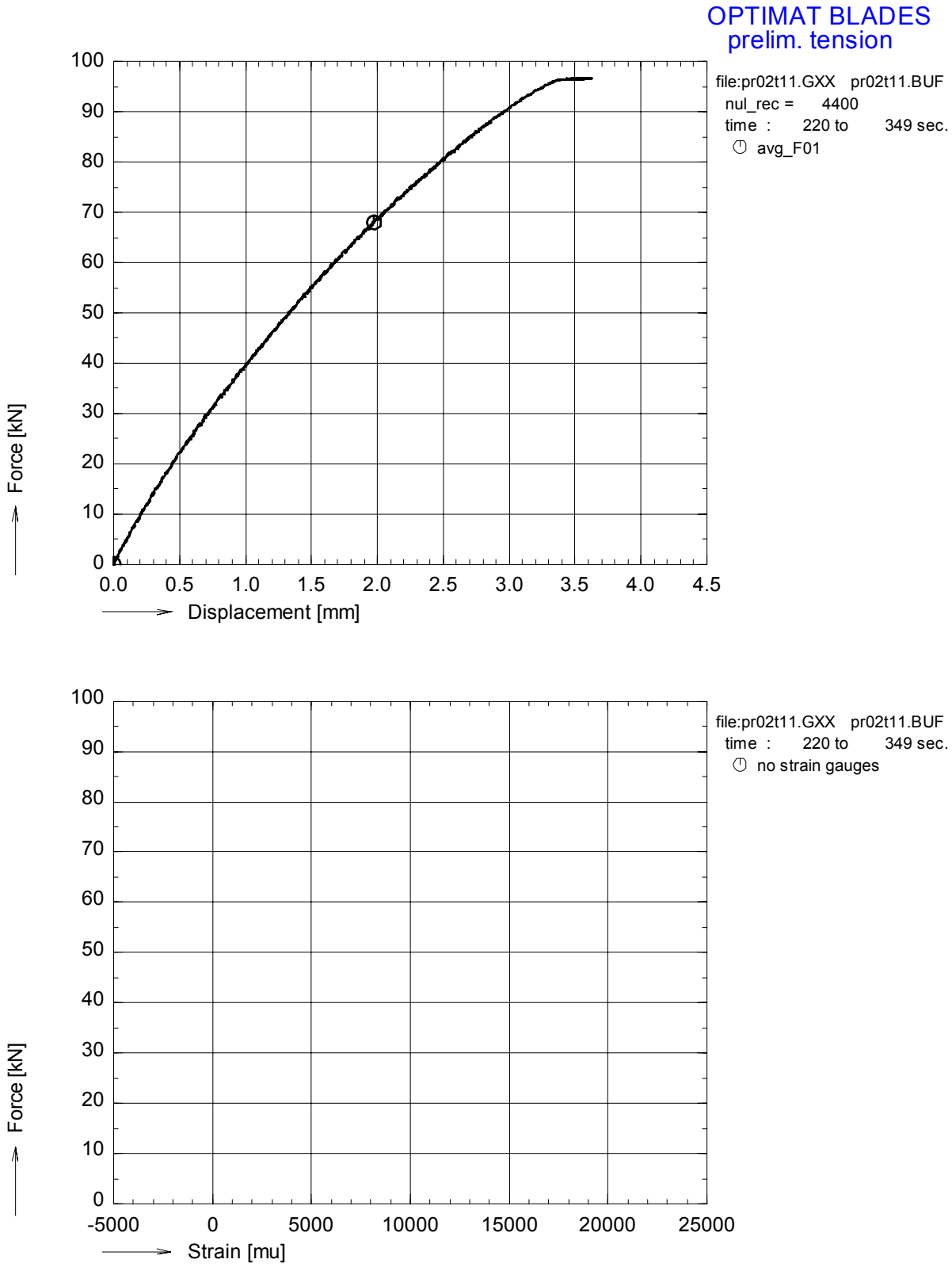

figure A 71: Axial tensile force vs. bench displacement and strains for pr02t11

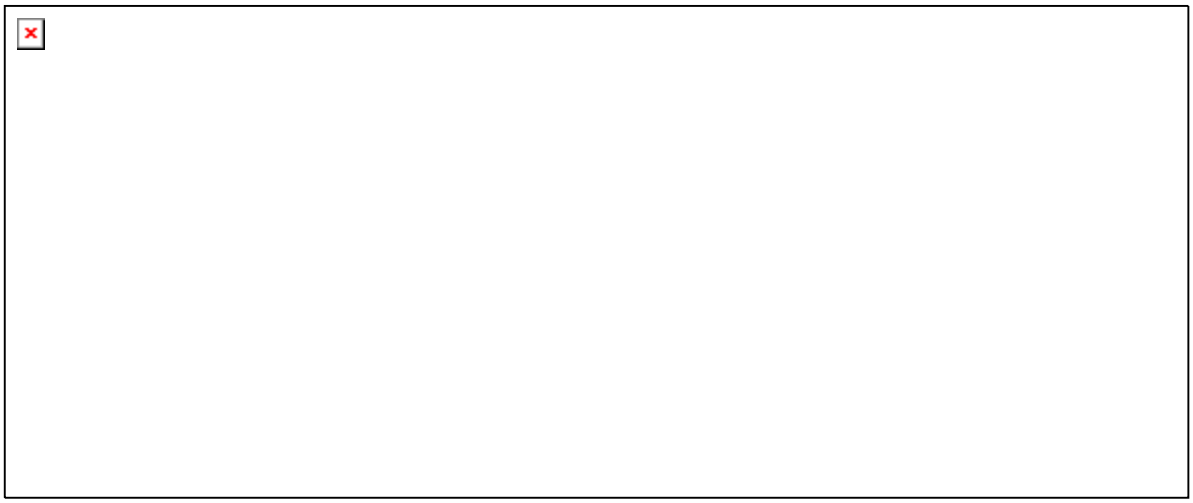

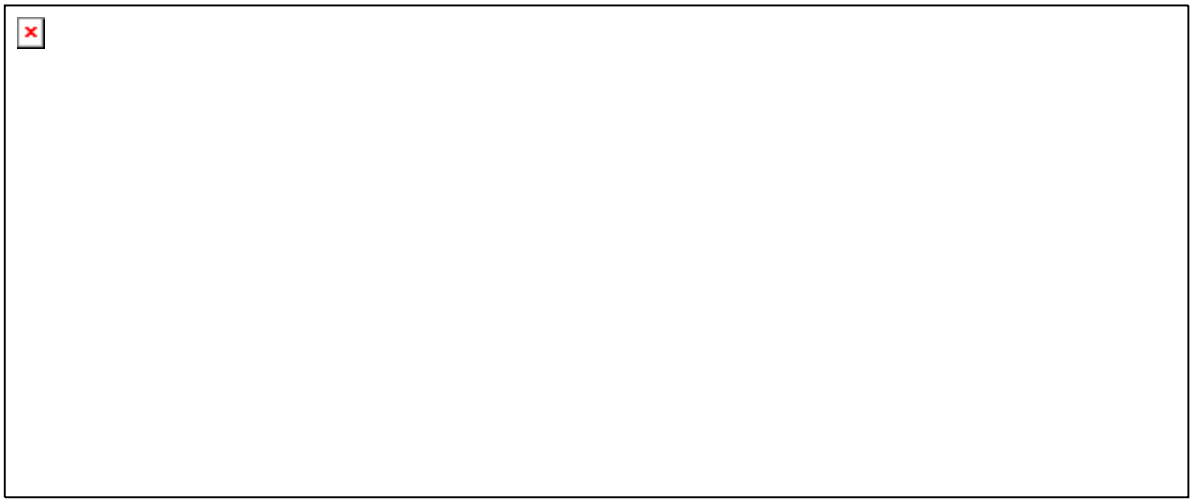

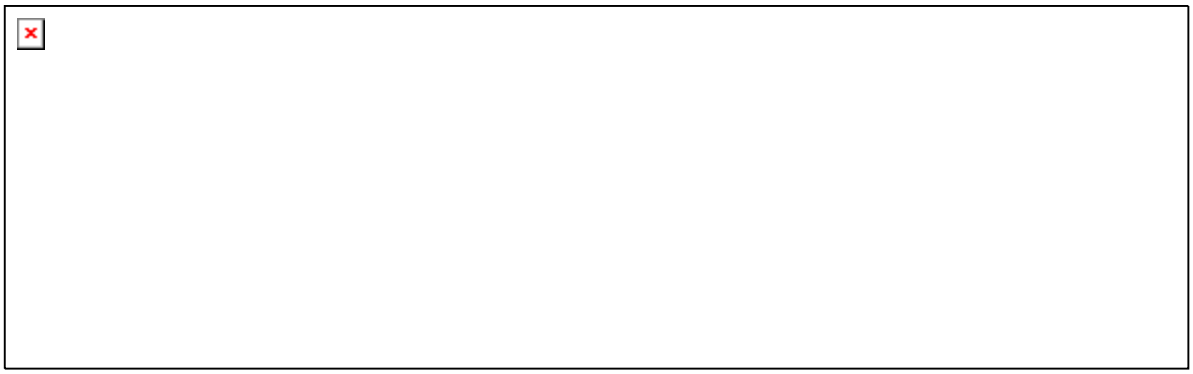

figure A 72: Photographs of failed specimen pr02t11 (resp. back, front, side)

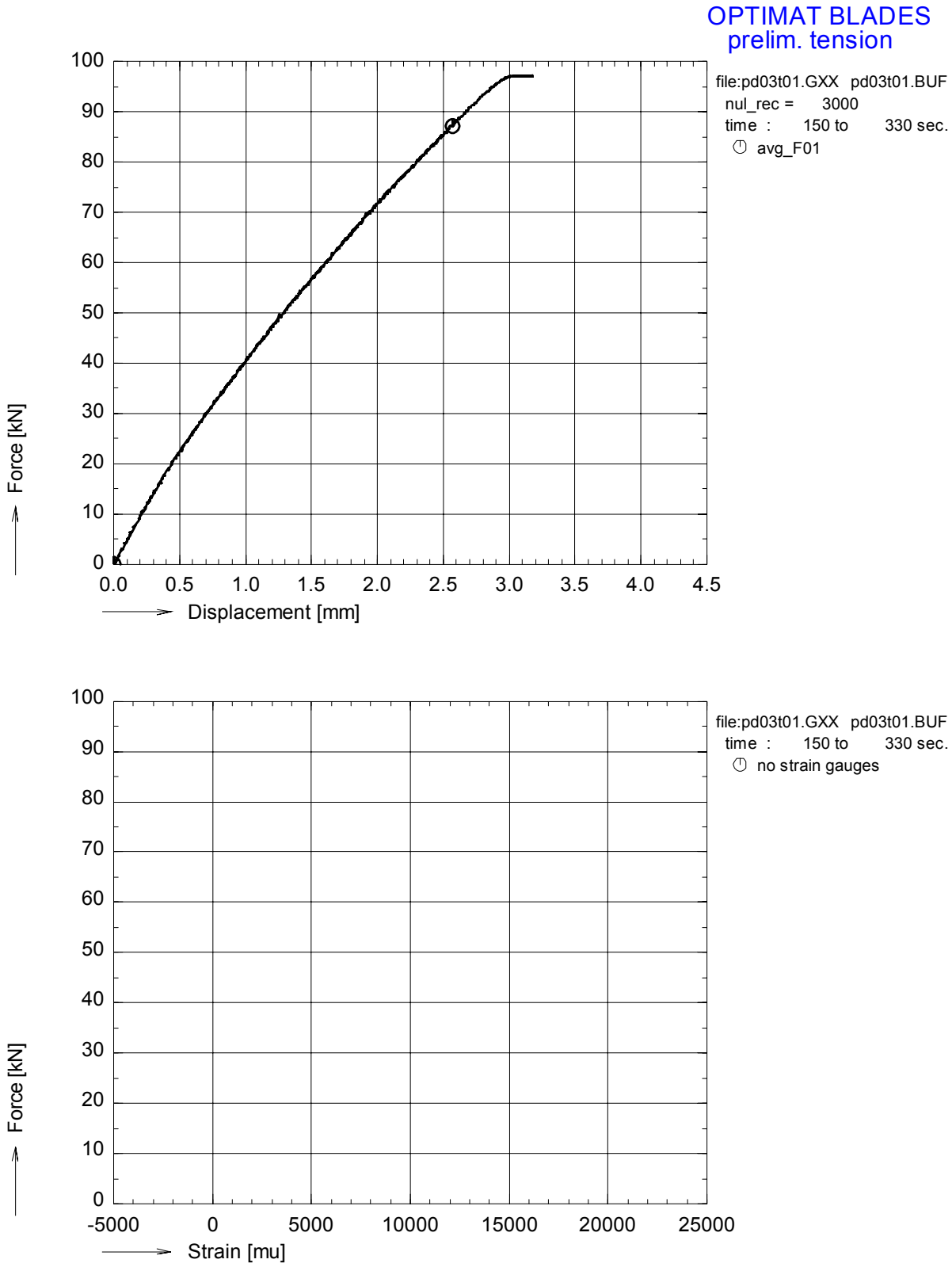

figure A 73: Axial tensile force vs. bench displacement and strains for pd03t01

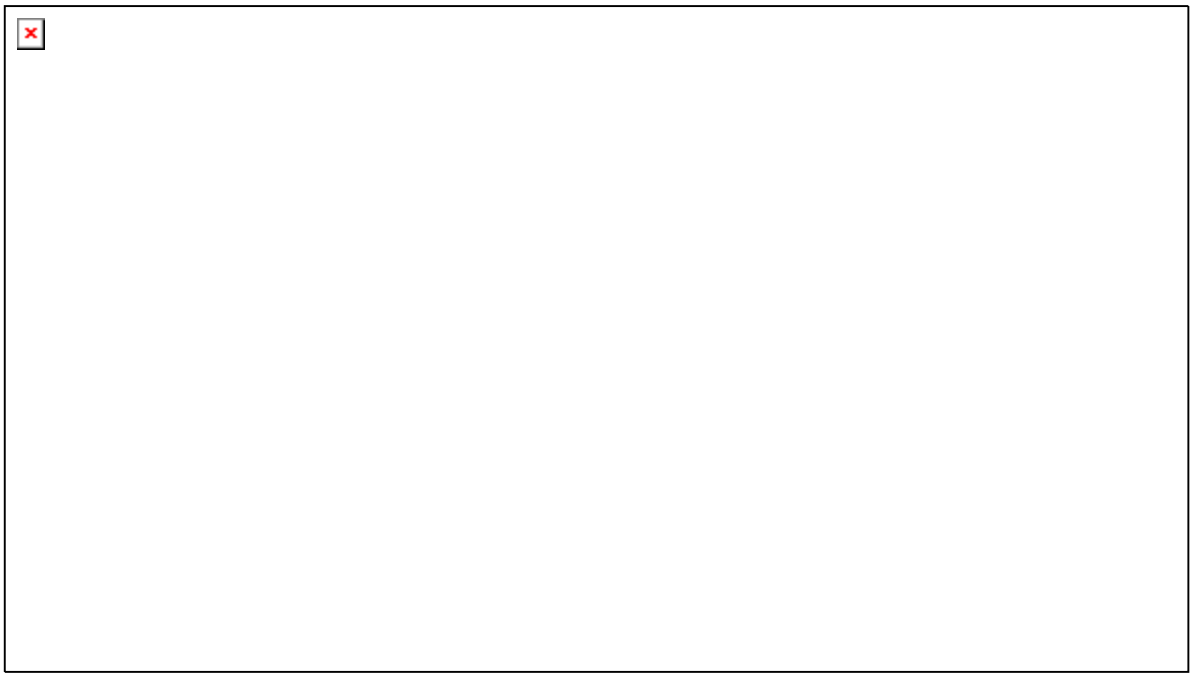

figure A 74: Photographs of failed specimen pd03t01 (top photograph: back side)

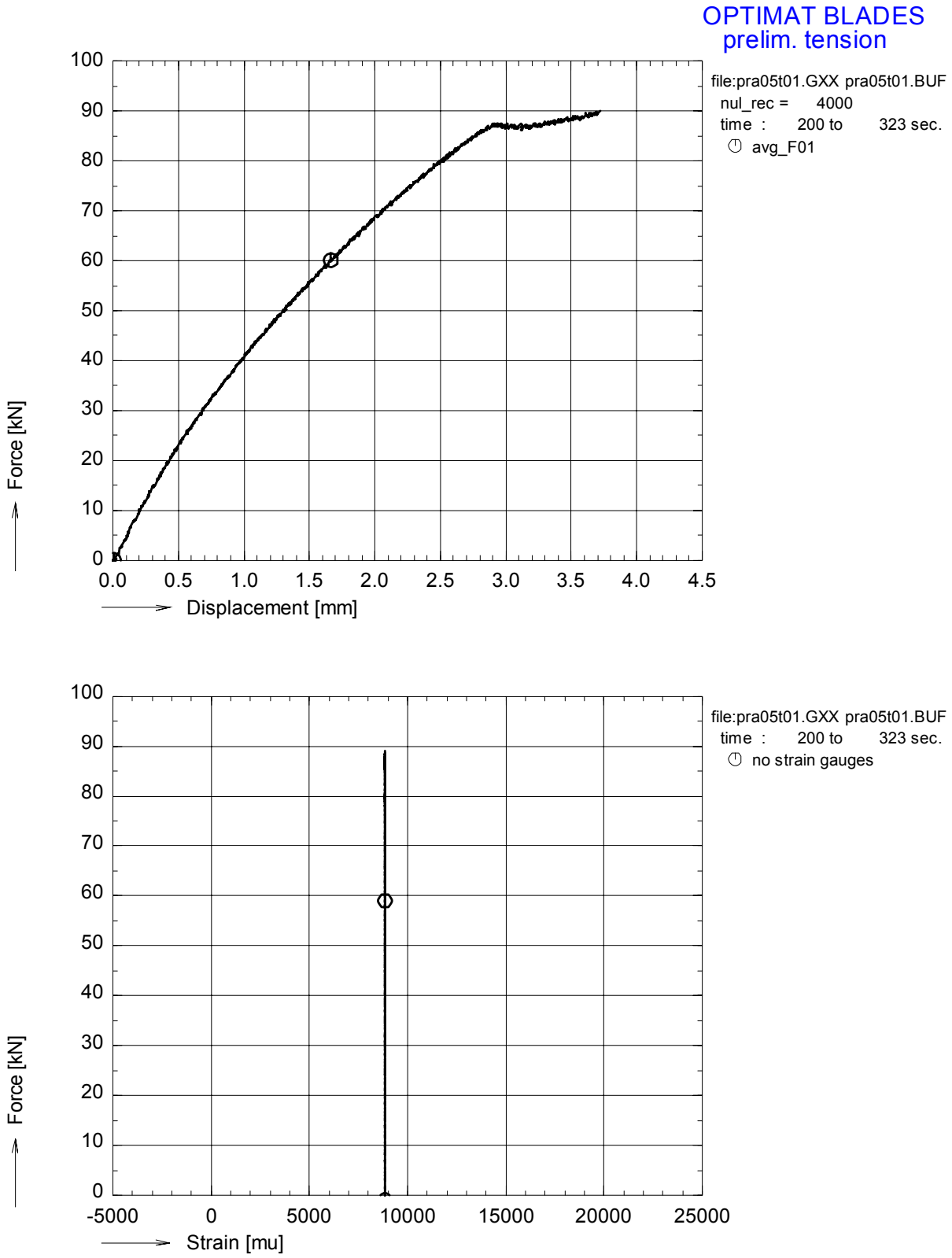

figure A 75: Axial tensile force vs. bench displacement and strains for pra05t01

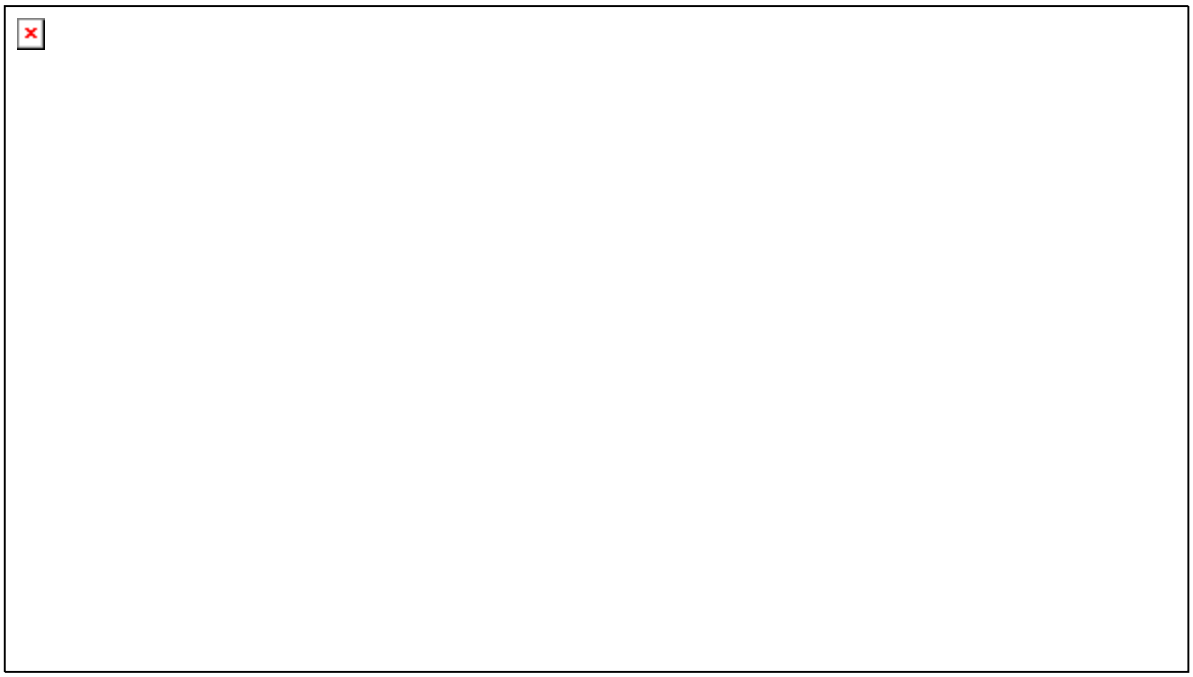

figure A 76: Photographs of failed specimen pra05t01

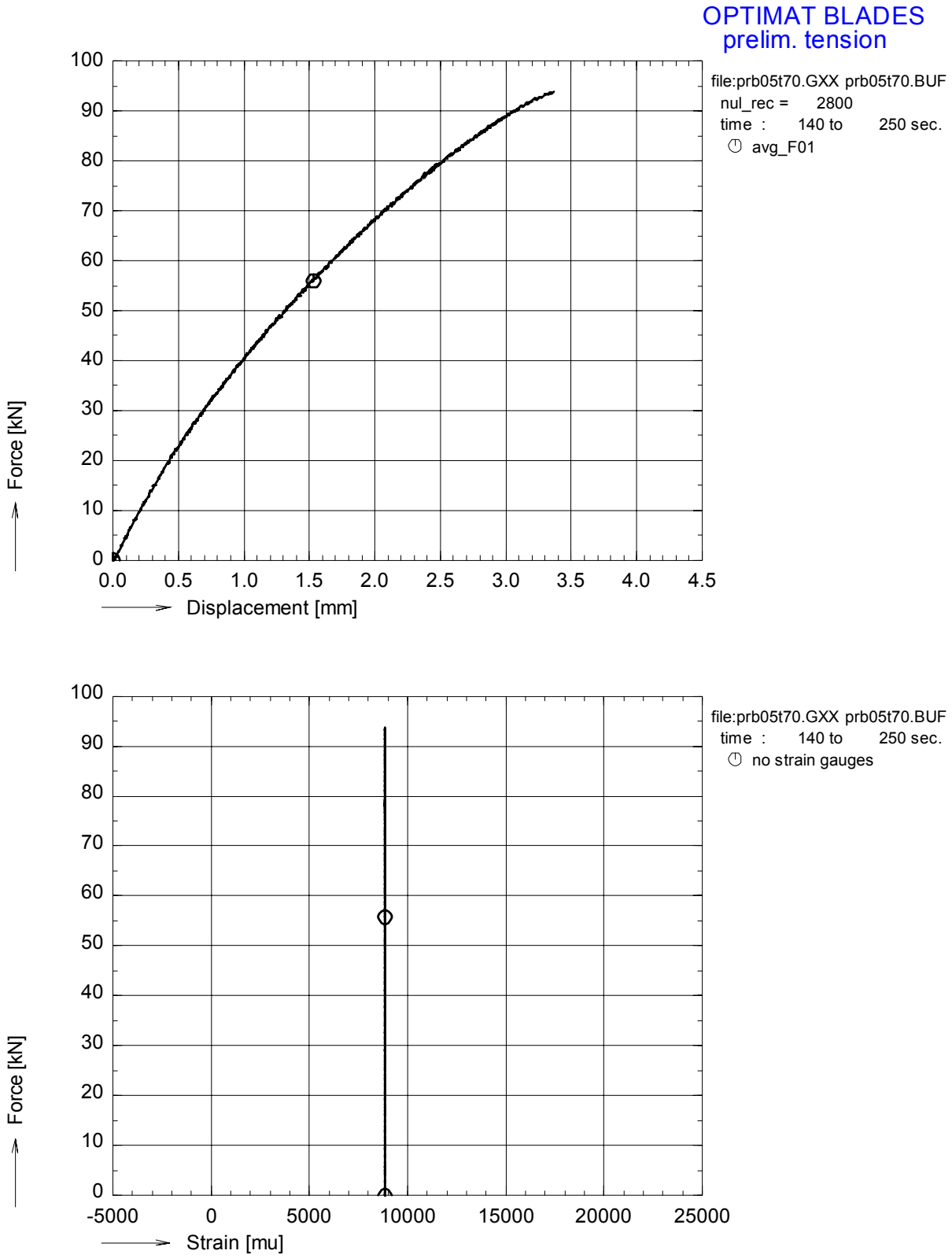

figure A 77: Axial tensile force vs. bench displacement and strains for prb05t70

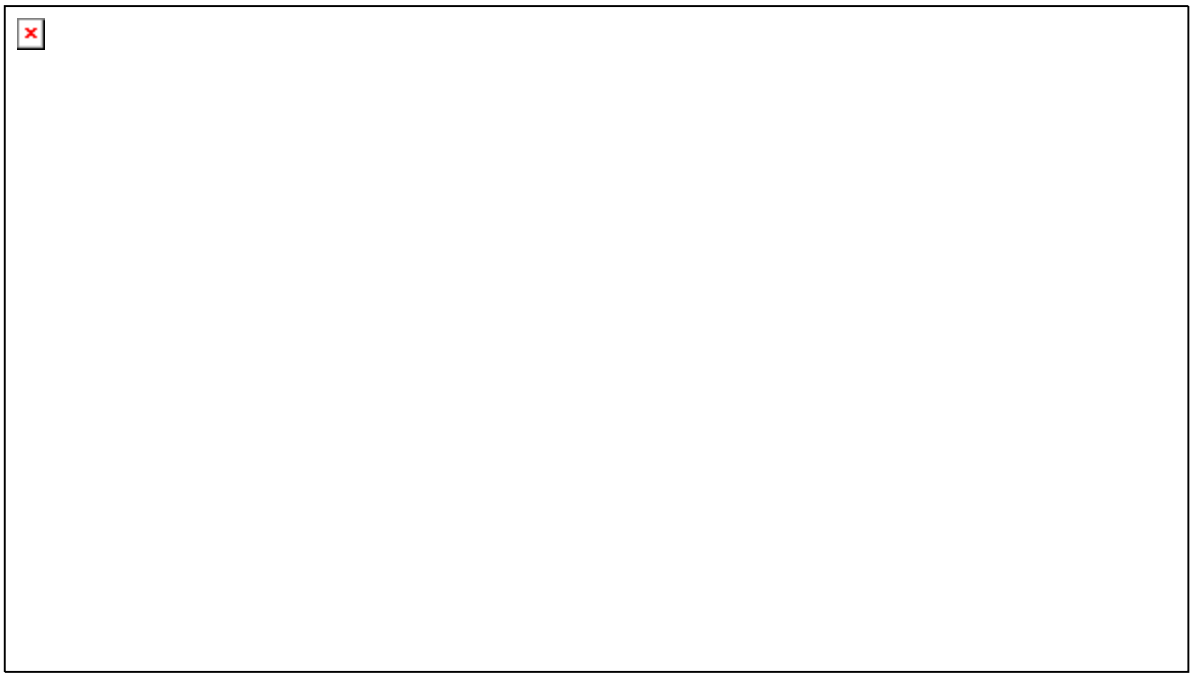

figure A 78: Photographs of failed specimen prb05t70

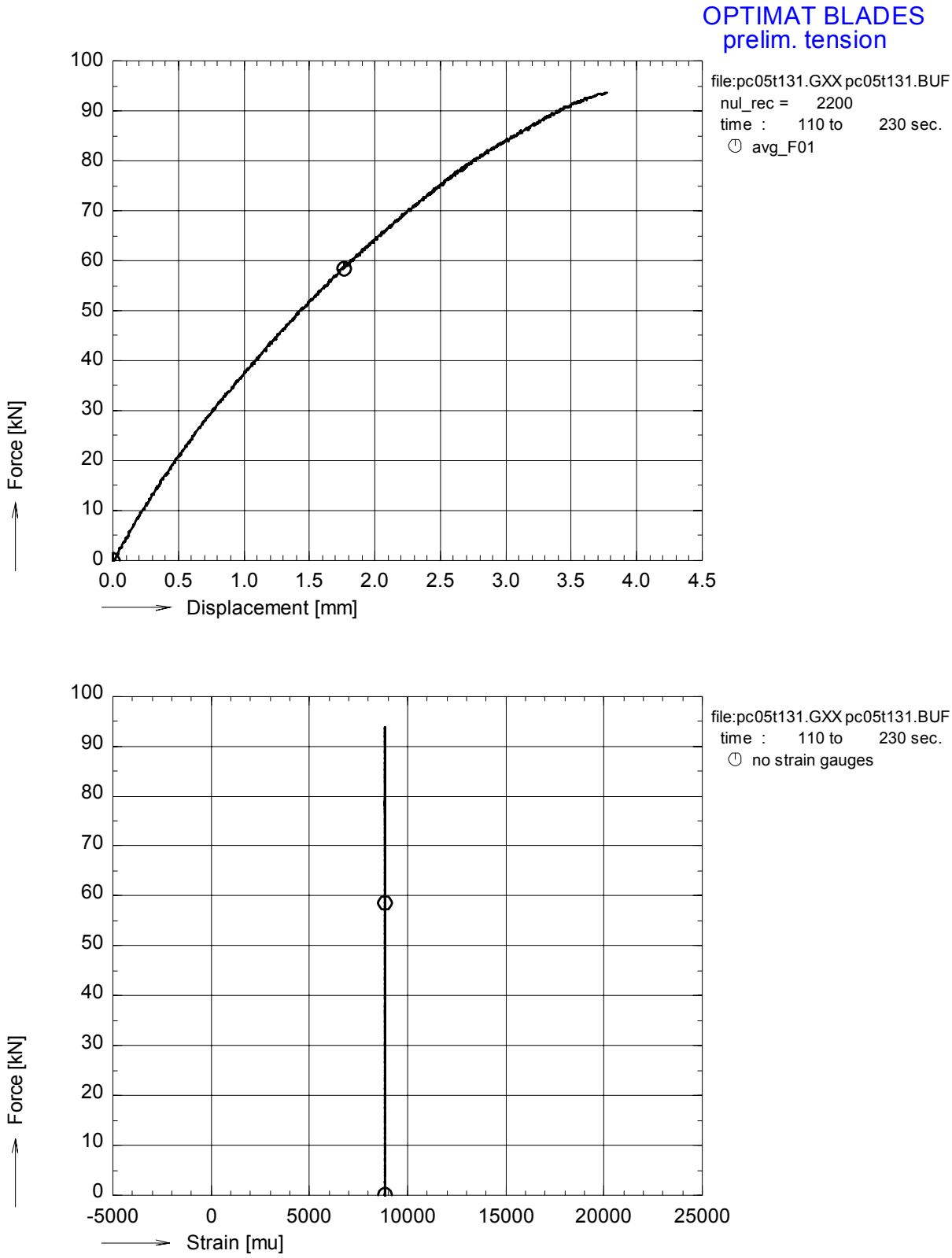

figure A 79: Axial tensile force vs. bench displacement and strains for pc05t131

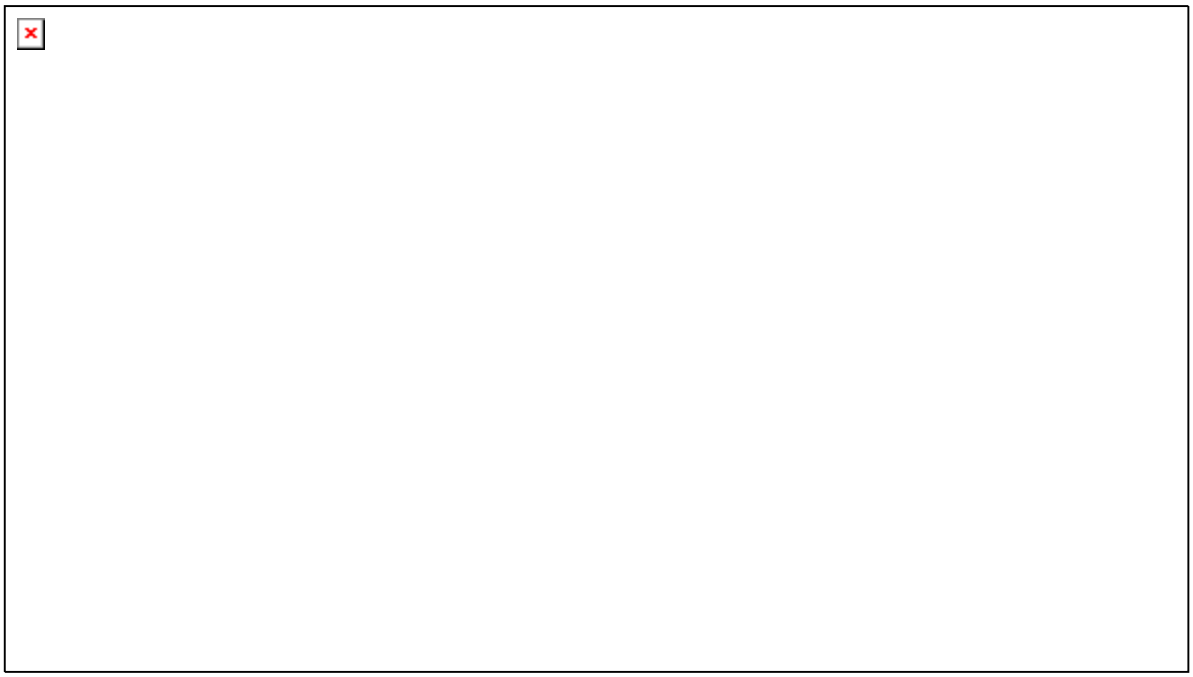

figure A 80: Photographs of failed specimen pc05t131

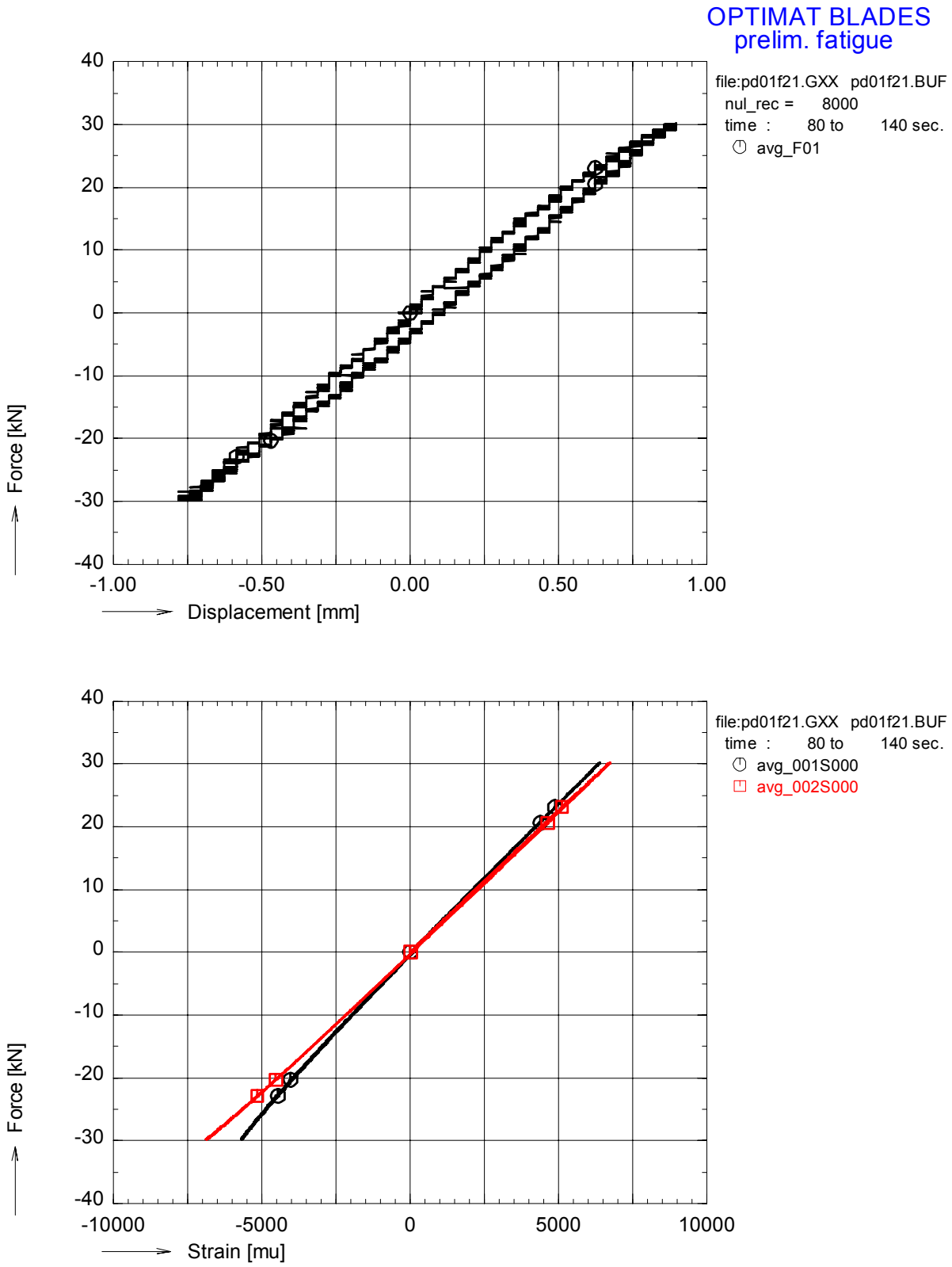

figure A 81: Force vs. bench displacement and strains during preceding slow cycle for pd01f21

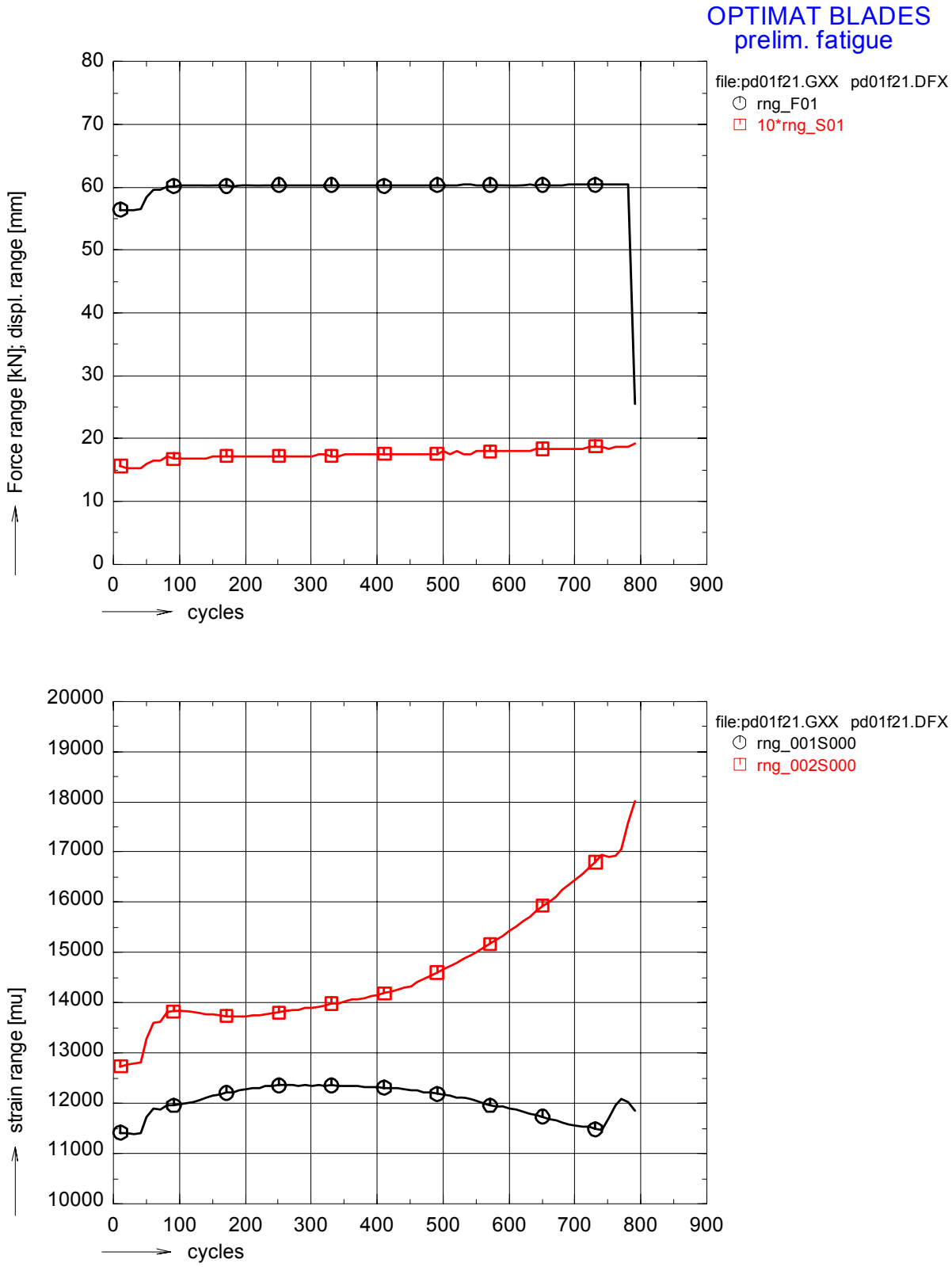

figure A 82: Ranges of force, bench displacement and strains during fatigue life for pd01f21

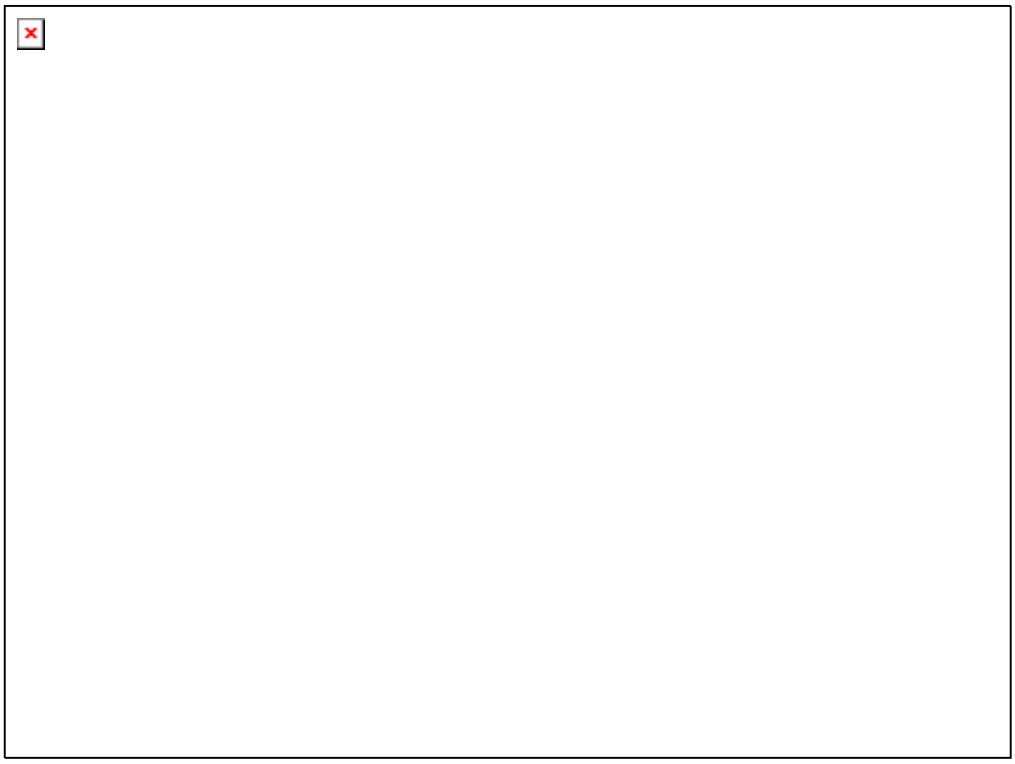

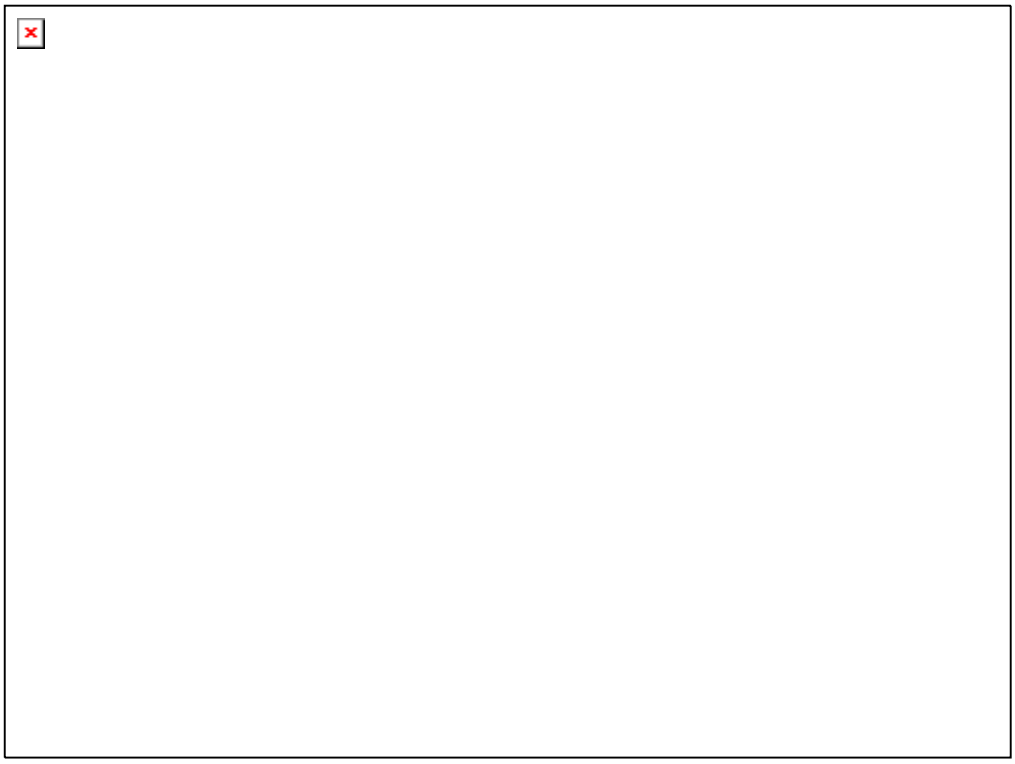

figure A 83: Photographs of failed specimen pd01f21

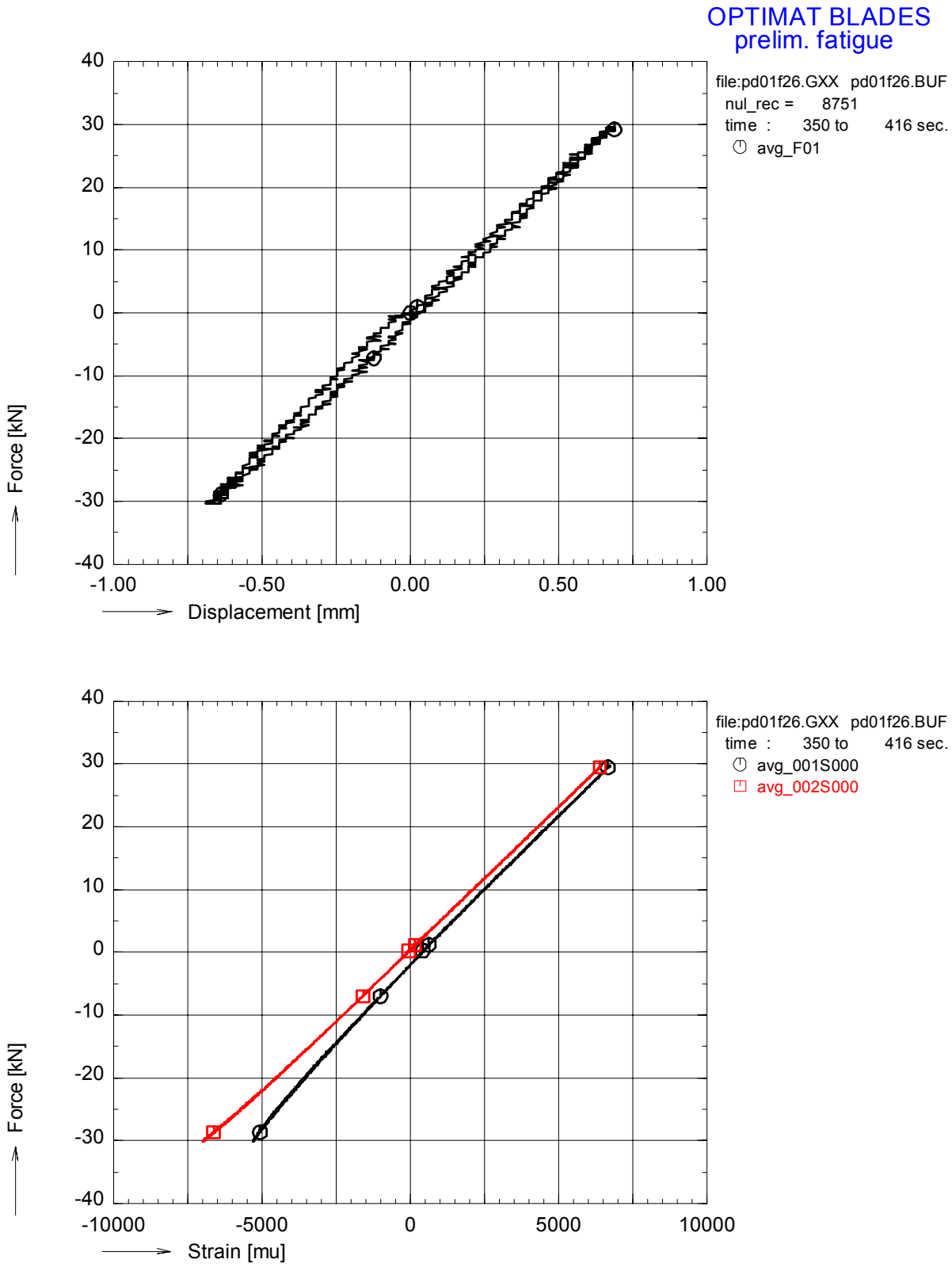

figure A 84: Axial force vs. bench displacement and strains during preceding slow cycle for pd01f26

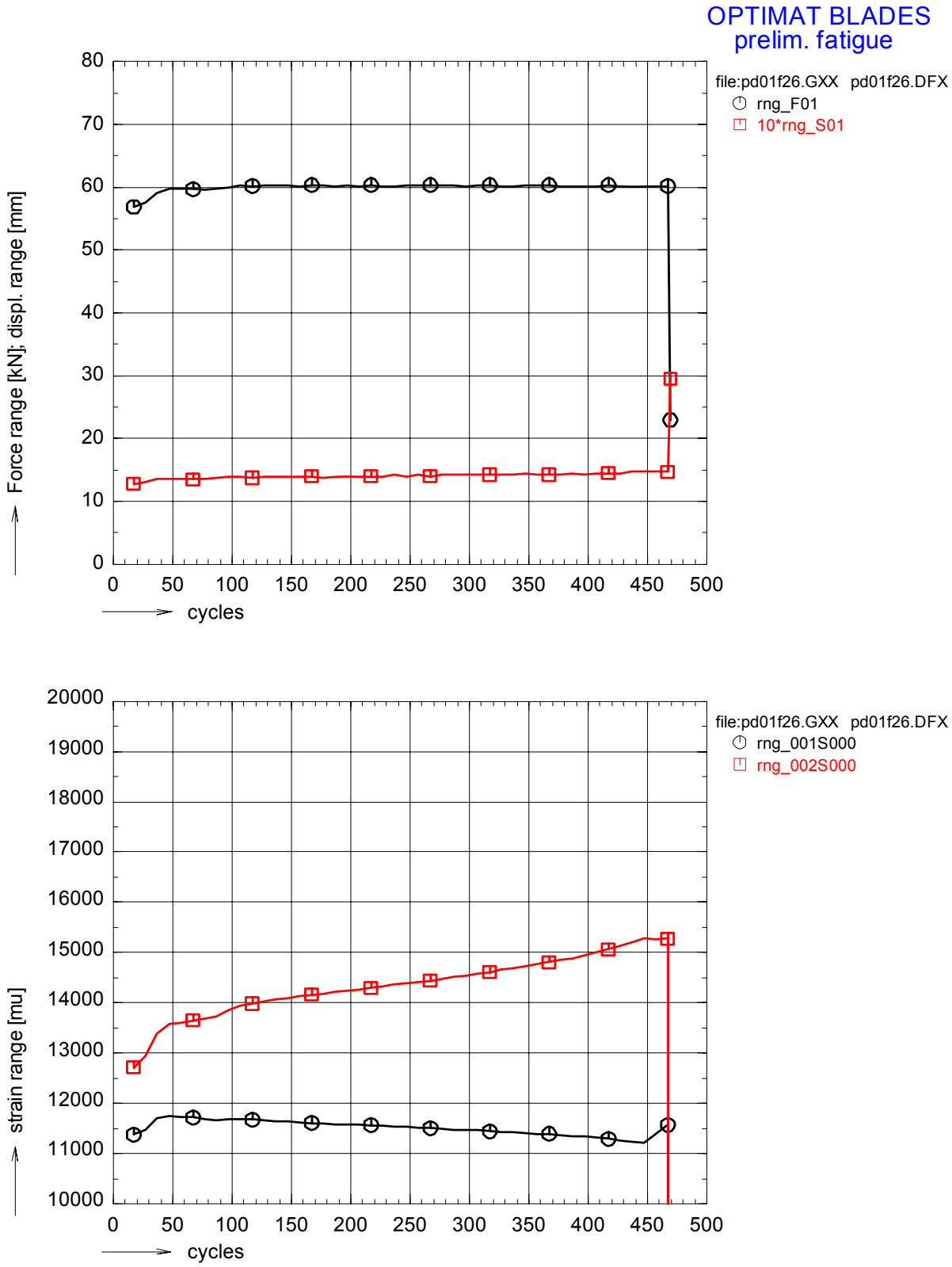

figure A 85: Ranges of force, bench displacement and strains during fatigue life for pd01f26

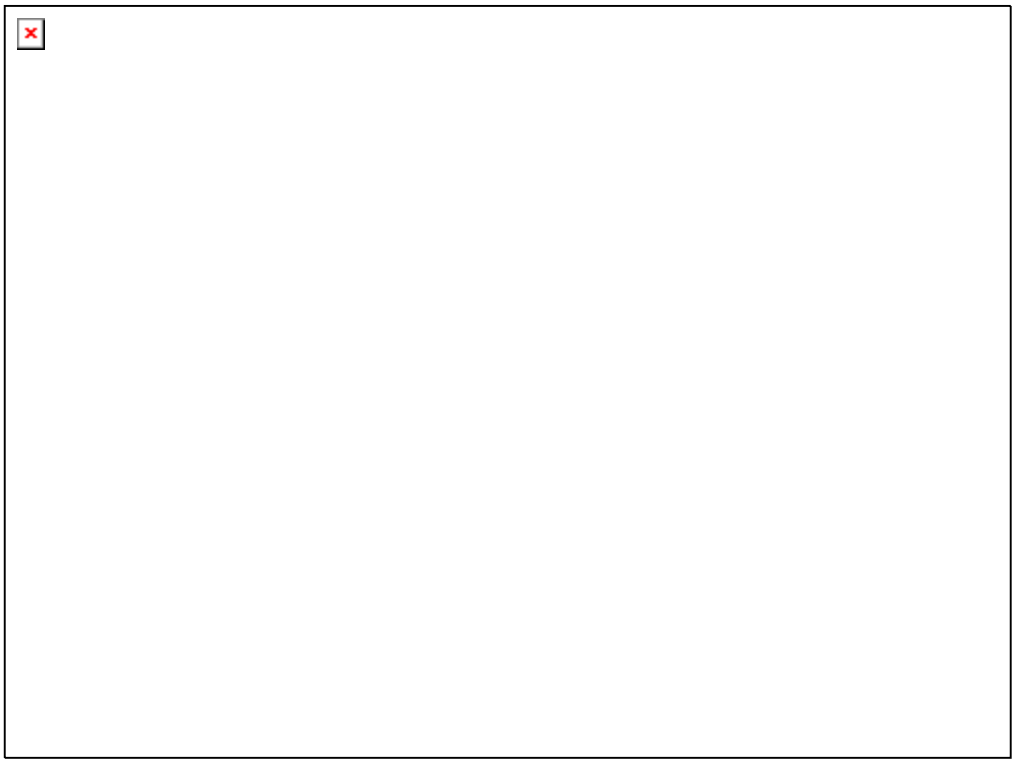

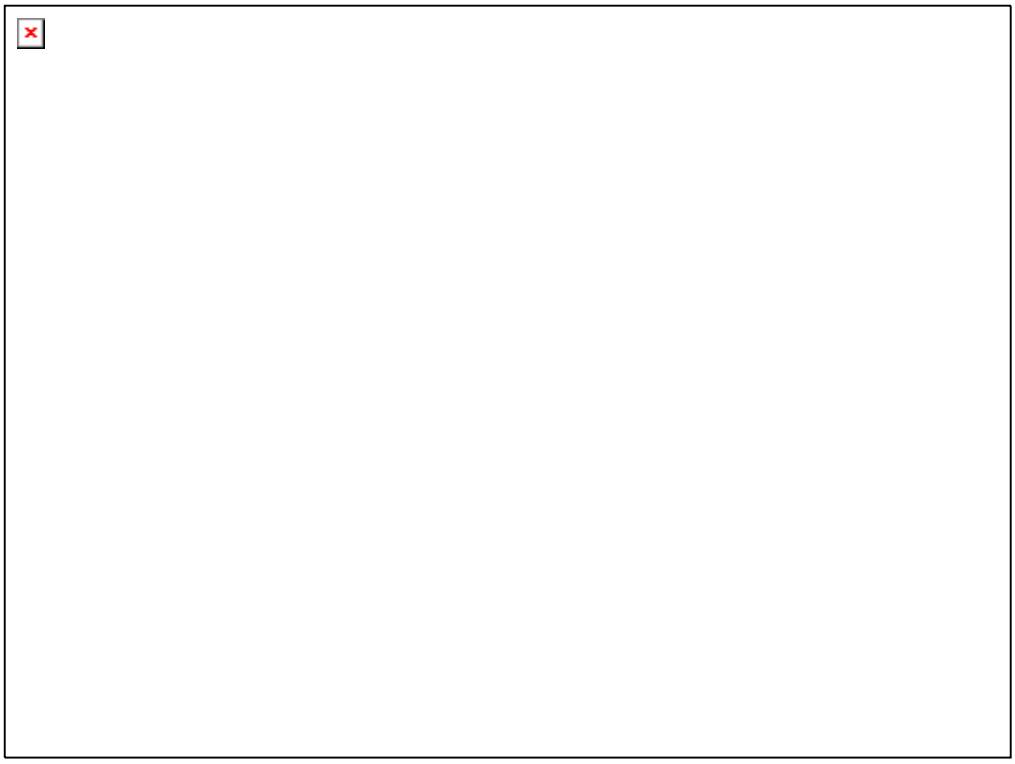

figure A 86: Photographs of failed specimen pd01f26

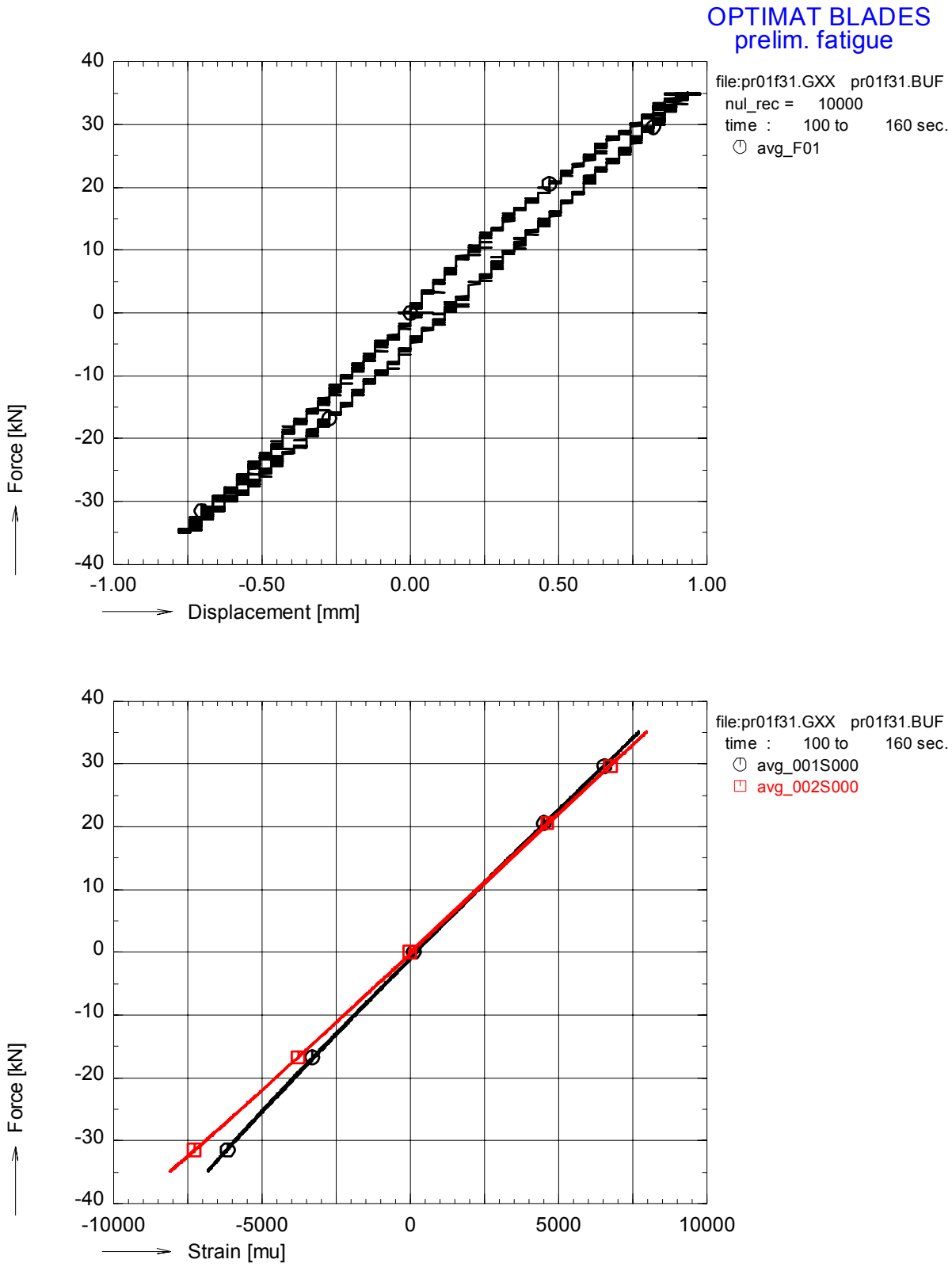

figure A 87: Axial force vs. bench displacement and strains during preceding slow cycle for pr01f31

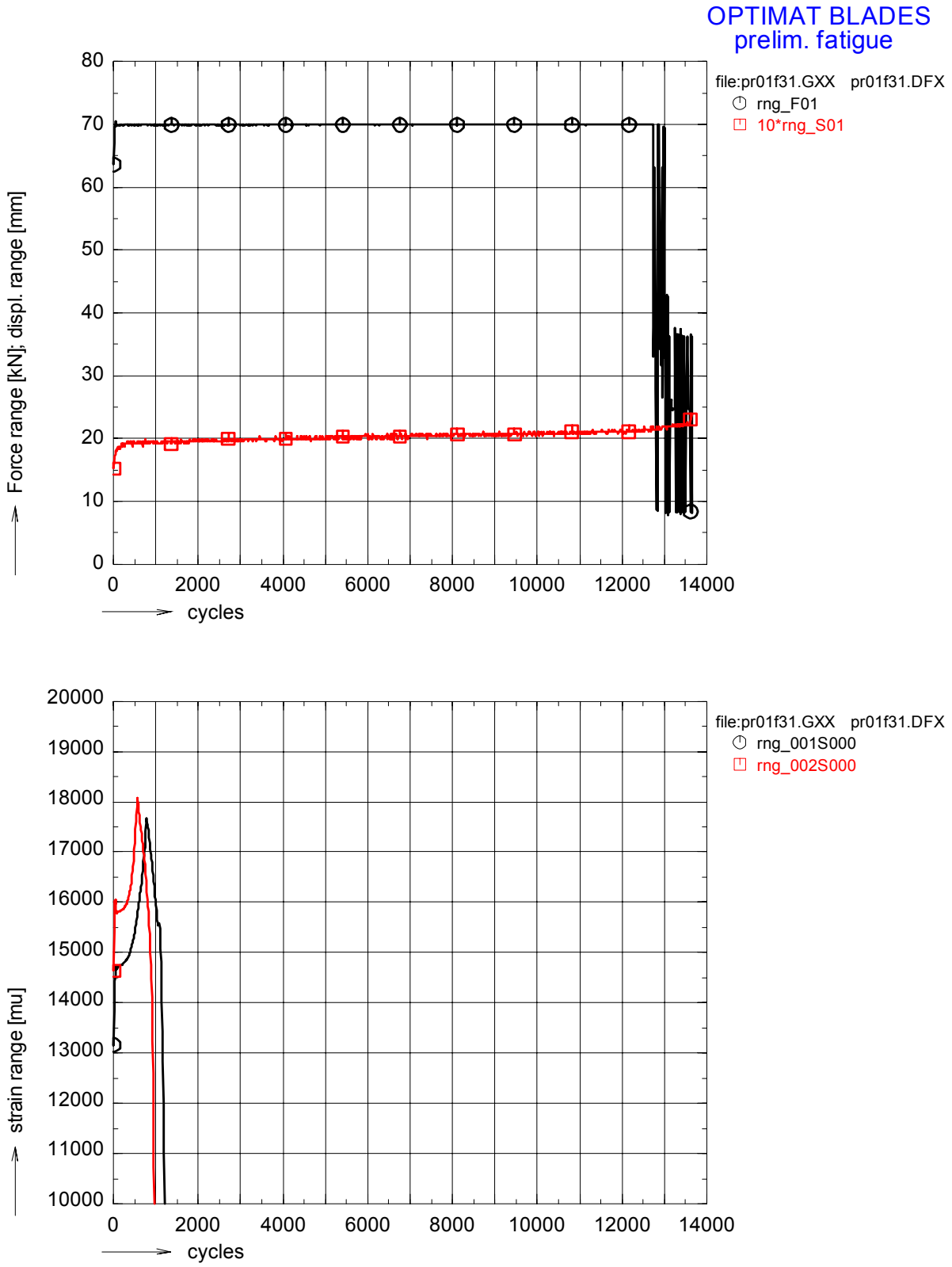

figure A 88: Ranges of force, bench displacement and strains during fatigue life for pr01f31

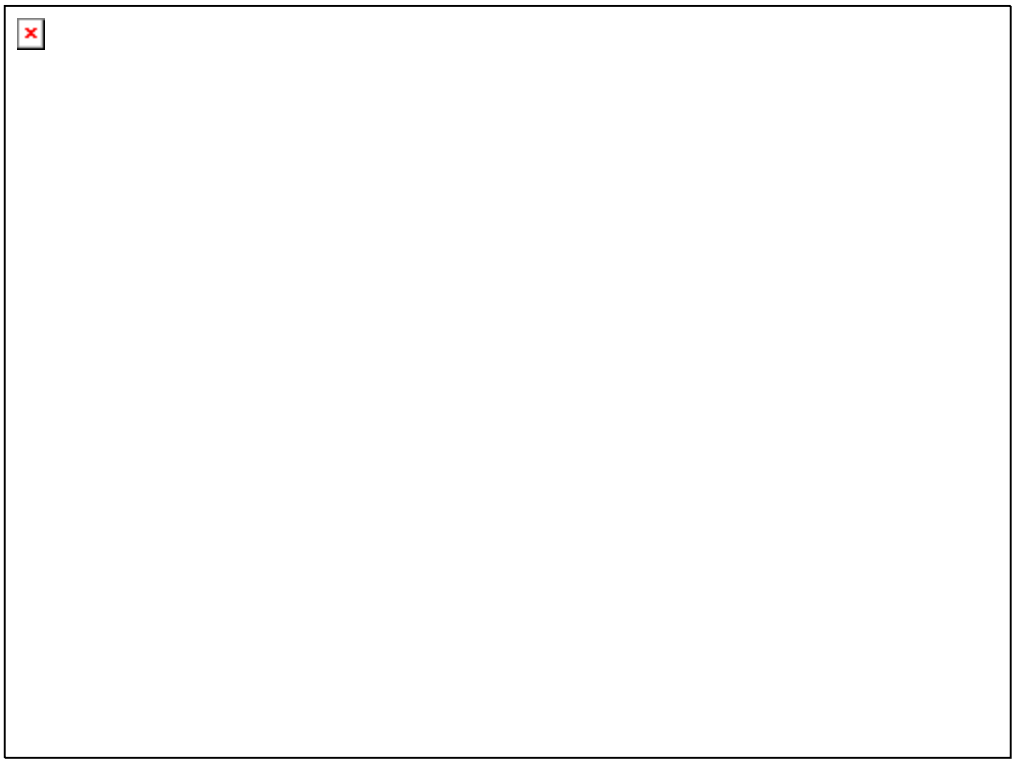

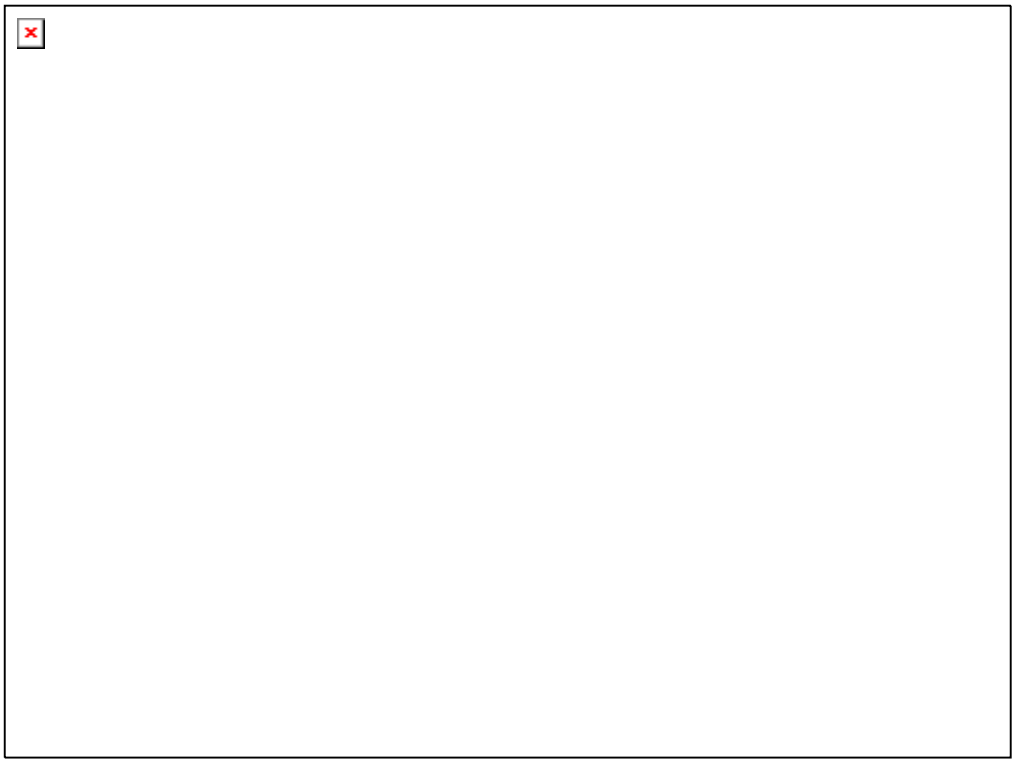

figure A 89: Photographs of failed specimen pr01f31

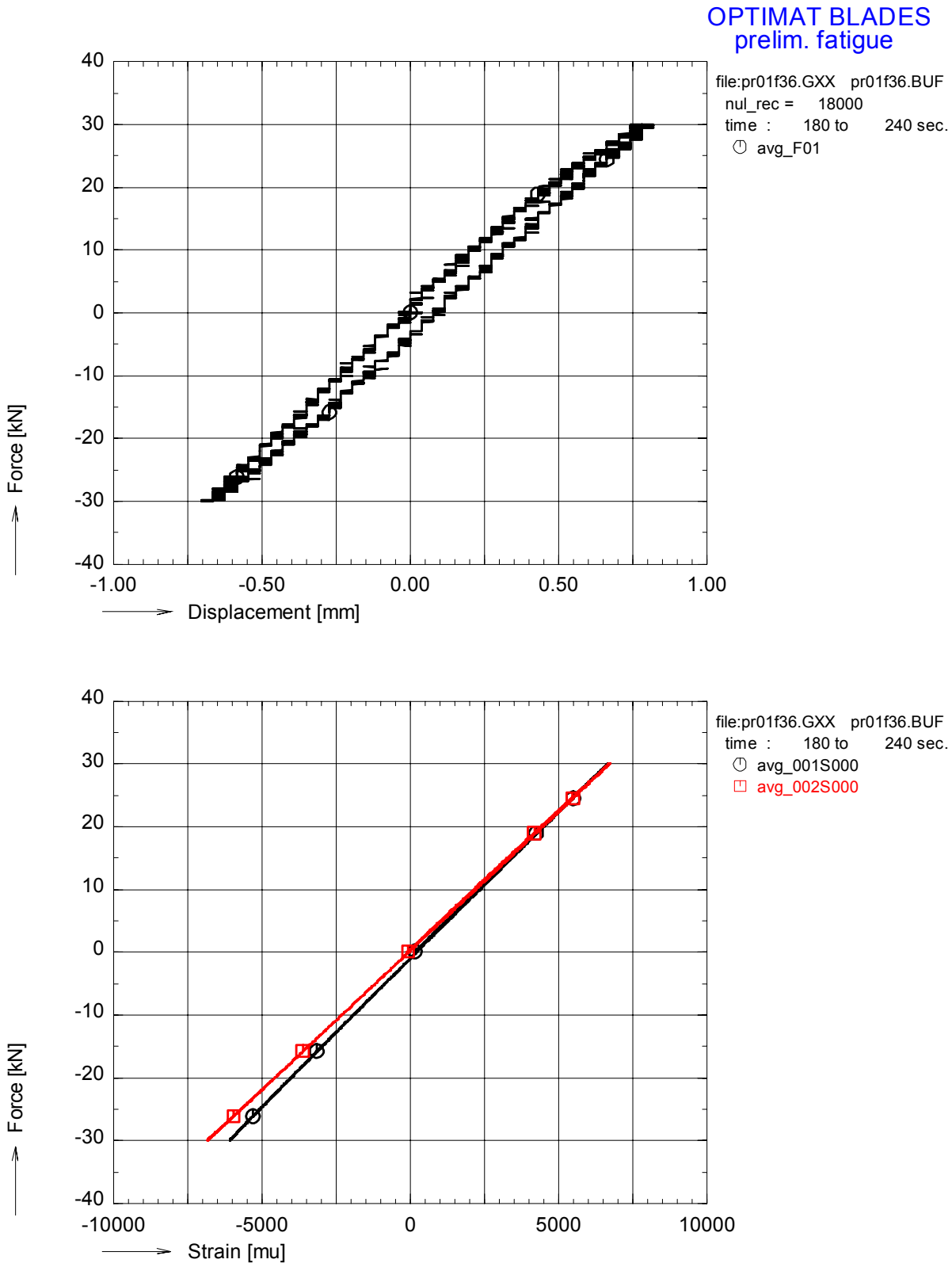

figure A 90: Axial force vs. bench displacement and strains during preceding slow cycle for pr01f36

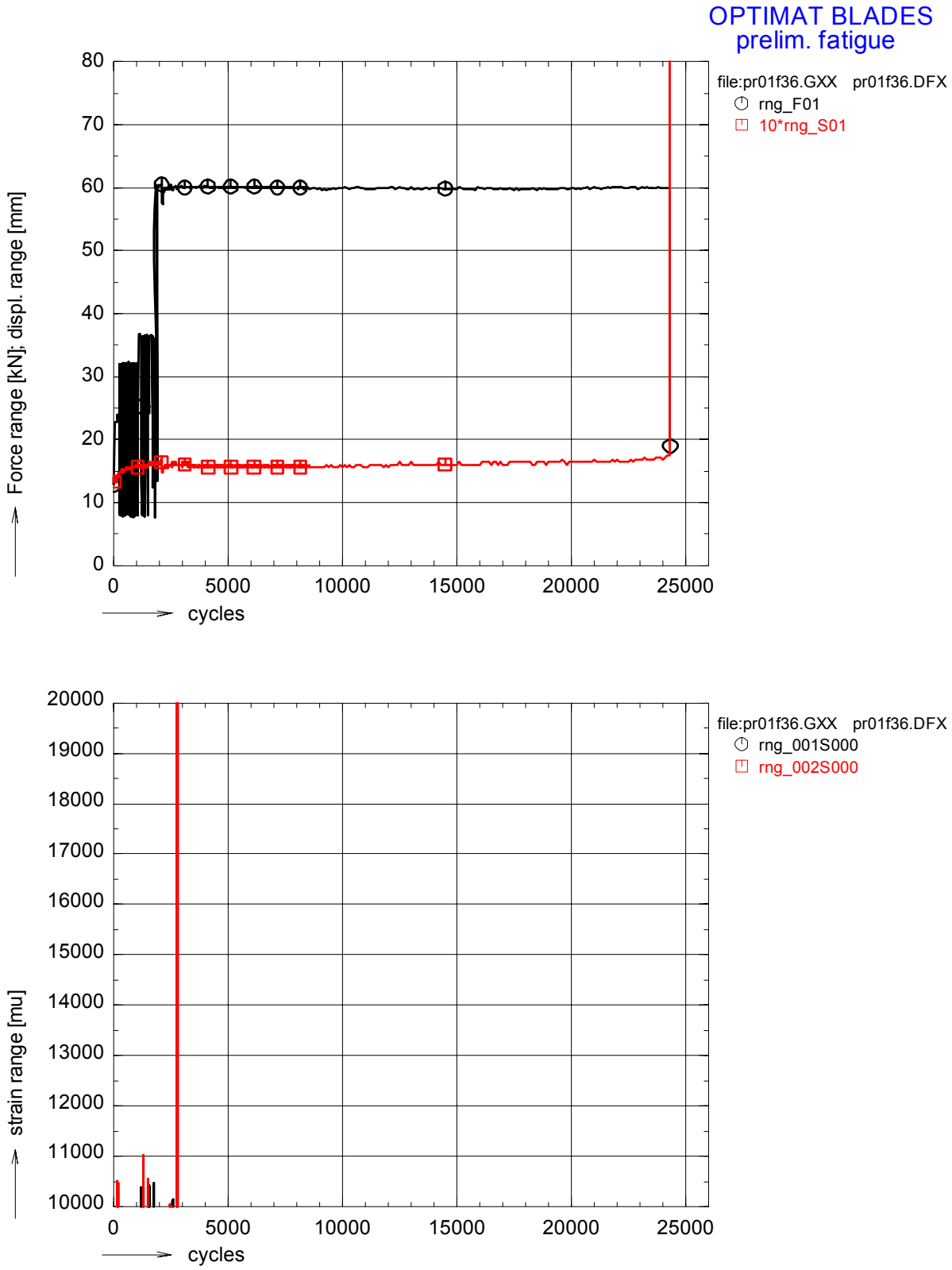

figure A 91: Ranges of force, bench displacement and strains during fatigue life for pr01f36

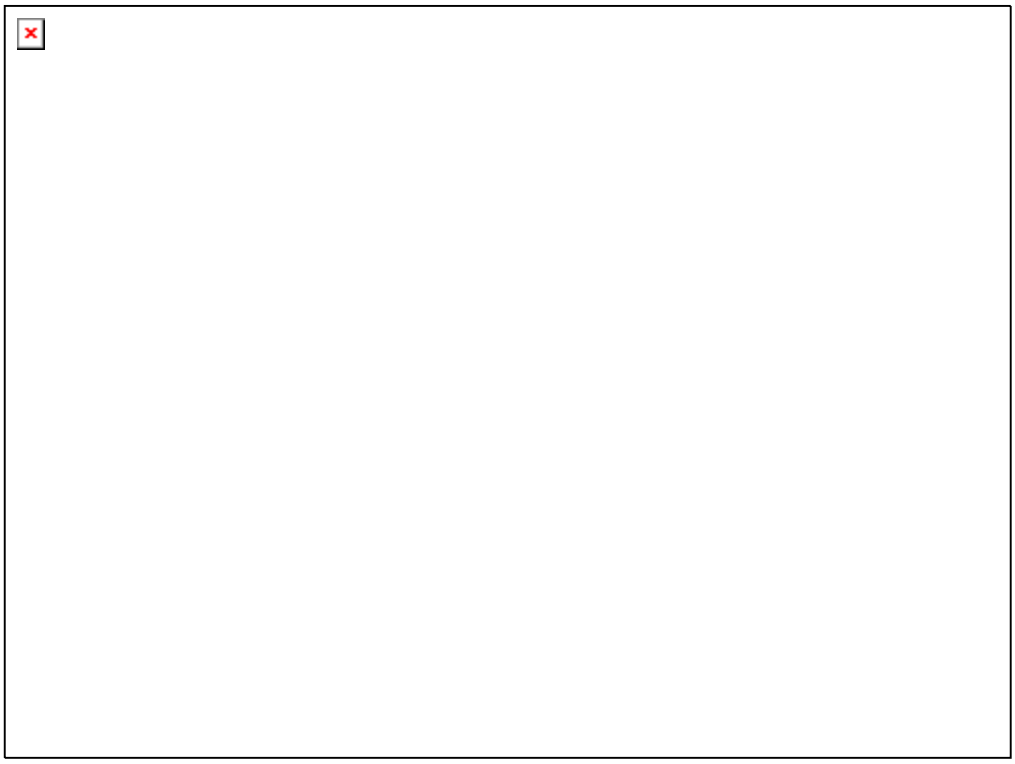

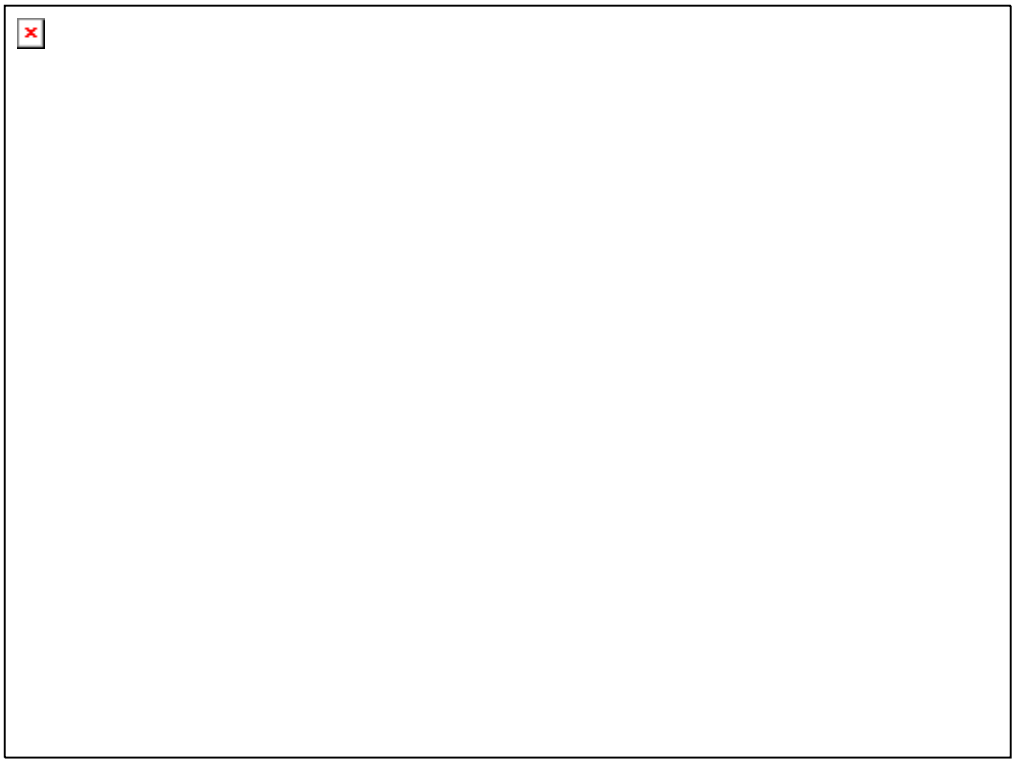

figure A 92: Photographs of failed specimen pr01f36

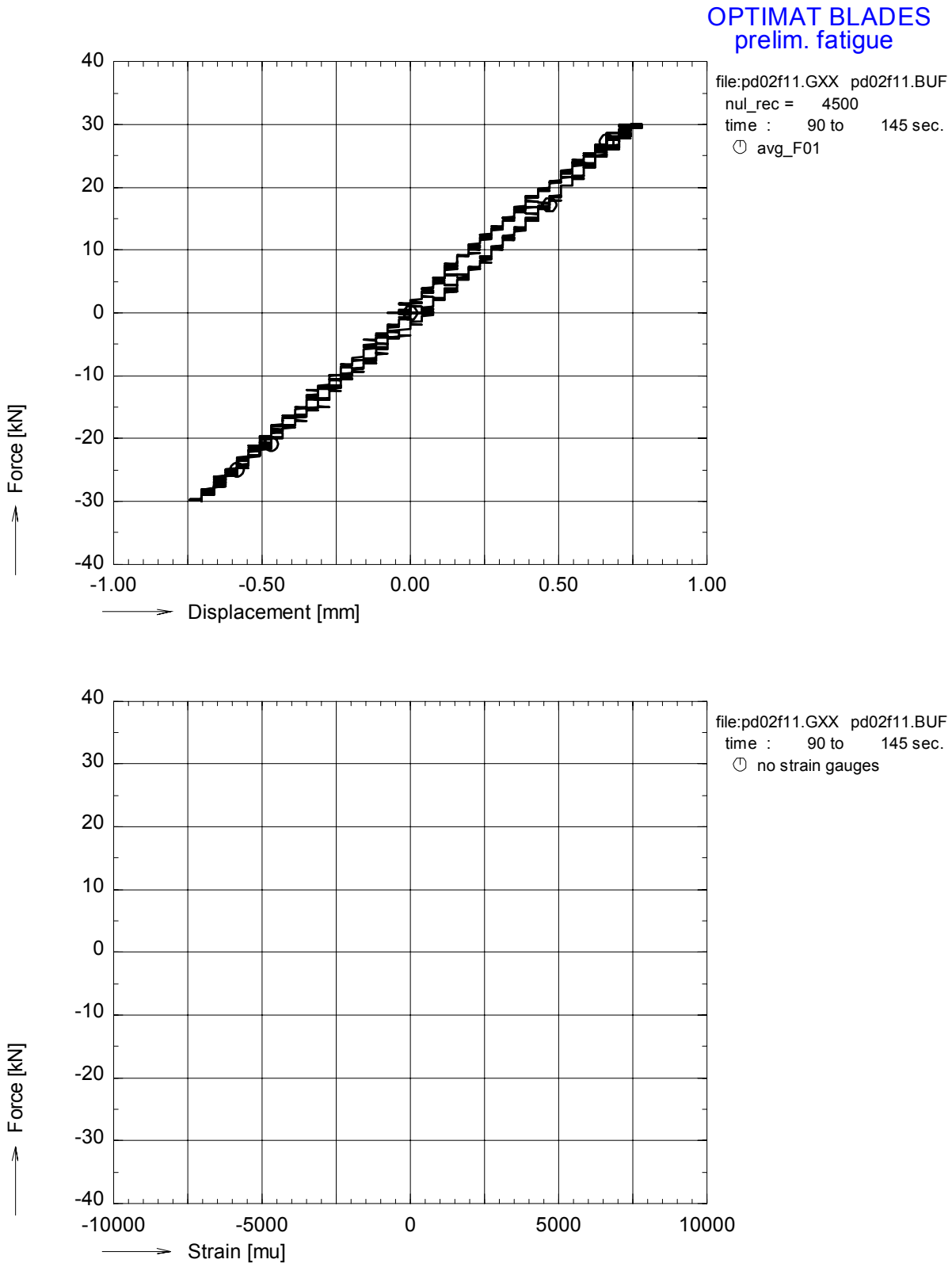

figure A 93: Axial force vs. bench displacement and strains during preceding slow cycle for pd02f11

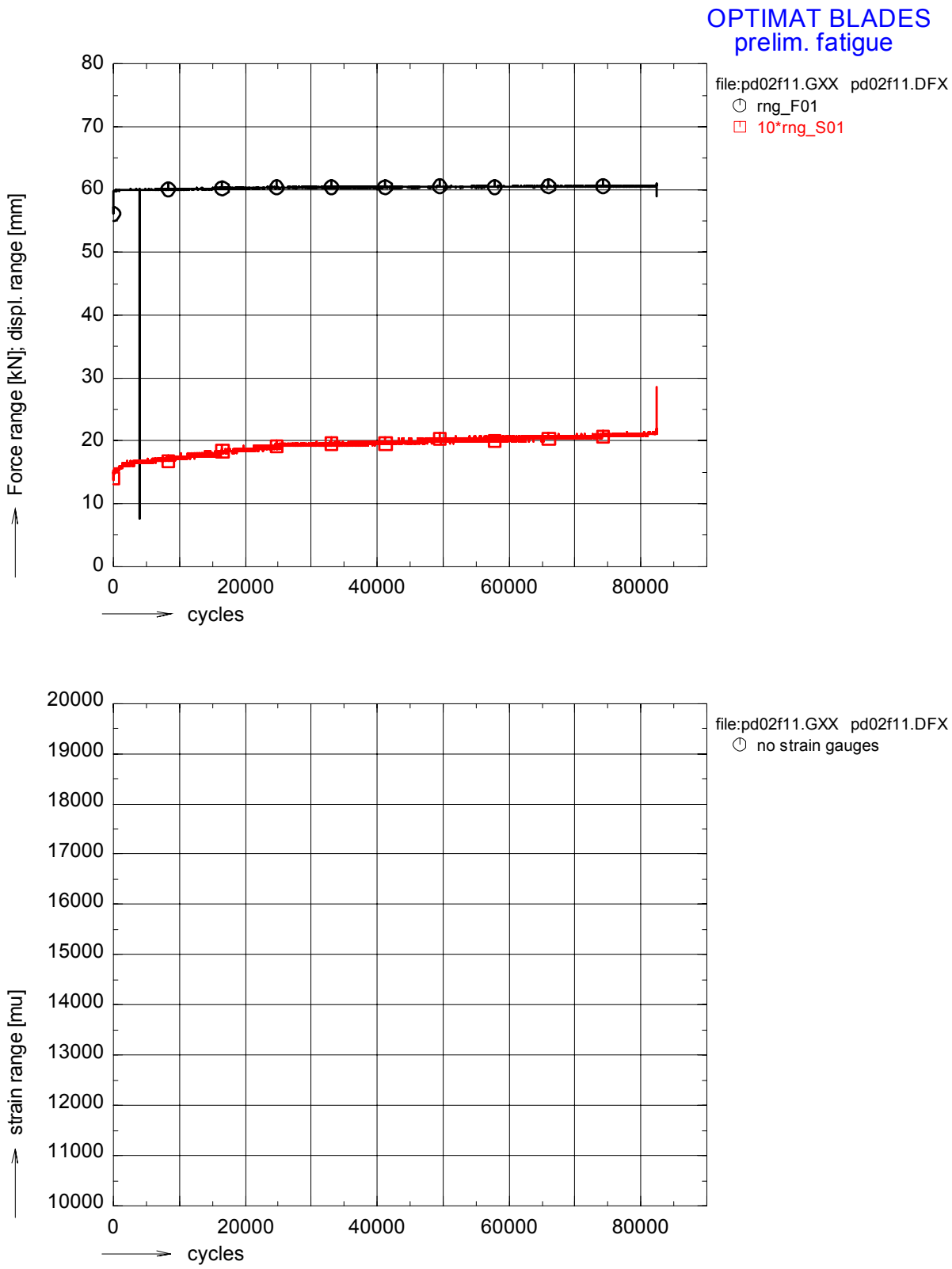

figure A 94: Ranges of force, bench displacement and strains during fatigue life for pd02f11

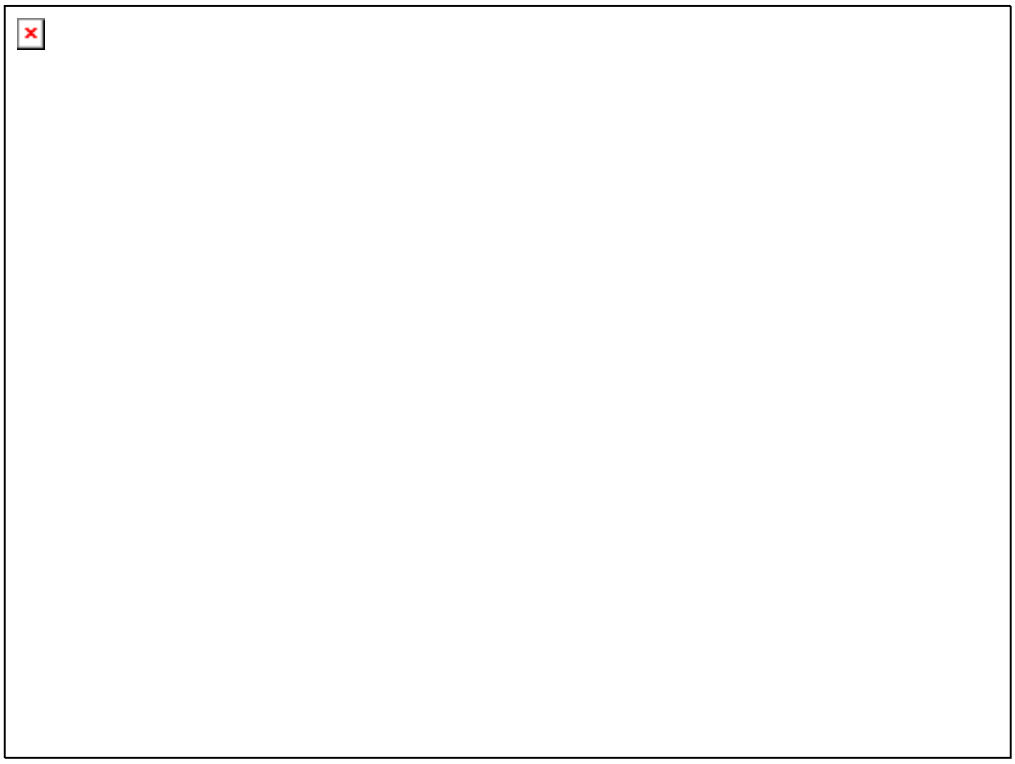

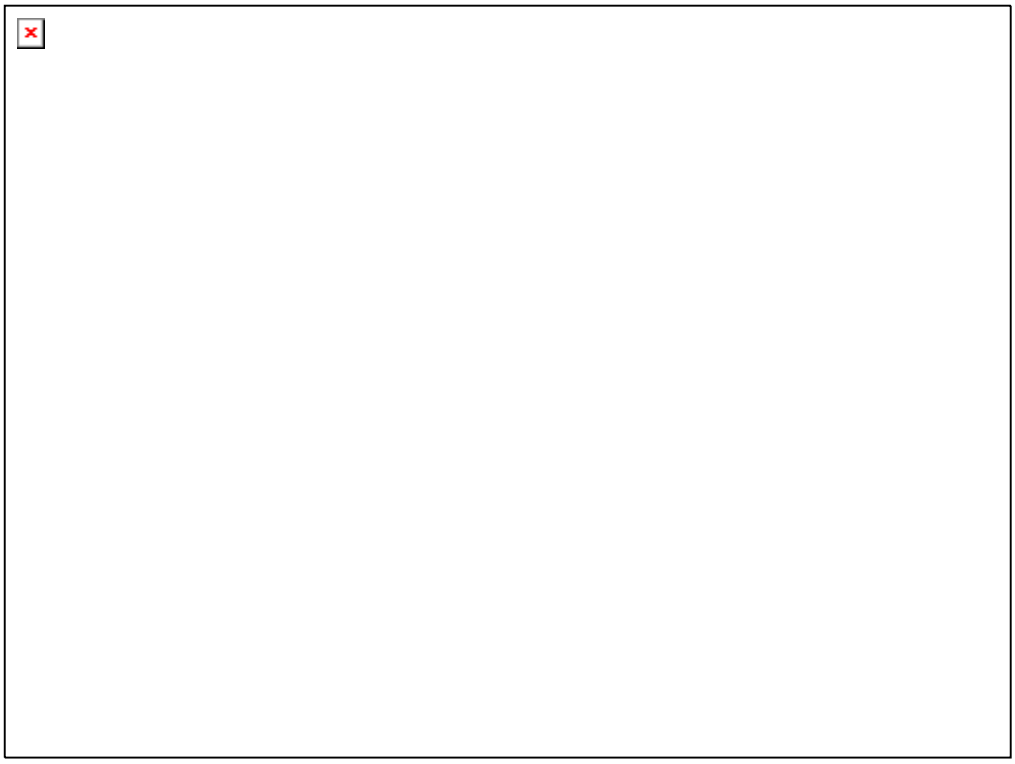

figure A 95: Photographs of failed specimen pd02f11

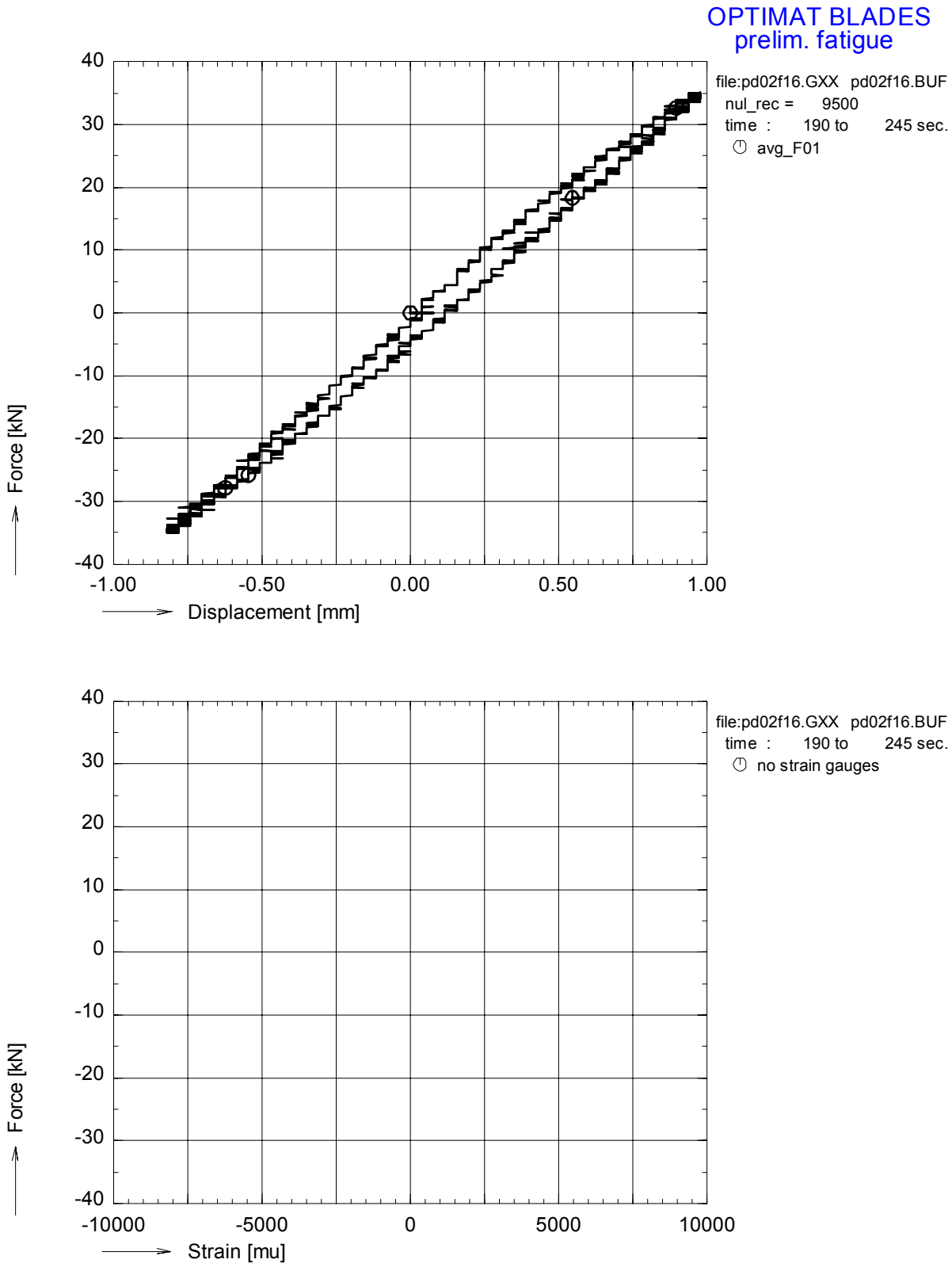

figure A 96: Axial force vs. bench displacement and strains during preceding slow cycle for pd02f16

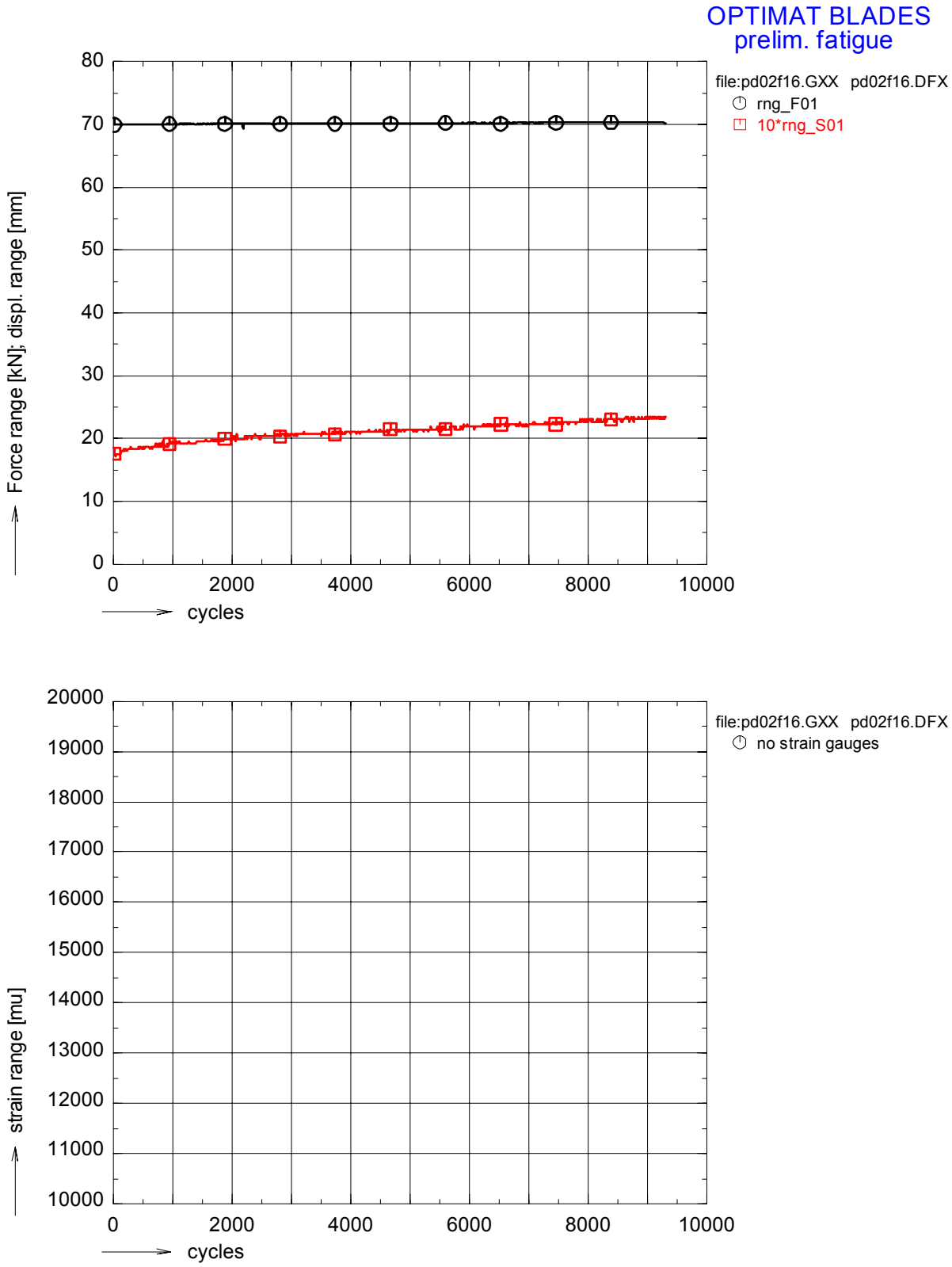

figure A 97: Ranges of force, bench displacement and strains during fatigue life for pd02f16

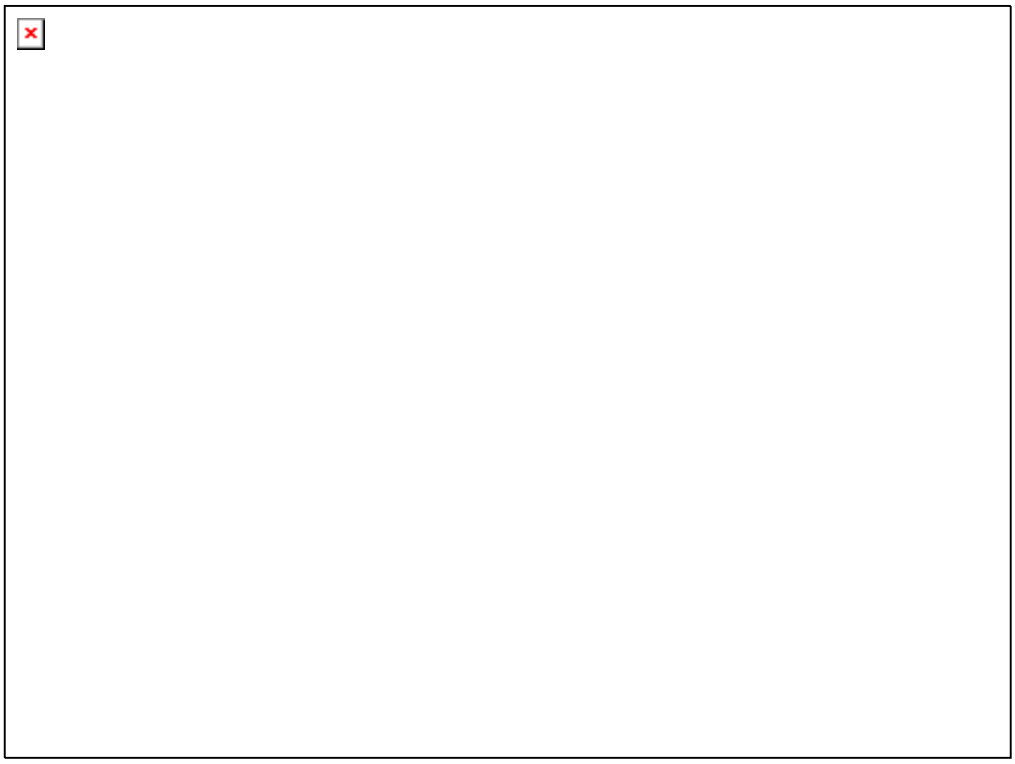

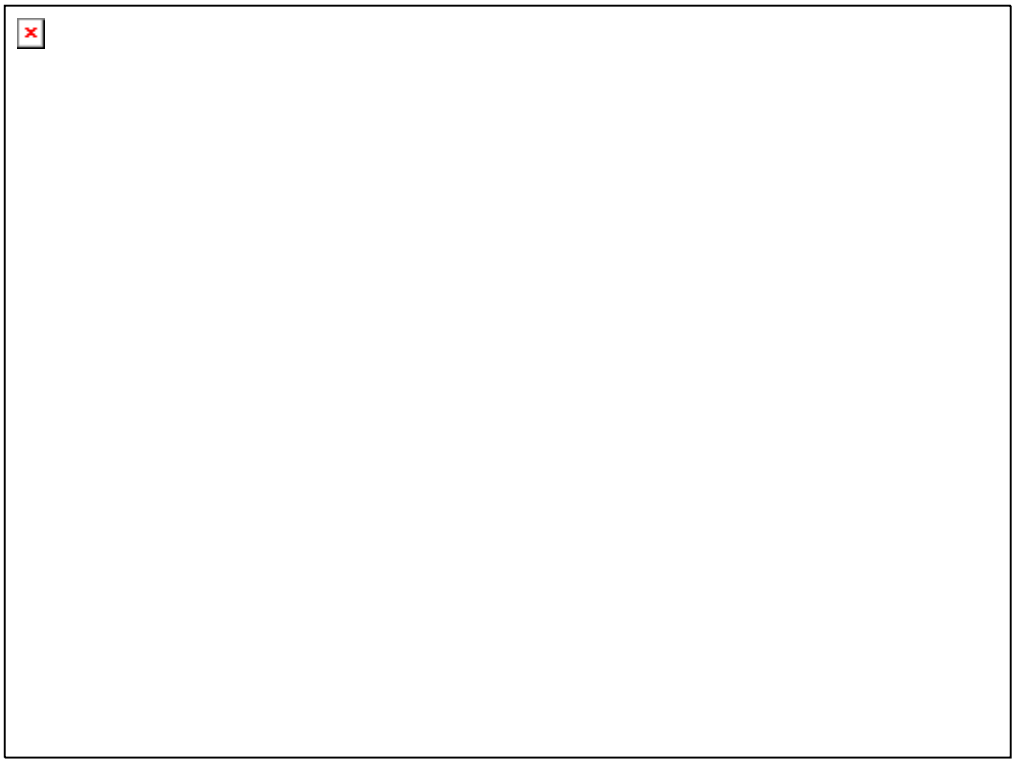

figure A 98: Photographs of failed specimen pd02f16

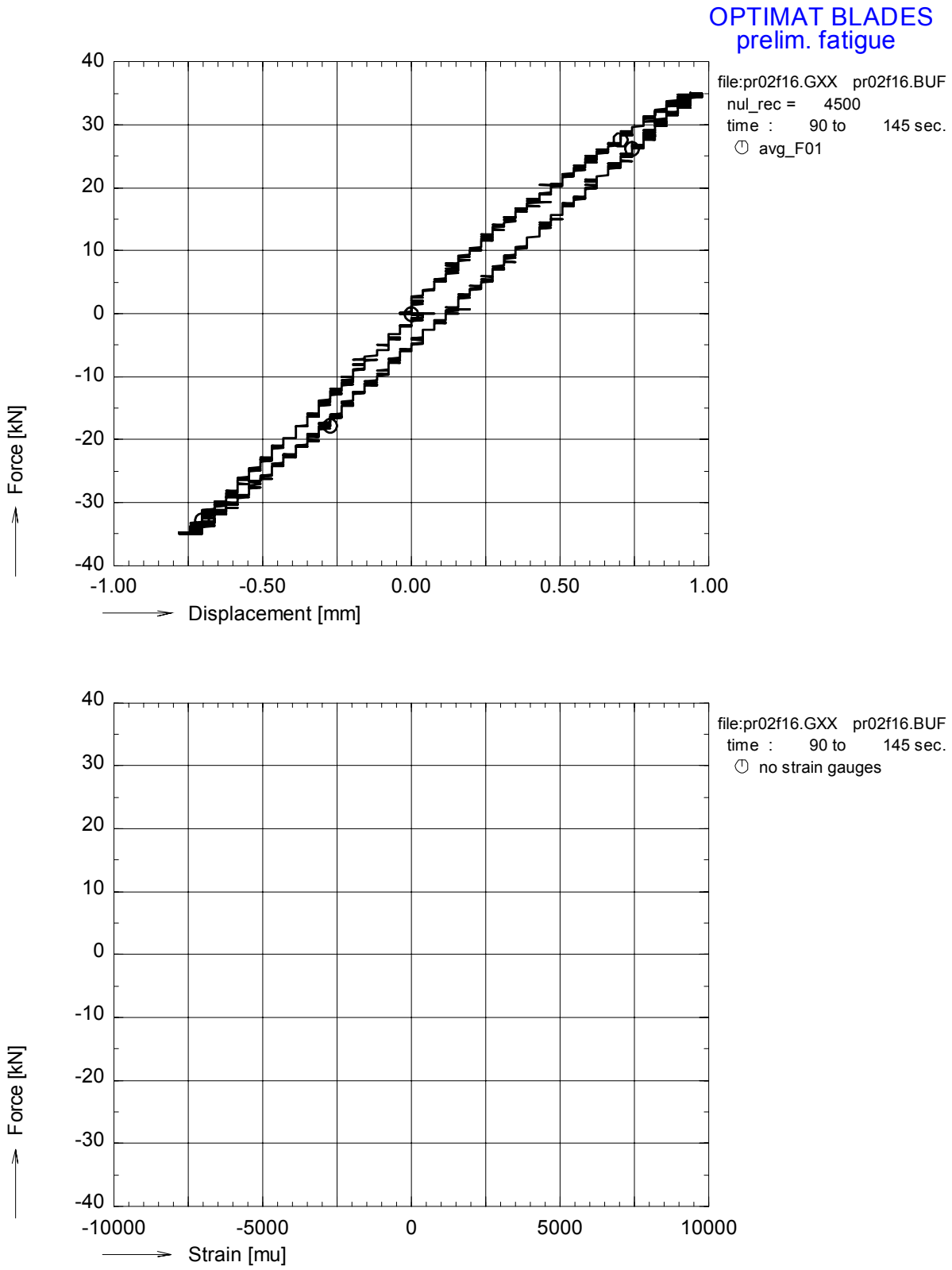

figure A 99: Axial force vs. bench displacement and strains during preceding slow cycle for pr02f16

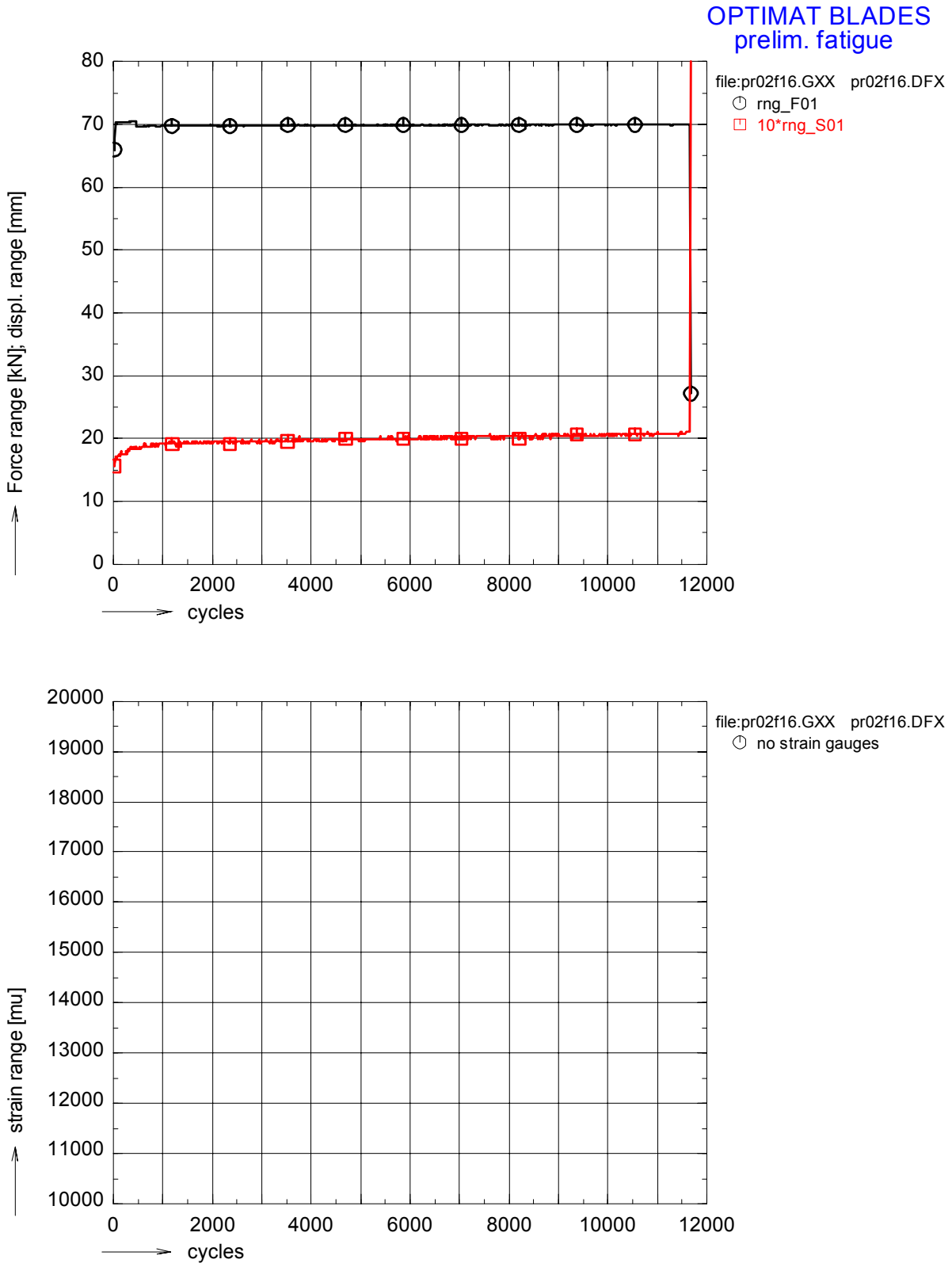

figure A 100: Ranges of force, bench displacement and strains during fatigue life for pr02f16

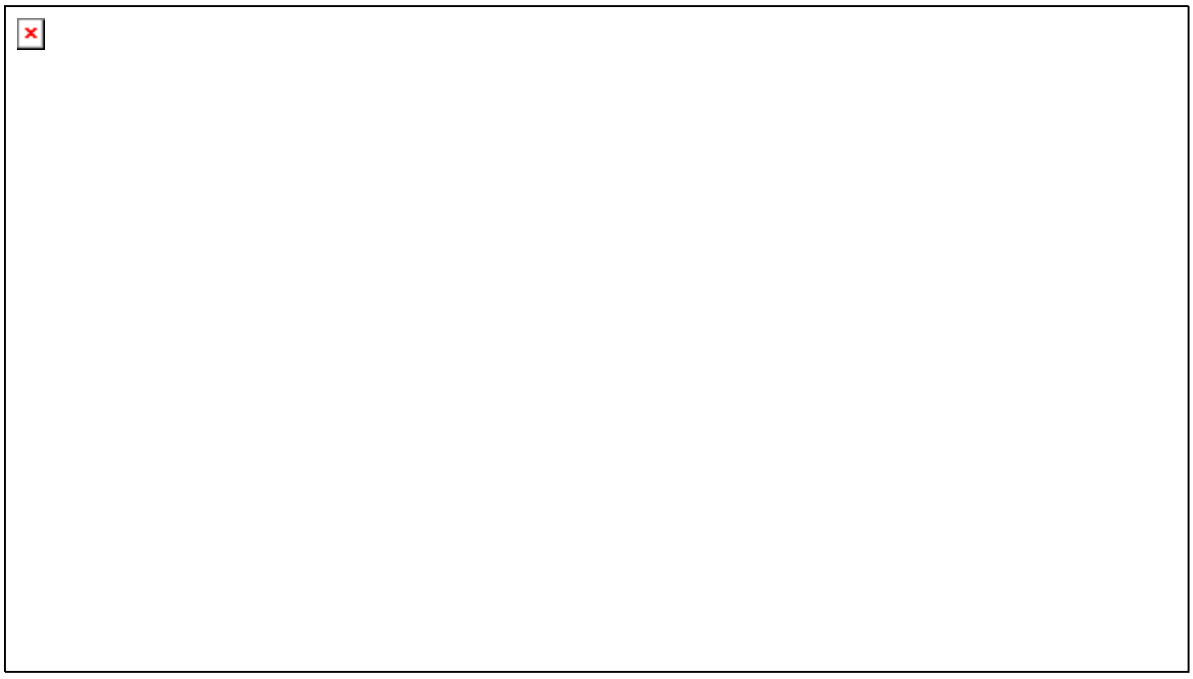

figure A 101: Photographs of failed specimen pr02f16

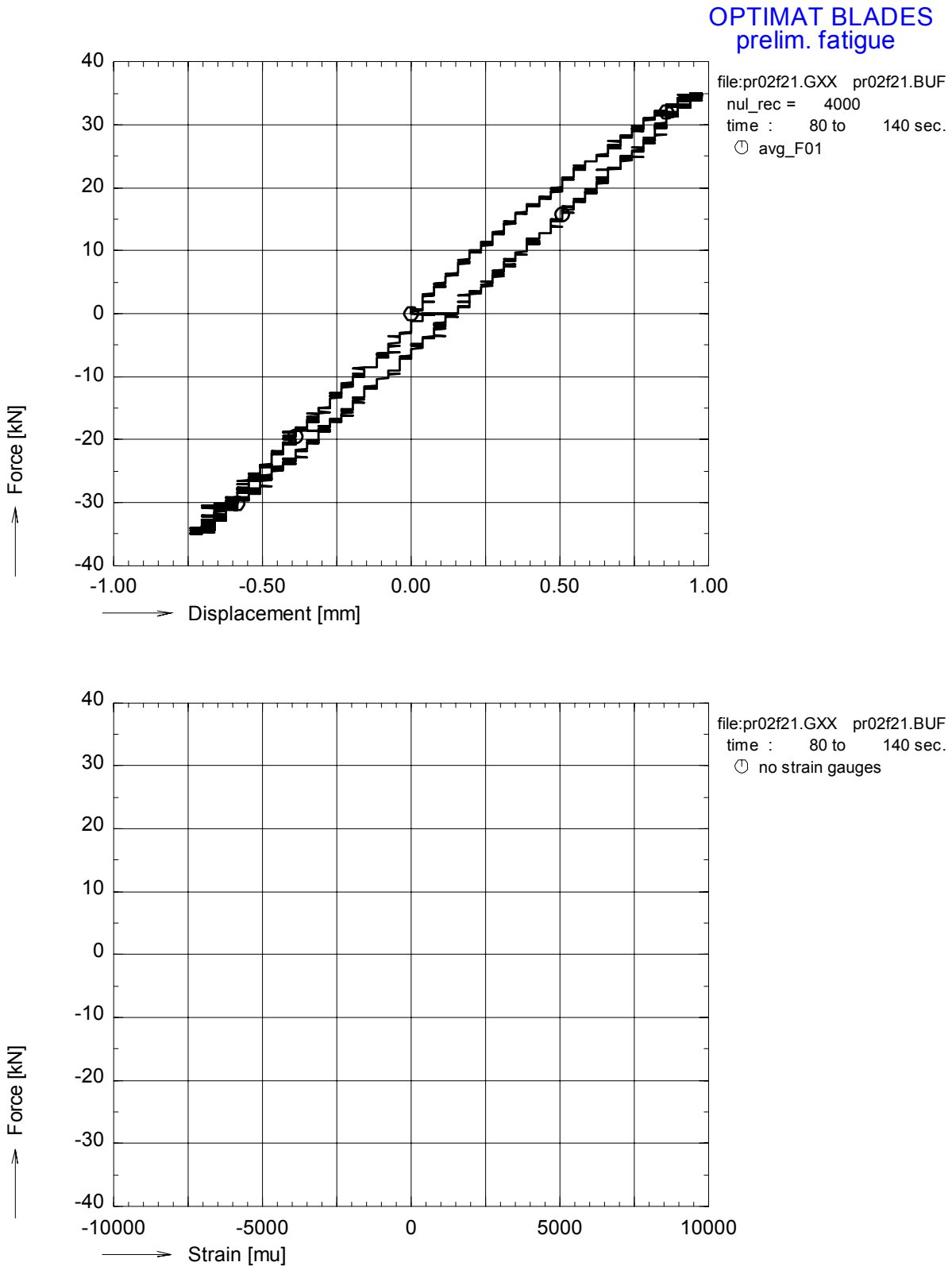

figure A 102: Axial force vs. bench displacement and strains during preceding slow cycle for pr02f21

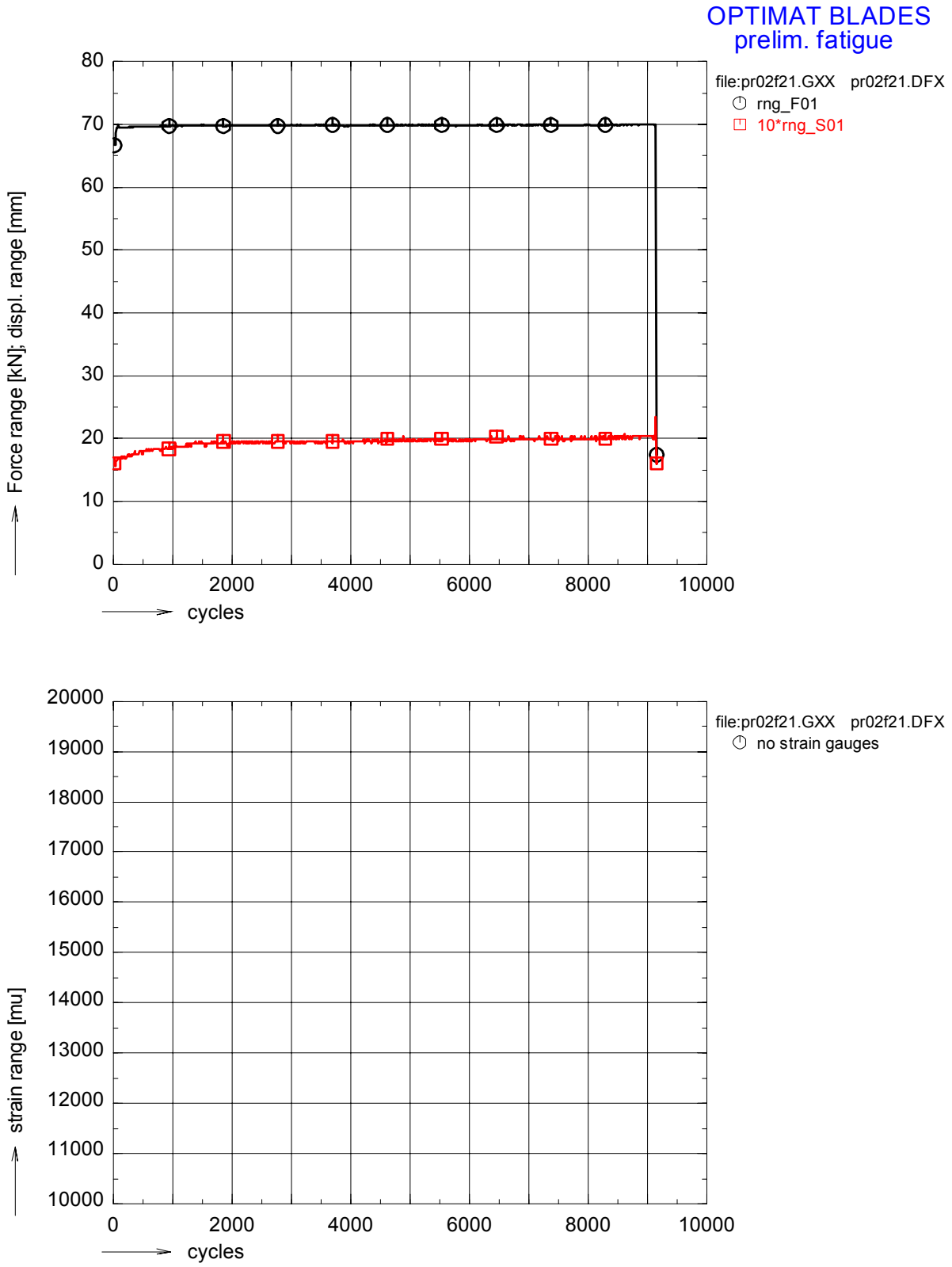

figure A 103: Ranges of force, bench displacement and strains during fatigue life for pr02f21

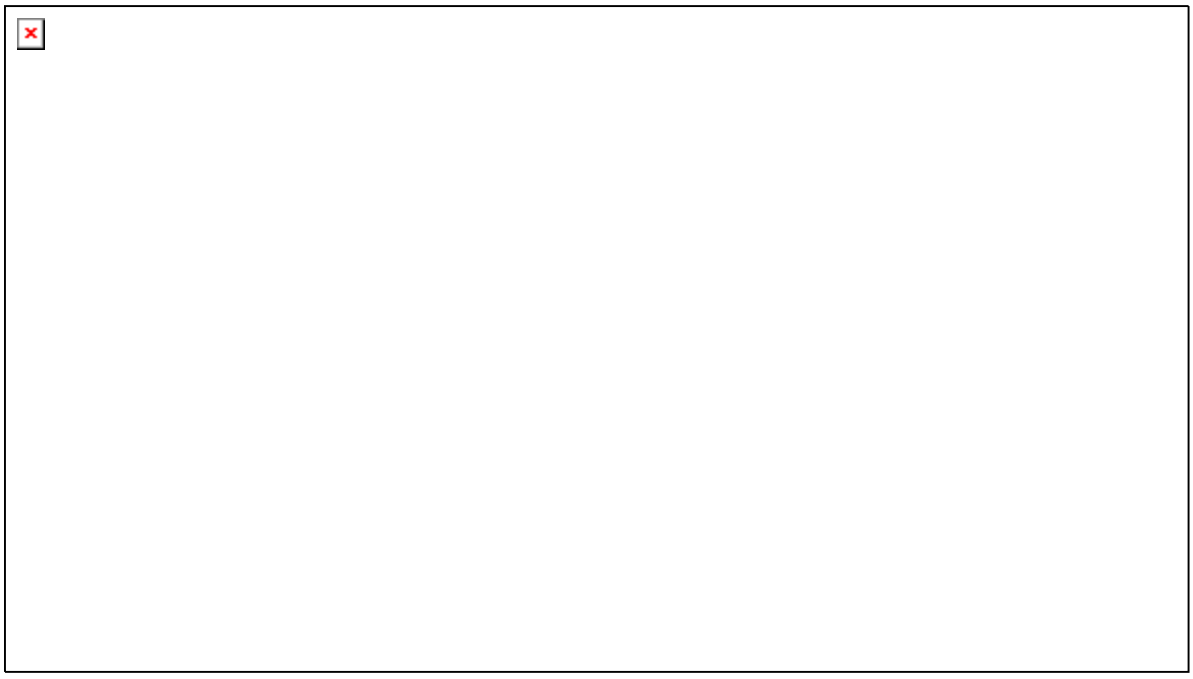

figure A 104: Photographs of failed specimen pr02f21

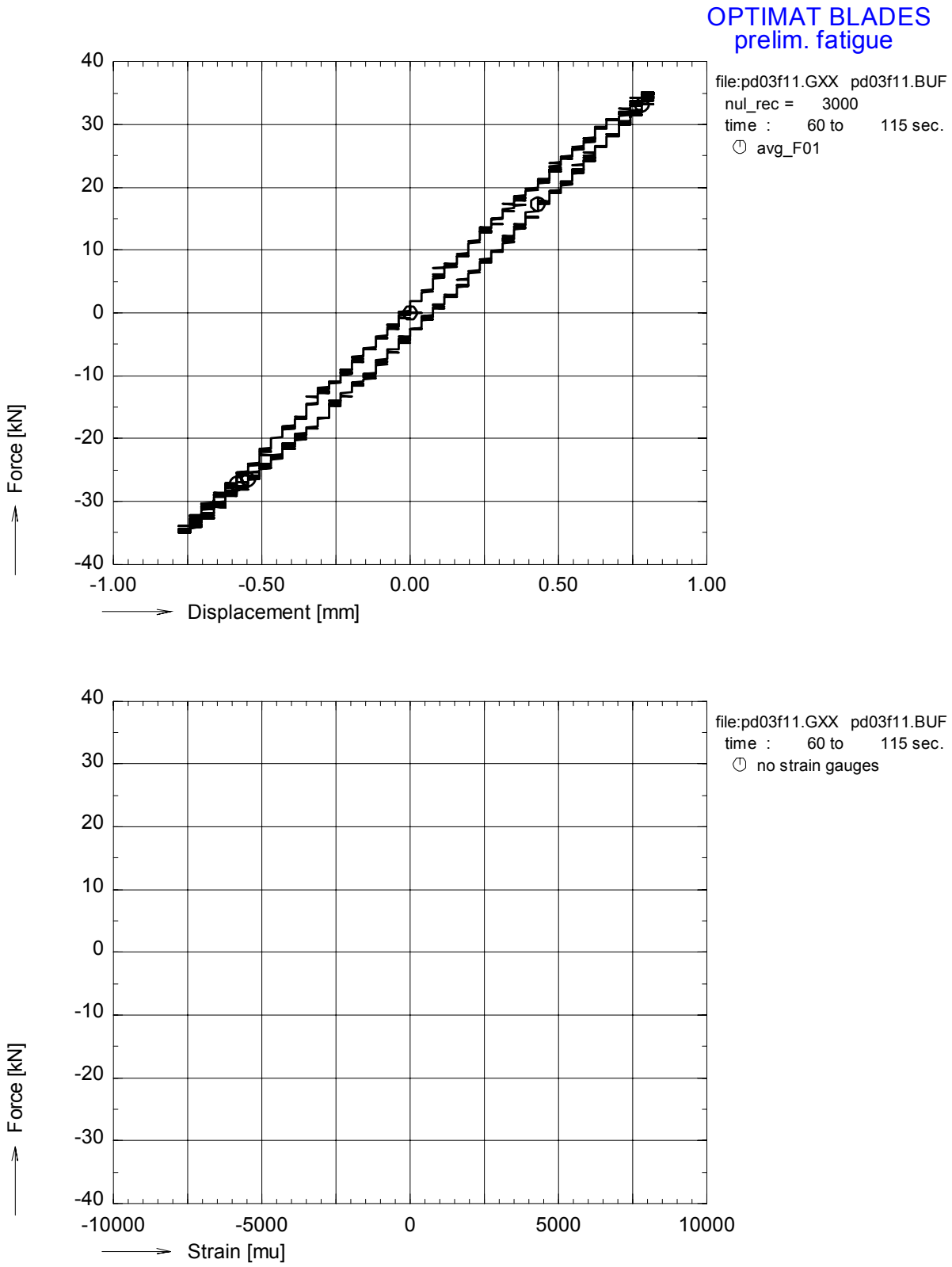

figure A 105: Axial force vs. bench displacement and strains during preceding slow cycle for pd03f11

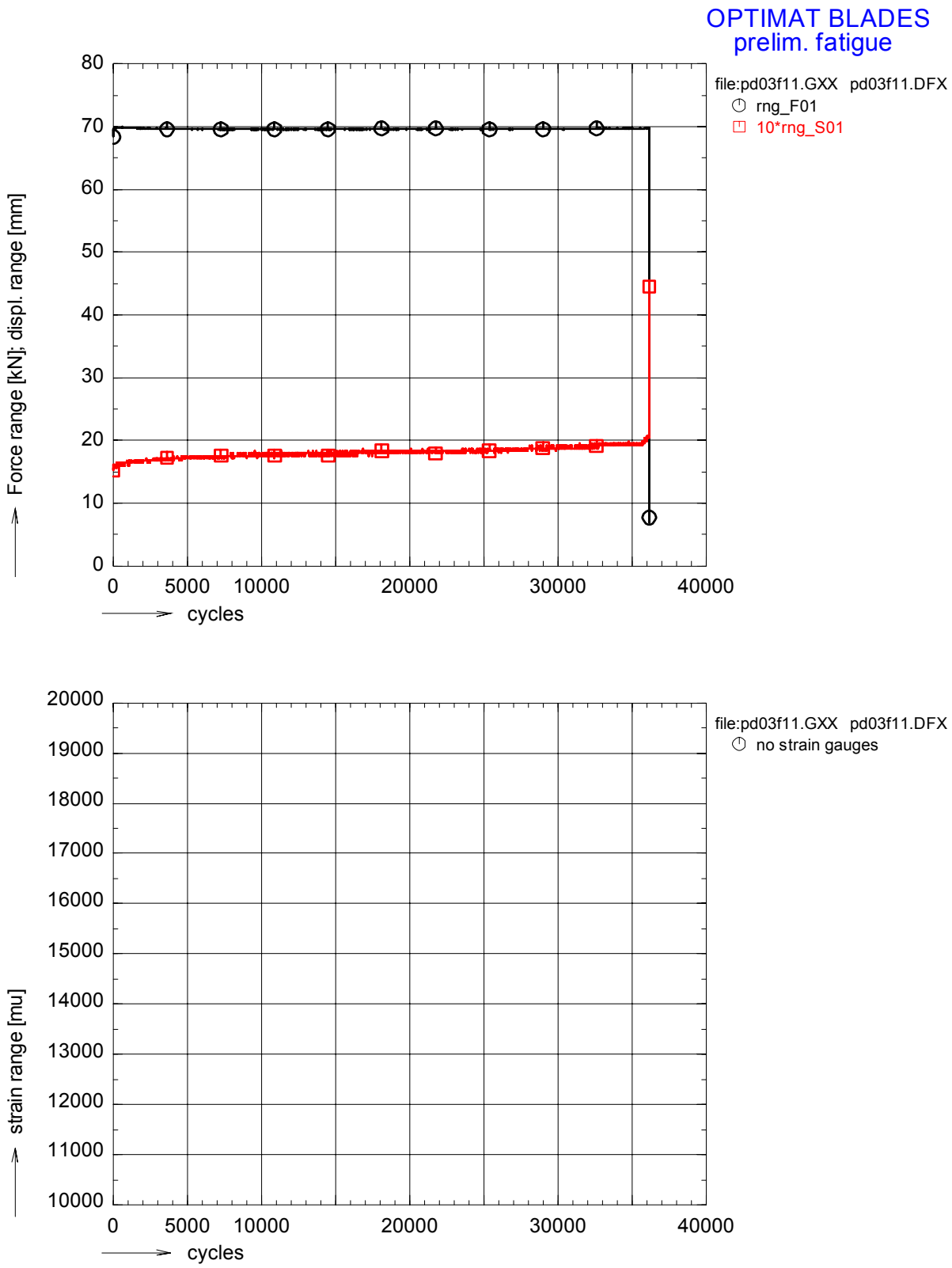

figure A 106: Ranges of force, bench displacement and strains during fatigue life for pd03f11

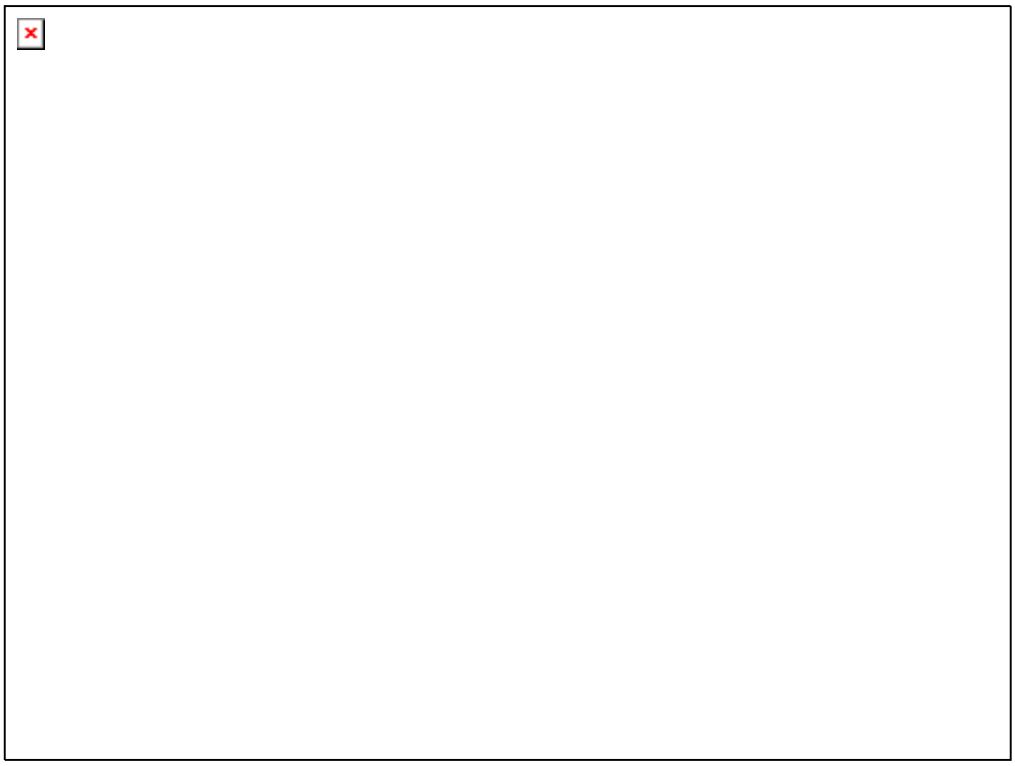

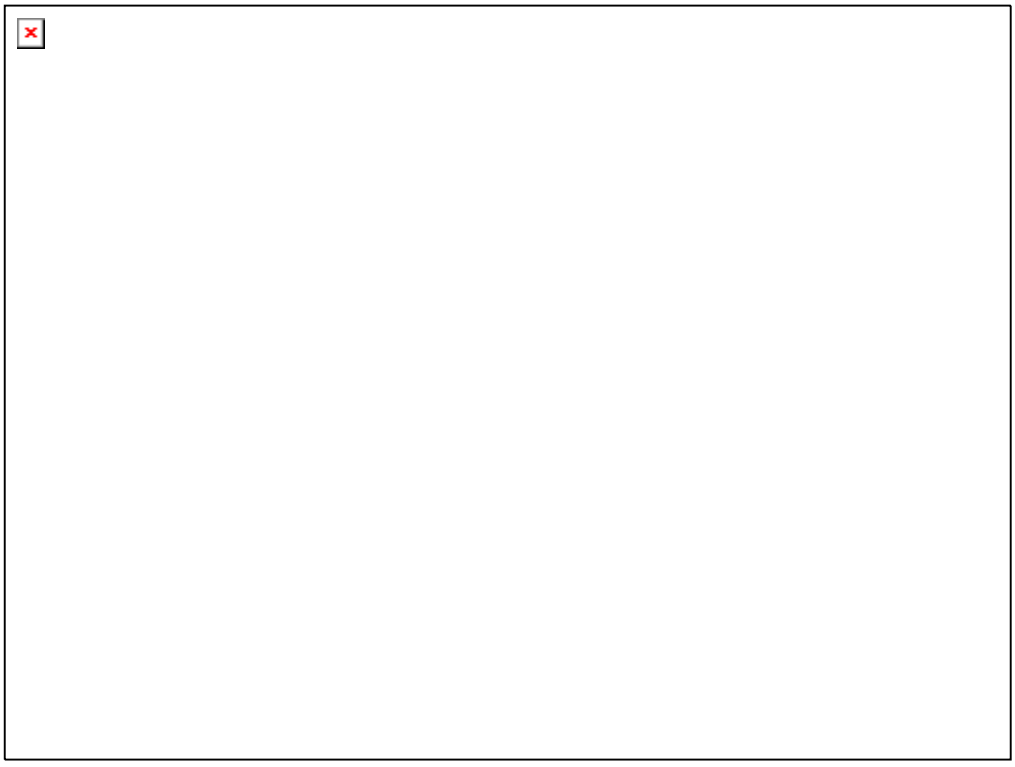

figure A 107: Photographs of failed specimen pd03f11

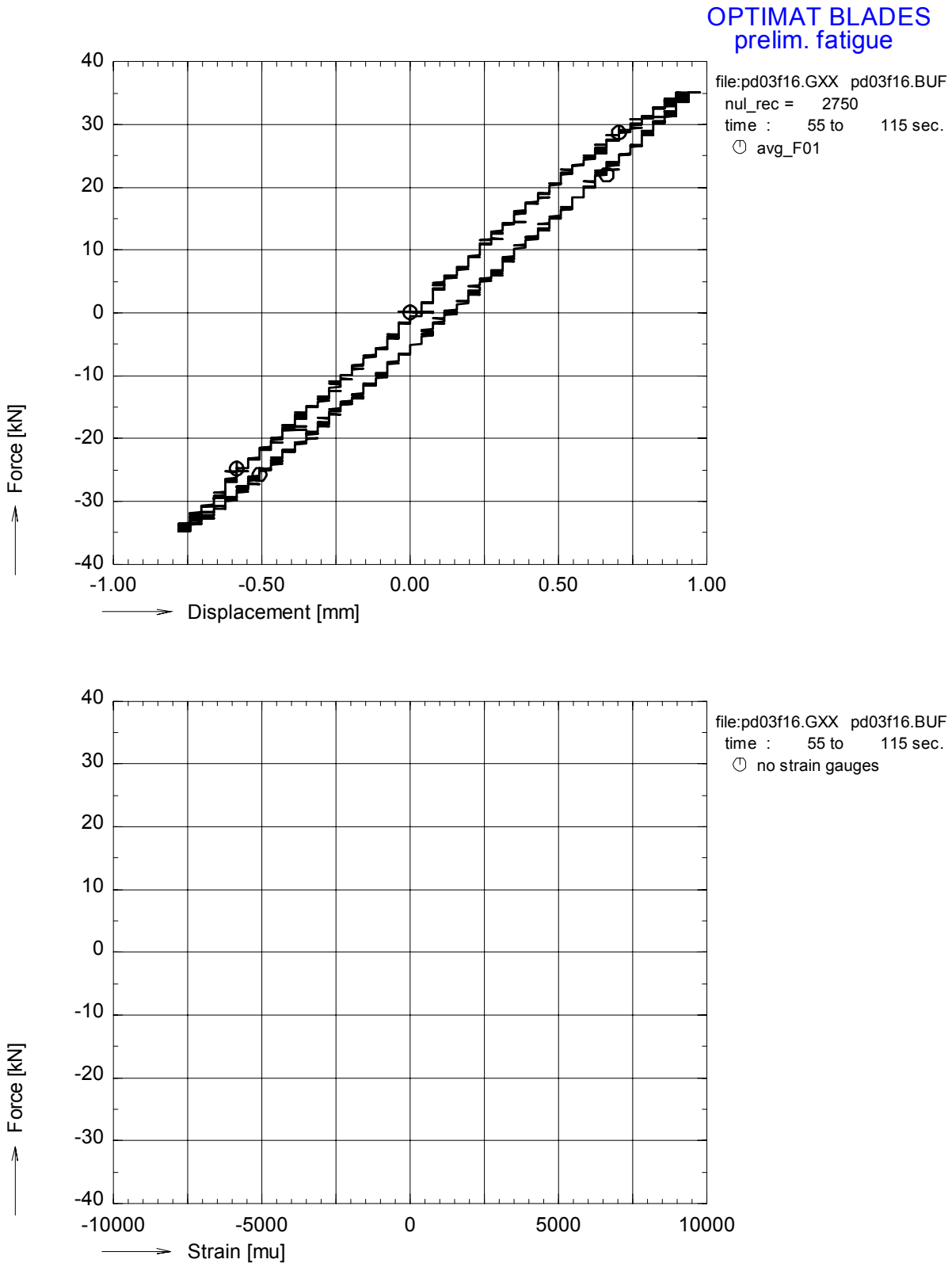

figure A 108: Axial force vs. bench displacement and strains during preceding slow cycle for pd03f16

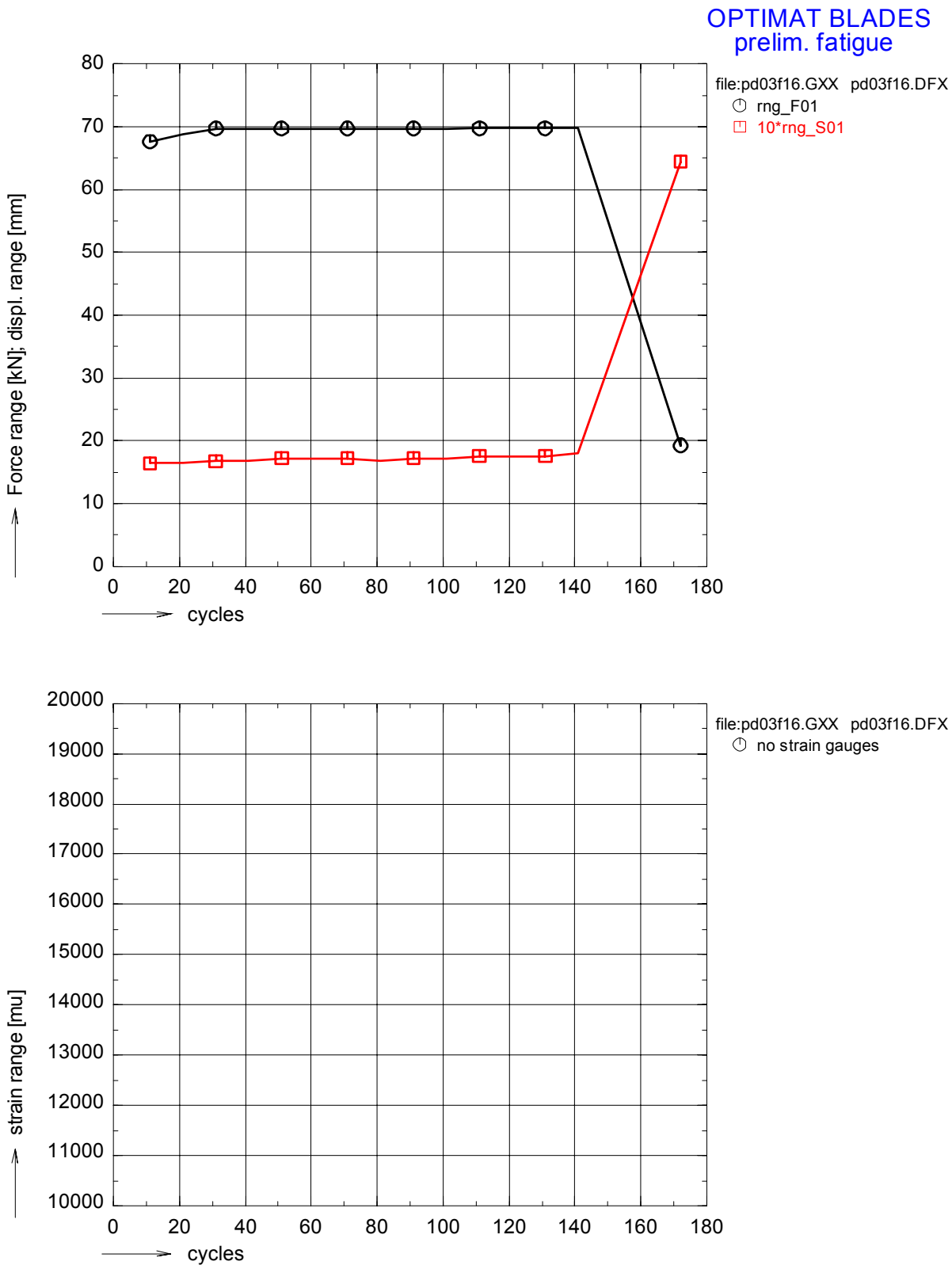

figure A 109: Ranges of force, bench displacement and strains during fatigue life for pd03f16

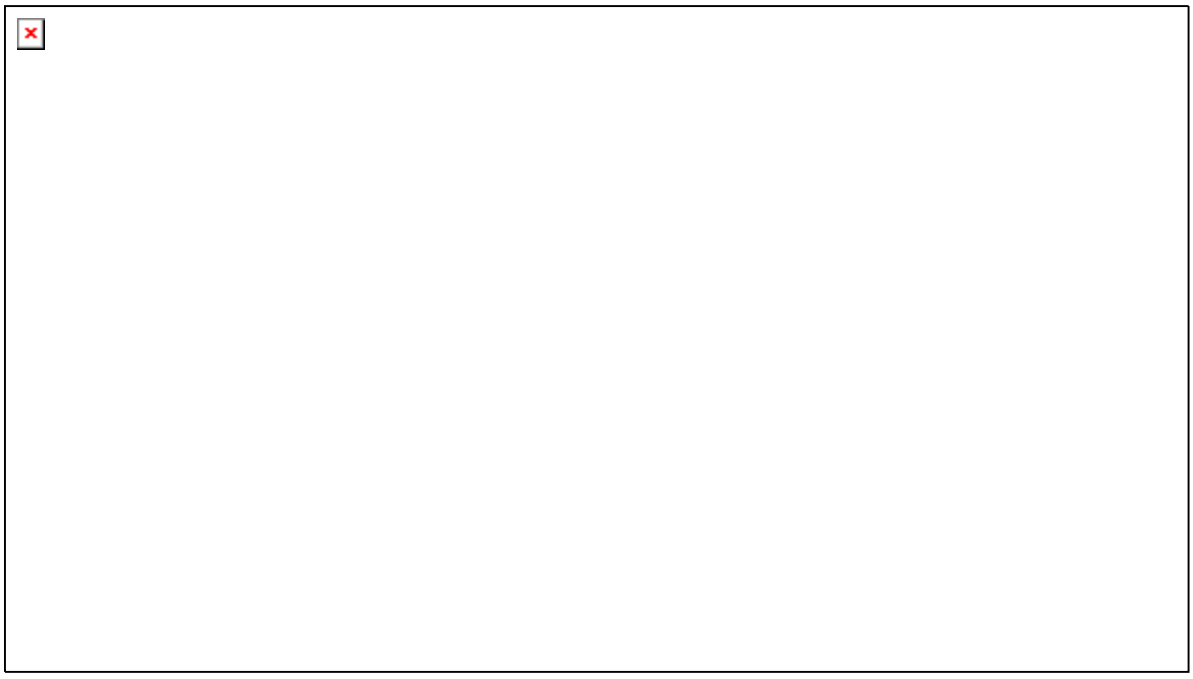

figure A 110: Photographs of failed specimen pd03f16

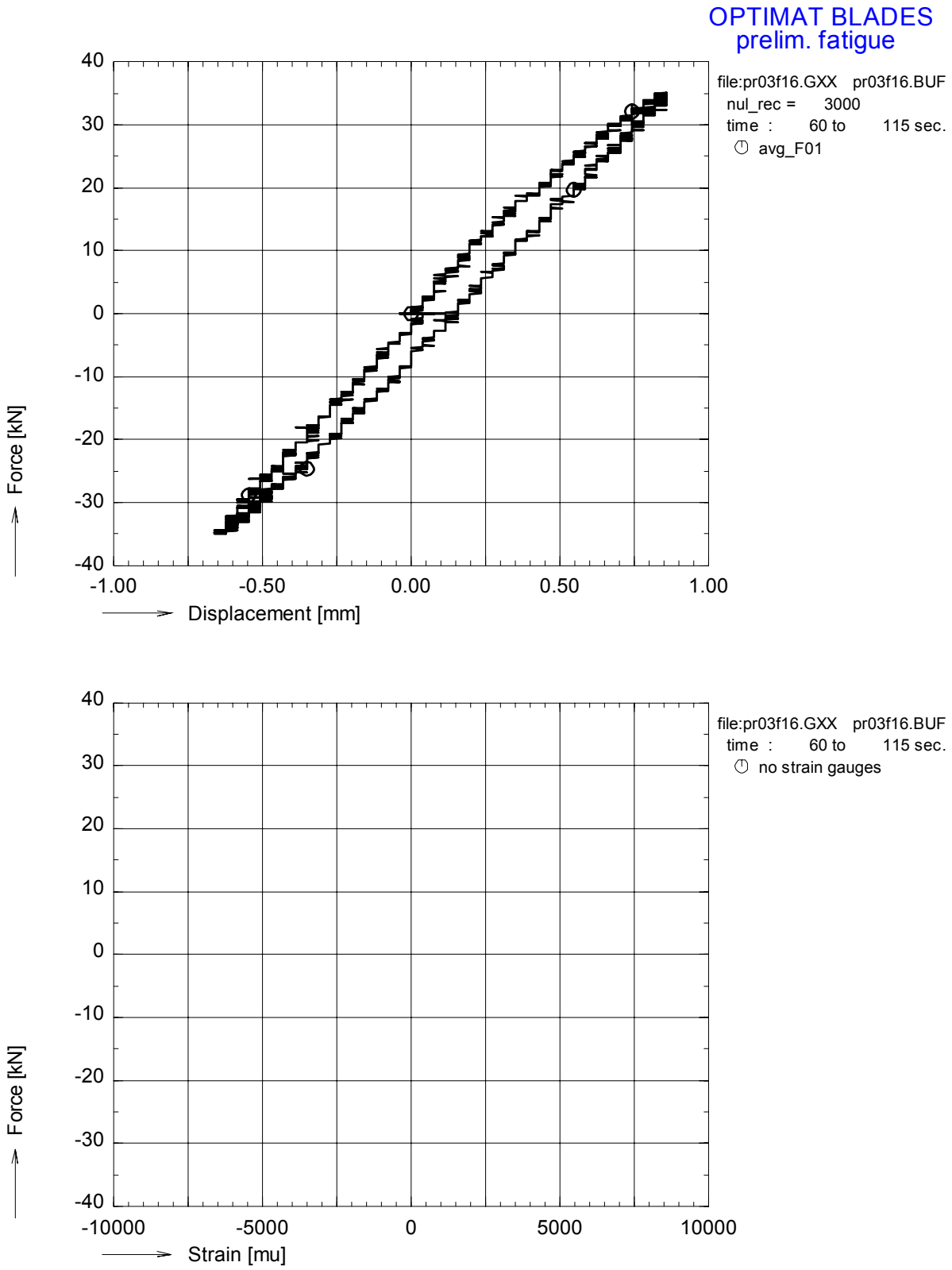

figure A 111: Axial force vs. bench displacement and strains during preceding slow cycle for pr03f16

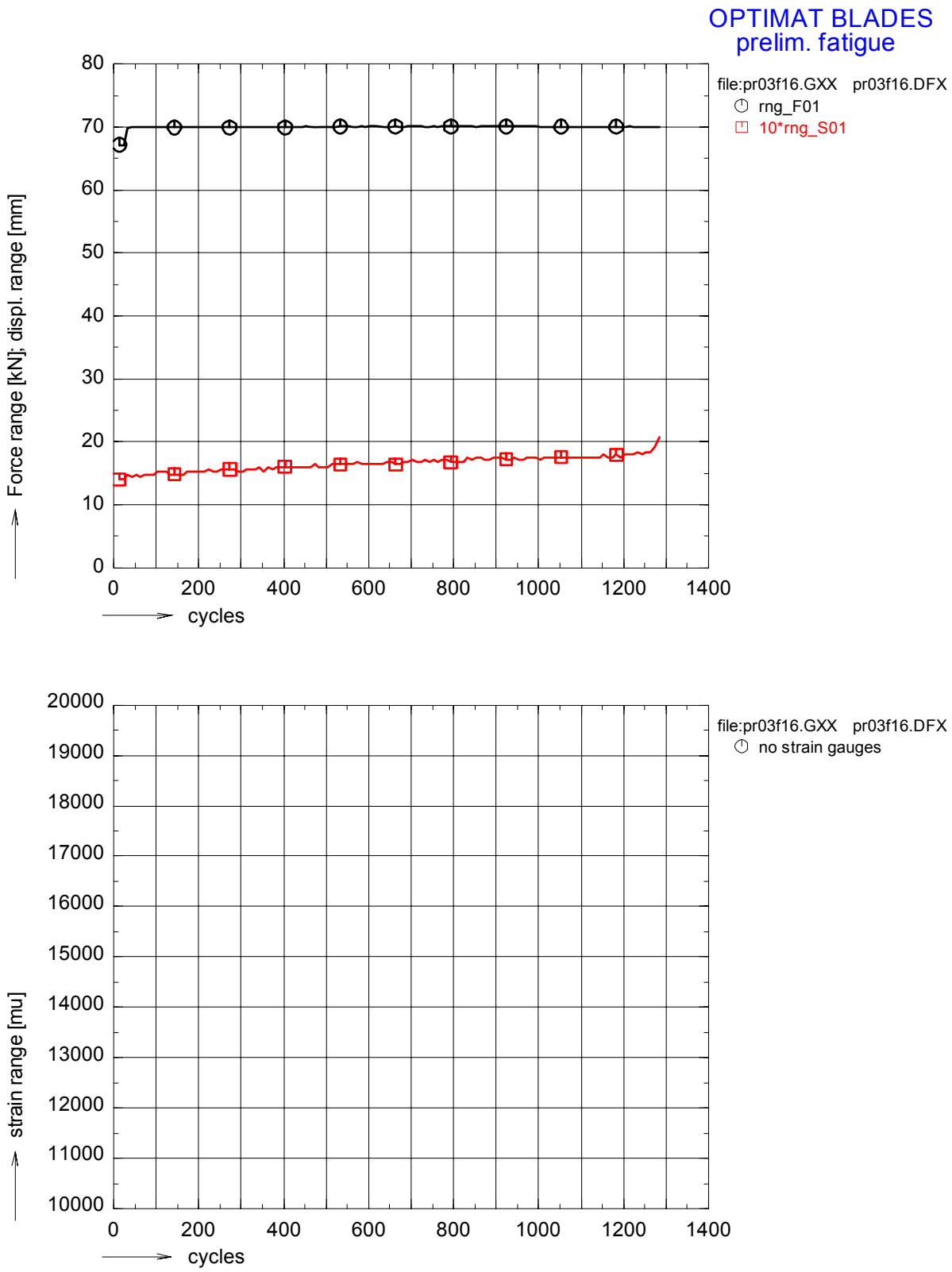

figure A 112: Ranges of force, bench displacement and strains during fatigue life for pr03f16

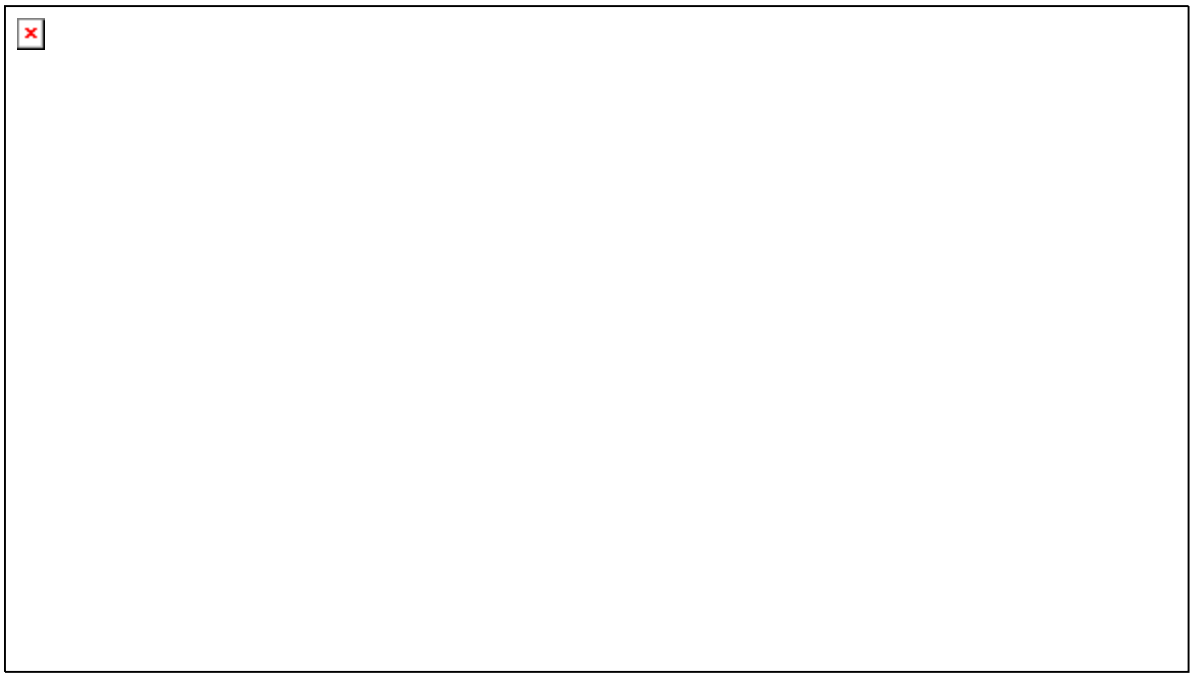

figure A 113: Photographs of failed specimen pr03f16

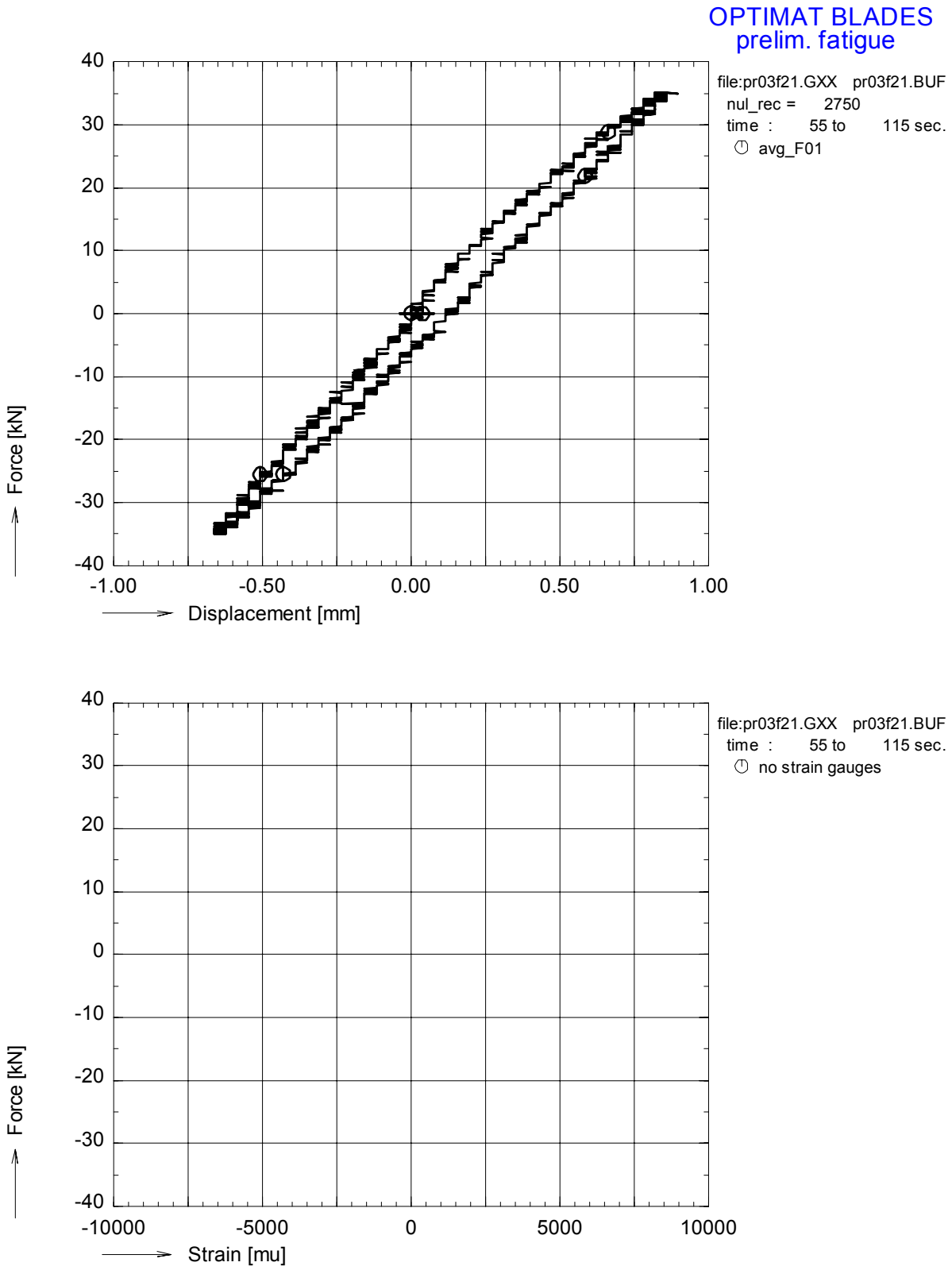

figure A 114: Axial force vs. bench displacement and strains during preceding slow cycle for pr03f21

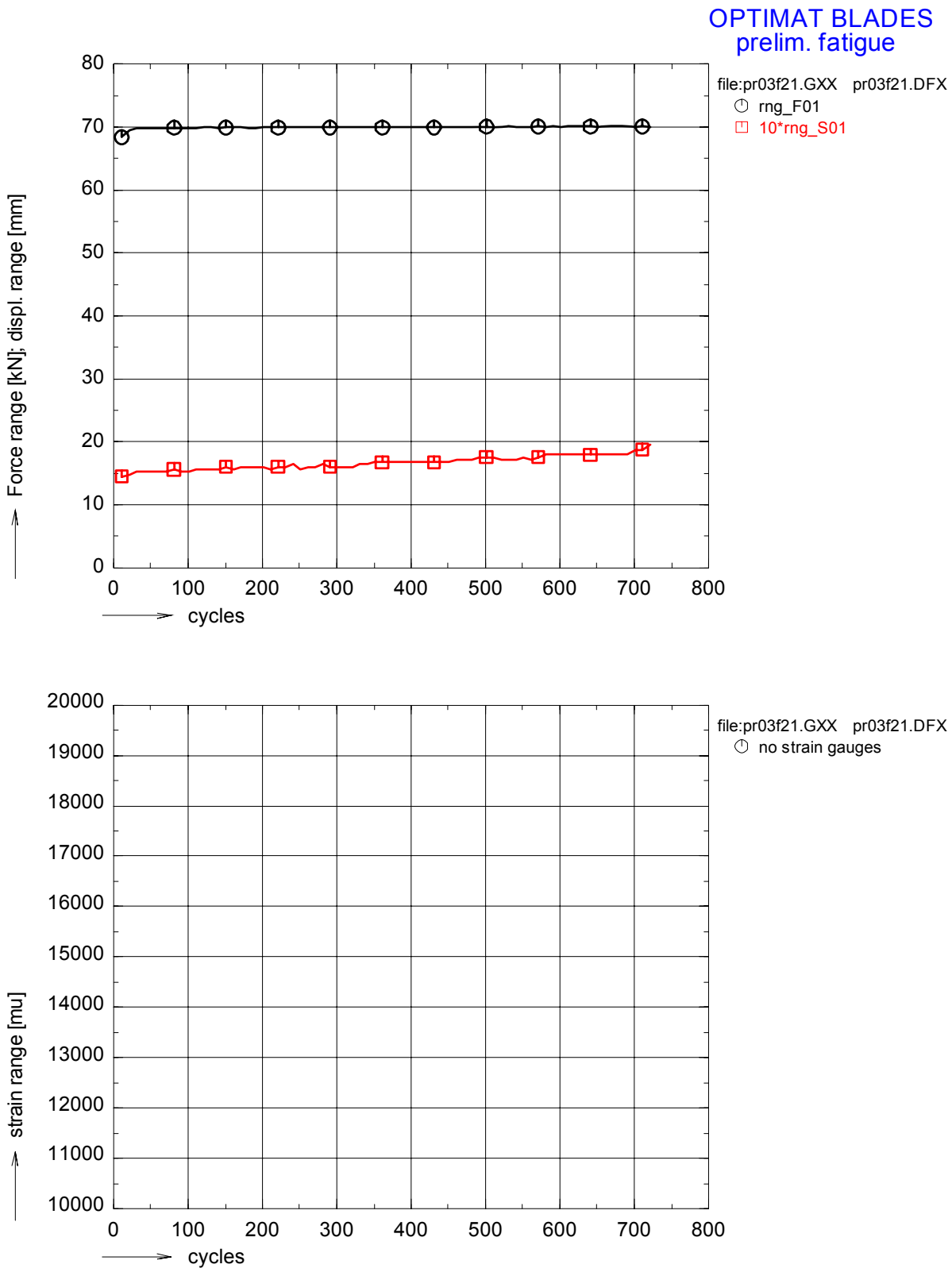

figure A 115: Ranges of force, bench displacement and strains during fatigue life for pr03f21

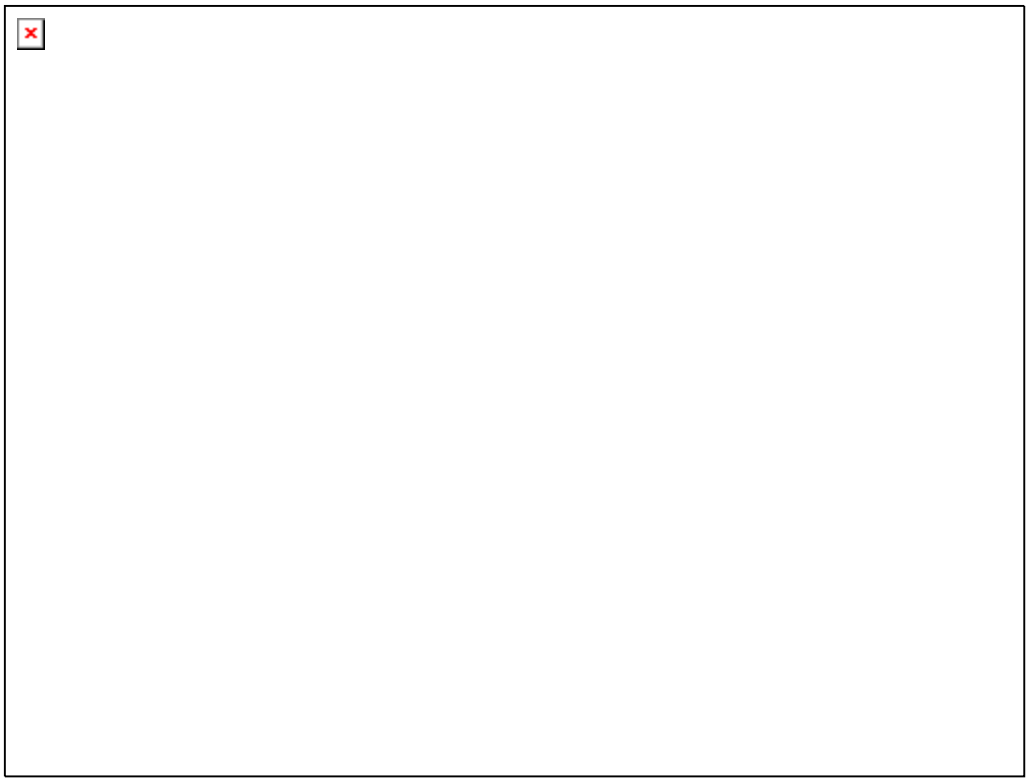

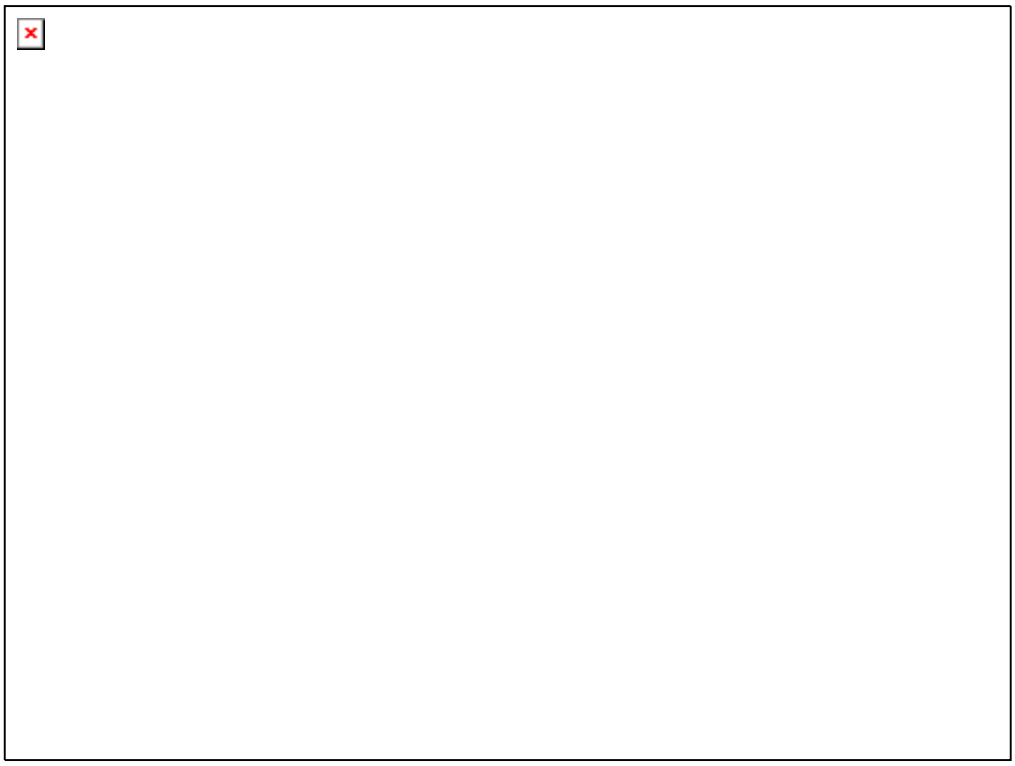

figure A 116: Photographs of failed specimen pr03f21